Physikalisch-Astronomische Fakultät

Thüringer Landessternwarte Tautenburg

The Frequency of Planets around A- and M-type stars

Dissertation zur Erlangung des akademischen Grades doctor rerum naturalium (Dr. rer. nat.)

vorgelegt dem Rat der Physikalisch-Astronomischen Fakultät der Friedrich-Schiller-Universität Jena

von M.Sc. Silvia Sabotta

geboren am 02. Januar 1990 in Mannheim

Referees:

1. Prof. Dr. Artie Hatzes
   Thüringer Landessternwarte Tautenburg
2. Prof. Dr. Konstanze Zwintz
   Univerität Innsbruck
   Institut für Astro- und Teilchenphysik
3. Prof. Dr. Magali Deleuil
   Aix-Marseille University, Marseille
   Laboratory of Astrophysics of Marseille (LAM)

Day of Disputation: February 17, 2021

Zusammenfassung

Bisher wissen wir noch relativ wenig über die Planetenhäufigkeit bei Sternen, die schwerer oder leichter sind als unsere Sonne (heiße und kühle Sterne). Die meisten Studien von Planetenhäufigkeiten wurden für sonnenähnliche Sterne durchgeführt. Wir müssen unser Wissen über die Planetenhäufigkeiten als Funktion der Sternenmasse erweitern, wenn wir Planetenentstehung vollständig verstehen wollen. Theoretische Planetenpopulationsmodelle werden zur Zeit auf Sterne mit anderen Massen erweitert. Zum Vergleich sind Planetenstatistiken von Beobachtungsdaten besonders wichtig.

Es ist allgemein anerkannt, dass Riesenplaneten in nahen Umlaufbahnen bis zu Perioden von 10 Tagen bei allen Sterntypen sehr selten sind. In dieser Arbeit überprüfe ich eine Hypothese von 166 zusätzlichen nahen Planetenkandidaten um A Sterne im Kepler Feld. Ich verwende Radialgeschwindigkeitsdaten von den 2 m Teleskopen in Tautenburg und Ondřejov um nahe Sternbegleiter auszuschließen. Mit einer statistischen Analyse von allen 2000 Kepler A Sternen, kann ich eine hohe Häufigkeit dieser Planetenart ausschließen. Ich finde eine Höchstgrenze der Häufigkeit von heißen Jupiters um A Sterne auf der Hauptreihe von 0.75 %. Das ist weniger oder gleich viel wie die Häufigkeit um sonnenähnliche Sterne.

Die Häufigkeit von Planeten um M Zwerge ist immer noch eine offene Frage. In dieser Arbeit präsentiere ich meine Analyse von 125 Sternen des CARMENES Surveys. Das Survey wurde für diese Sterne beendet weshalb wir eine erste statistische Analyse durchführen können. Zu diesem Zweck, berechne ich die Nachweisgrenzen für jeden Stern. Von diesen Nachweisgrenzen leite ich Planetenhäufigkeiten mit zwei Methoden ab. Mit der ersten Methode bilde ich eine durchschnittliche Anzahl der Sterne um die ein Planet entdeckt werden könnte in verschiedenen Periode-Masse Bins ("Periode-Masse Bin Methode"). Mit der zweiten Methode schätze ich die Anzahl der Planeten, die wir mit unseren Beobachtungsdaten nicht entdecken konnten, anhand der entdeckten Planeten ab ("Nicht-Entdeckte Planeten Methode"). Ich kann eine Höchstgrenze von 1.4 % für die Häufigkeit von heißen Jupiters setzen. Für kleine Planeten ergeben die beiden Methoden

sehr unterschiedliche Ergebnisse. Die Ergebnisse der ersten Methode (66 % für Perioden bis zu 100 Tagen) stimmen mit den Häufigkeiten von von kleinen Planeten bei G Sternen überein. Die zweite Methode resultiert mit 1.8 Planeten pro Stern in einer sehr viel höheren Häufigkeit von kleinen Planeten. Diese höhere Häufigkeit stimmt mit dem überein, was wir von Transitsurveys über Planeten um M Zwerge wissen. Ich zeige, dass das CARMENES survey in der Zukunft mit 200 Messungen pro Stern bei 10 zufällig ausgewählten inaktiven Sternen, diese Diskrepanz auflösen kann.

Abstract

We still know relatively little about the planet frequency around stars that are more or less massive than the Sun (hot and cool stars). Most occurrence rate studies were done on stars that are solar-like. We have to increase our knowledge on planet frequencies as a function of stellar mass, if we want to fully understand planet formation. Theoretical planet population models are currently extended to stars with other masses. For comparison, planet statistics from observational data are particularly important.

It is generally accepted that giant planets in close orbits up to periods of 10 days are very rare around all kinds of stars. In this thesis I test a hypothesis of 166 additional close-in planet candidates around A-type stars in the *Kepler* field. I utilize radial velocity data from the Tautenburg and Ondřejov 2 m telescopes to rule out a close-in stellar companion. With a statistical analysis of all 2000 Kepler A stars, I can rule out a high frequency of this kind of planets. I find an upper limit of 0.75 % on the hot Jupiter frequency around main-sequence A-type stars. This is less or equal the frequency of hot Jupiters around solar-like stars.

The frequency of planets around M dwarfs is still an open question. In this thesis I present my analysis of 125 stars of the CARMENES survey. The survey is finished on those stars which allows us to make a first statistical analysis. To this end I compute observational detection limits for each of the stars. From the detection limits I infer the occurrence rates with two methods. With the first method I average the number of stars around which a planet could be detected in several period-mass bins ("period-mass bin method"). With the second method I estimate the number of planets that could be missed due to observational biases based on the actual planet detections ("missed planets method"). For hot Jupiters around M dwarfs I can place an upper limit of 1.4 %. For small mass planets the two methods give very different results. The results of the first method (66 % for periods up to 100 d) are consistent with G star frequencies of small mass planets. The second method results in a much higher small planet frequency of 1.8 planets per star. Those higher occurrence rates are consistent with what we

know from transiting surveys of planets around M dwarfs. I show that the CARMENES survey in the future will be able to resolve this discrepancy with 200 measurements per star of 10 randomly selected inactive targets.

Contents

List of Tables

List of Figures

Chapter 1

Introduction

We still know relatively little about the planet occurrence around main-sequence stars that are more and less massive than the Sun (hot and cool stars). The mass of a star is its most fundamental parameter and influences the formation and evolution of its planets. As of today[1], the Extrasolar Planets Encyclopedia on `exoplanet.eu` lists 4482 planets (Schneider et al. 2011). Only 33 of them orbit main-sequence stars with effective temperatures between $T_{\rm eff} = 7300 - 10\,000$ K (A-type stars). Most of what we know about planets around A-type stars, we know from planets around "retired A stars" – A stars that have evolved to giant stars. But there are some recent studies that question the planetary nature of these signals (e.g. γ Draconis or Aldebaran Hatzes et al. 2018; Reichert et al. 2019). For the M stars ($T_{\rm eff} = 2300 - 4100\,{\rm K}$) the sample is larger with around 300 detected planets. The vast majority of planet detections is still around stars with spectral types between F6 and K0. As a consequence most occurrence rate studies were done on the so-called FGK stars. To fully understand planet formation mechanisms it is necessary to extend this scale to lower ($0.08\,{\rm M}_\odot < M_\star < 0.7\,{\rm M}_\odot$) and higher ($1.5\,{\rm M}_\odot < M_\star < 2.5\,{\rm M}_\odot$) mass stars.

[1] last update Aug. 6, 2020

Planet formation theories can be tested in two different ways: with single objects or statistically. A planet formation model needs to be capable of reproducing all of the diverse exoplanets that are observed. If a theory fails to predict a certain planet type, it needs to be revised.

The most prominent example is the first exoplanet 51 Peg b (Mayor & Queloz 1995) – a close-in giant planet around a solar type star. Before its discovery, it was believed that giant planets form *in situ* in a region where the stellar irradiance is weak enough such that volatiles can condensate – beyond a so-called "snow or ice line". This region was expected to be around 4 AU to 5 AU for stars of solar type and lower mass (Boss 1995). The very close orbit of 51 Peg b therefore came as a surprise. The most adopted explanation up to date is that it formed further out in the protoplanetary disk and then migrated inwards – so called type II migration (Lin et al. 1996). One challenge of this migration theory is that it requires a halting mechanism such that planets are prevented from falling into their star (e.g. Plavchan & Bilinski 2013). Another suggested scenario for the formation of 51 Peg is that a two Jupiter system could become dynamically unstable – one planet would be ejected and the other left in a close-in circular orbit (Rasio & Ford 1996). Other models claim that *in situ* formation of 51 Peg is possible but unlikely (Bodenheimer et al. 2000).

Pätzold & Rauer (2002) claim that massive planets are engulfed by their host stars through tidal interactions. This hypothesis is challenged by discoveries of very close giant planets with periods of less than 1 d. Nielsen et al. (2020) discovered a 3.2 7 M_{Jup} planet in a 0.98 d orbit of a K4-dwarf and Jackman et al. (2019) found a brown dwarf companion to an M-type host star in an orbit as short as 0.675 d.

Still up until now after several thousands of discovered exoplanets, new benchmark objects are uncovered. One example is a giant planet published by Morales et al. (2019), which orbits a very low mass star. This discovery shows that not a single formation mechanism can explain all the planets known up to date. The two major formation mechanisms, disk instability (Boss 2006) and pebble (Lambrechts & Johansen 2012) or core accretion (Pollack et al. 1996; Alibert et al. 2005), are possibly both needed to explain the exoplanet diversity. Another very interesting planetary system, cannot be formed *in situ*. The A type planet host star HR 8799 hosts four massive exoplanets. They were detected with the direct imaging method and have masses of $M_{\mathrm{pl}} = 7\,\mathrm{M_{Jup}} - 9.2\,\mathrm{M_{Jup}}$ at orbital distances of 16.4 AU to 68 AU (Marois et al. 2008; Marois et al. 2010). The innermost planet is too close-in to be formed by disk instability at this location while the outermost planet is too far out for *in situ* formation via core-accretion.

With the emergence of planet population synthesis, we are able to compare observations and theory on a statistical level as well. Those large sets of artificial planets, formed within the core accretion scenario, can be directly compared to planet frequencies from observations (e.g. Emsenhuber et al. 2020a,b; Schlecker et al. 2020). Those planet population models are currently extended to low mass stars (Burn et al. 2020). Hence, planet statistics for this kind of stars is important.

Planet formation depends crucially on the host star properties. Important host star parameters that have to be considered are the host star metallicity and the host star mass. The dependence of giant planet occurrence on the metallicity of the host star is well established (e.g. Fischer & Valenti 2005). This relation seems to hold for even smaller planets with Neptune or Super Earth size around K stars in comparison to FG stars (Wang et al. 2018).

In this thesis I focus on the planet frequencies vs. stellar mass. A star's evolution depends heavily on its mass. It is thus obvious that the formation and evolution of a planet also depends on the host star mass. Nevertheless, a relation between host star mass and planet occurrence rate, is not as well established as that between metallicity and giant planet occurrence. One way how the host star mass influences planet formation is via the protoplanetary disk. The host star mass affects the protoplanetary disks in several ways. The mass of the disk is observed to be dependent on the mass of the host star (Andrews et al. 2013). The disk lifetime of stars more massive than the sun is around two times shorter than that of disks around solar-like or less massive stars (Williams & Cieza 2011). The location of the "snow line" is dependent on the luminosity of the star. Observations also indicate that there is a cutoff location in the disk, inside which planet formation and migration become unlikely. This region is also stellar mass dependent (Mulders et al. 2015).

These effects influence planet formation mechanisms. A more massive disk provides more material for planet formation such that we would expect a higher frequency of gas giants. A shorter disk lifetime on the other hand could mean that the disk is already depleted of material before the runaway gas accretion – necessary to form a giant planet in the core accretion scenario – or type II migration could be effective (Burkert & Ida 2007; Currie 2009). The location of the "snow line" of hotter stars is further out, therefore planets around this type of stars are expected to form in longer orbits. Taking these effects into account, theories predict a lower frequency of close-in massive planets around both A- and M-type stars than around G-type stars (e.g. Ida & Lin 2005; Alibert et al. 2011). The giant planet occurrence for longer periods on the other hand is expected to increase with stellar mass (Kennedy & Kenyon 2008).

These theoretical predictions interplay with what is known from observations. For example: the core accretion theory predicted a low number of planets with several Earth masses in closer orbits (e.g. Ida & Lin 2008) and had to be revised after Howard et al. (2010) found several planets in exactly this period-mass region. Gathering more information on the exoplanet statistics thus brings us a step closer to fully understand planet formation processes.

Planet frequency studies of A- and M-type stars are still rare. For A-type stars they have to ultimately focus on giant planet occurrence rates as lower mass or size planets are mostly not observable. In the following sections I will first give an overview on what is known about the close-in giant planet frequencies of solar-like stars followed by a comparison to A-type stars. In this thesis I will test the hypothesis of a very high close-in giant planet planet occurrence rate of 8.4 % suggested by Balona (2014). I will use radial velocity data from the Tautenburg and Ondřejov high resolution spectrographs at the 2 m telescopes and data from the *Kepler* space telescope. The entire analysis is the content of chapter 2. The second goal of this thesis is to refine the statistics we have about planets around M dwarfs. Later in this chapter I will show what is known about giant and small planets around G-type stars in order to compare those values to the sparse results we have for main-sequence M-type stars. Apart from an expected lower giant planet occurrence rate, it is specifically interesting if the small planet occurrence is higher for stars with lower mass. I will present what I learned from the **C**alar **A**lto high-**R**esolution search for **M** dwarfs with **E**xo-earths with **N**ear-infrared and optical **E**chelle **S**pectrographs (CARMENES) in chapter 3. My conclusions are placed in chapter 4.

1.1 Close-in giant planets around G-type stars

The first exoplanet discovered was a hot Jupiter, but further discoveries showed that this kind of planet is in fact relatively rare. Hatzes & Rauer (2015) define giant planets from the planet densities to have masses from 0.3–60 Jupiter masses (100–20 000 Earth masses). The International Astronomical Union (IAU) currently defines the limiting mass for thermonuclear fusion of deuterium as a criterion for the upper mass limit of a planet (e.g. Boss et al. 2007). Above this limit they are called "brown dwarfs". This limit corresponds to a mass of $13\,\mathrm{M_{Jup}}$ (e.g. Spiegel et al. 2011). Several authors confirm that this mass limit does not correspond to a breakpoint in the mass-density or mass-radius relation, e.g. Bashi et al. (2017) or Chen et al. (2017). Therefore, I adopt the definition of Hatzes & Rauer (2015) as my definition of giant planets.

One of the most cited studies of planet occurrence rates from radial velocity (RV) is that of Cumming et al. (2008), who analyzed data from the Keck Planet Search with a total number of 475 stars that were observed for around 8 years. They did not find any close-in planets ($P_{\mathrm{pl}} < 10\,\mathrm{d}$) with masses $M_{\mathrm{pl}} \sin i > 2\,\mathrm{M_{Jup}}$ for FGK stars although their sample is almost complete in this regime. The fraction of planets with masses $M_{\mathrm{pl}} \sin i > 1\,\mathrm{M_{Jup}}$ they have obtained, is only 0.4 % and that of planets with masses $M_{\mathrm{pl}} \sin i > 0.3\,\mathrm{M_{Jup}}$ is 1.5 %.

Wright et al. (2012) have reanalyzed data of 836 stars from the Lick and Keck Planet Searches. They reduced selection effects that were probably present in the Cumming et al. (2008) analysis. The hot Jupiter occurrence rate they found is 1.2 % but they define hot Jupiters to have masses in the range from $0.1\,\mathrm{M_{Jup}}$ to $13\,\mathrm{M_{Jup}}$. Although they did not publish a frequency of planets more massive than $0.3\,\mathrm{M_{Jup}}$, I can estimate it from their results. Nine of their detected planets have masses higher than $0.3\,\mathrm{M_{Jup}}$ and in the total sample there are 10 planets. Accordingly, the frequency of planets more massive than $0.3\,\mathrm{M_{Jup}}$ in their sample should be roughly 1.1 %. Howard et al. (2010) also used data from the Keck observatory and obtained a close-in giant planet frequency of 1.6 %.

Another large RV-survey was a combination of the High Accuracy Radial velocity Planet Searcher (HARPS) and CORALIE results by Mayor et al. (2011). They used 822 non-active stars. Their survey indicates an increase of giant planet occurrence towards longer periods and a low frequency for close-in massive planets of 0.9 %. They included planets with $M_{\mathrm{pl}} \sin i > 0.16\,\mathrm{M_{Jup}}$. Had they included only those with masses $> 0.3\,\mathrm{M_{Jup}}$ their occurrence rate would even be as low as 0.5 %. On the other hand, Wittenmyer et al. (2020) recently published a giant planet occurrence rate from the radial velocity Anglo Australian Planet Search (AAPS) around 203 stars of $1.5^{+3}_{-0.7}\,\%$.

One other way to find planets is through transit surveys. During a transit the light from the star is partially blocked by the planet that is orbiting in line of sight. If we compare RV and transit data we have to keep in mind that they probe a different parameter space – transit surveys obtain an occurrence rate based on the radius of the planet whereas radial velocities give the $M \sin i$ of a planet. Several authors have tried to establish a relation between mass and radius of planets. Bashi et al. (2017) find two different mass-radius relations for large and small planets. A large planet, according to them, is a planet with mass of $M_{\mathrm{pl}} > 0.39\,\mathrm{M_{Jup}}$ with a corresponding radius of $R_{\mathrm{pl}} > 12.1\,\mathrm{R_{\oplus}}$. Chen et al. (2017) find a similar inflection point for the mass-radius relation at $M_{\mathrm{pl}} > 0.41\,\mathrm{M_{Jup}}$ corresponding to roughly $R_{\mathrm{pl}} > 13\,\mathrm{R_{\oplus}}$. Petigura et al. (2017) argue that giant planets can have radii down to $R_{\mathrm{pl}} = 8\,\mathrm{R_{\oplus}}$. This is true also for the studies mentioned above. The parameter space from transit and RV survey will not fully overlap, no matter which radius definition is used.

Howard et al. (2012) have found a close-in giant planet occurrence rate that is lower – only 0.4 % – than that obtained by RV studies. They have studied G and K stars observed with the *Kepler* space telescope. They have included all planets with radii from 8–24 $R_\oplus$. Fressin et al. (2013) cleaned the sample from false positives and reached the same conclusion. Their definition of a giant planet is for planets with radii as small as 6 $R_\oplus$. Petigura et al. (2018) have also reanalyzed the hot Jupiter frequency with the same limits on the planet radius as Howard et al. (2012) but shifted slightly to hotter stars and with a slightly larger range of $\log g$ of the host stars. They found a hot Jupiter frequency of 0.57 %.

From the COnvection, ROtation et Transits planétaires (CoRoT) satellite Deleuil et al. (2018) determined a hot Jupiter frequency of 0.98 ± 0.26 % for F5 to K5 stars. Their choice of host stars is comparable in terms of stellar effective temperature to that of Howard et al. (2012). But on the other hand they define all planets with radii larger than 5 $R_\oplus$ as giant planets. This is adding planets in the range $R_{\mathrm{pl}} = 5 - 8\,R_\oplus$ to the statistics which may account for the larger occurrence rate compared to Kepler.

Zhou et al. (2019b) published the first statistical analysis of data obtained with the Transiting Exoplanet Survey Satellite (TESS). Their hot Jupiter definition is slightly different than that of Howard et al. (2012) with planets having radii in the range 9–17 $R_\oplus$ considered as a giants. They claim that with 0.41 % their result is consistent with that of Howard et al. (2012). Nevertheless they do not consider two of the main differences between their study and the *Kepler* study. Howard et al. (2012) included only G and K stars and planets with $R_{\mathrm{pl}} = 8 - 9\,R_\oplus$. The two studies should therefore be compared only in their overlap region of G-type stars for which Zhou et al. (2019b) report a giant planet occurrence of 0.7 ± 0.3 %. This occurrence rate increases if they include planets with radii of 8-9 $R_\oplus$ as well. Using the occurrence rates from Petigura et al. (2018) the results overlap within their error bars.

Table 1.1 summarizes the results of those surveys. If the same mass/radius limit is applied throughout the different surveys, the hot Jupiter frequency around FGK stars is in between 0.4 % and 1.6 %.

paper	method	mass/radius range	frequency
Cumming et al. (2008)	RV	$M_{\mathrm{pl}} > 0.3\,\mathrm{M_{Jup}}$	$1.5^{+0.6}_{-0.6}\,\%$
Howard et al. (2010)	RV	$M_{\mathrm{pl}} > 0.31\,\mathrm{M_{Jup}}$	$1.6^{+1.2}_{-0.8}\,\%$
Mayor et al. (2011)	RV	$M_{\mathrm{pl}} > 0.3\,\mathrm{M_{Jup}}$	$0.5^{+0.4}_{-0.4}\,\%$
Wright et al. (2012)	RV	$M_{\mathrm{pl}} > 0.3\,\mathrm{M_{Jup}}$	$1.1^{+0.6}_{-0.6}\,\%$.
Howard et al. (2012)	transit	$R_{\mathrm{pl}} > 8\,\mathrm{R_{\oplus}}$	$0.4^{+0.1}_{-0.1}\,\%$
Fressin et al. (2013)	transit	$R_{\mathrm{pl}} > 6\,\mathrm{R_{\oplus}}$	$0.43^{+0.05}_{-0.05}\,\%$
Petigura et al. (2018)	transit	$R_{\mathrm{pl}} > 8\,\mathrm{R_{\oplus}}$	$0.57^{+0.14}_{-0.12}\,\%$
Deleuil et al. (2018)	transit	$R_{\mathrm{pl}} > 5\,\mathrm{R_{\oplus}}$	$0.98^{+0.26}_{-0.26}\,\%$
Zhou et al. (2019a)	transit	$R_{\mathrm{pl}} > 9\,\mathrm{R_{\oplus}}$	$0.7^{+0.3}_{-0.3}\,\%$
Wittenmyer et al. (2020)	RV	$M_{\mathrm{pl}} > 0.3\,\mathrm{M_{Jup}}$	$1.5^{+3}_{-0.7}\,\%$.

Table 1.1: Close-in giant planet occurrence rate around main-sequence G-type stars

1.2 Close-in giant planets around A stars

Up to now there are still very few detected planets around A stars. This could be due to observational biases or due to a hampered planet formation around this type of stars.

According to the Extrasolar Planets Encyclopedia[2] on `exoplanet.eu`, only 33 planets are observed around stars with temperatures of 7300–10 100 K. None of these discoveries are due to radial velocity surveys, 18 are identified by transiting surveys and 15 by direct imaging. Although radial velocity surveys did not find planets around A stars, RVs are important to confirm the planetary nature of transit signals and ideally also to find the mass of the planet. In table 1.2 I list all known close-in ($P_{\mathrm{pl}} < 10\,\mathrm{d}$) A star planets with some of their properties. Despite the small sample size it is still possible to obtain upper limits on the A star planet population of close-in planets.

[2]last update Aug. 6, 2020

planet name	star SpT	period (d)	mass (M_{Jup})
WASP 33 b (Collier Cameron et al. 2010)	A5	1.22	2.8[1]
KELT-9 b (Gaudi et al. 2017)	A0	1.48	2.9[2]
Kepler 13 A b (Borucki et al. 2011)		1.76	8.0[3]
HATS-70 b (Zhou et al. 2019a)		1.89	12.9
MASCARA-1 b (Talens et al. 2017)	A8	2.15	3.7
HAT-P-57 b (Hartman et al. 2015)	A8V	2.47	1.8[4]
WASP-189 b (Anderson et al. 2018)[5]	A6IV-V	2.72	2.1
HAT-P-70 b (Zhou et al. 2019b)		2.74	6.8[4]
MASCARA-4 b (Dorval et al. 2020)	A3V	2.82	3.1
KELT-17 b (Zhou et al. 2016)	A	3.08	1.3
WASP-178 b (Hellier et al. 2019) or KELT-26 b (Rodríguez Martínez et al. 2019)[5]	A1V	3.34	1.4[4]
KELT-20 b (Lund et al. 2017) or MASCARA-2 b (Talens et al. 2018)	A2V	3.47	3.5[4]
KELT-21 b (Johnson et al. 2018)	A8V	3.61	3.9[4]
TOI-503 b (Šubjak et al. 2020)	A	3.67	53.6
KELT-25 b (Rodríguez Martínez et al. 2019)[5]	A	4.40	21
KELT-19 A b (Siverd et al. 2018)	A8V	4.61	4.1[4]
HAT-P-69 b (Zhou et al. 2019b)		4.79	3.6

Table 1.2: Known close-in planets around A-type stars

[1] Lehmann et al. (2015) [2] Borsa et al. (2019) [3] Shporer et al. (2011)

[4] upper limit

[5] not yet peer reviewed

1.2.1 RV-surveys

RV-surveys are not particularly suitable for the detection of planets around main-sequence A stars. Those stars have very few lines and they are rapid rotators. Rapid rotation leads to broadened and shallow spectral lines. Finding the center of the line, which is used for RV determination, thus is more difficult. I will discuss the challenges of A star radial-velocities in detail in section 2.2.2.

One option to bypass those difficulties is to look at A stars that have evolved from the main-sequence. Giant stars are cooler and rotate more slowly. Therefore, they have more spectral lines which are less broadened. This makes them good targets for precise radial velocities. Reffert et al. (2015) observed around 380 massive evolved stars with masses of $1\,\mathrm{M}_\odot$ to more than $3\,\mathrm{M}_\odot$. They even observed 113 stars that are more massive than $2.5\,\mathrm{M}_\odot$. Their findings suggest that there is an increase of giant planet occurrence rate from stars with $M_\star = 1\,\mathrm{M}_\odot$ ($\approx 2\,\%$) to stars with $M_\star = 2\,\mathrm{M}_\odot$ ($\approx 5\,\%$) in periods up to 840 d. Going to higher masses there is again a decrease in planet frequency. A-type stars typically have masses from $1.5\,\mathrm{M}_\odot$ for WASP-33 (Collier Cameron et al. 2010), $2\,\mathrm{M}_\odot$ for Kepler-13 A (Shporer et al. 2011; Szabó et al. 2011) up to $2.5\,\mathrm{M}_\odot$ for KELT-9 (Gaudi et al. 2017). This would translate to a giant planet occurrence rate of around 15 % for retired A stars from Reffert et al. (2015). Nevertheless, they did not observe a single hot Jupiter. As their sample should be complete for close-in giant planets, this is evidence of a very low hot Jupiter rate of less than 0.3 % around evolved A stars. Johnson et al. (2007) have already concluded that planets around intermediate mass stars typically have orbital periods that translate to semimajor axes larger than 0.8 AU (as compared to 0.1 AU for the very close-in planets).

One explanation for the absence of close-in massive planets around evolved stars could be that host stars engulf their planets as they develop from the main-sequence. This hypothesis is supported by Villaver & Livio (2009) and Villaver et al. (2014) who determined a higher probability of giant planets to be engulfed by their host star. Stephan et al. (2018) predict that only 30 %

of hot Jupiters in binary systems would survive to the white dwarf phase of their host stars. The other explanation is that migration after gas depletion of the protoplanetary disk is less effective around higher mass stars such that the giant planets stay in larger orbits.

Furthermore, some of these discoveries of planets around "retired A stars" have recently been questioned. Hatzes et al. (2018) suggest that oscillatory convective modes could mimic a planetary signal in the RV data of the star γ Draconis. The signal, that seemed to be of planetary nature first, later disappeared but re-appeard with a phase shift. Similar observations were made for Aldebaran (Reichert et al. 2019). Therefore an independent planet frequency analysis of main-sequence A-type stars is useful to constrain planet migration scenarios.

A first such study was done with the HARPS spectrograph (Pepe et al. 2002). It included 108 main-sequence stars from B9V to F9V (Borgniet et al. 2017). The sample was divided into more massive ($M_\star > 1.5\,\mathrm{M}_\odot$) and less massive stars. The challenge of A star RV measurements becomes clear by the fact that even close-in planets which are Saturn like ($M_{\mathrm{pl}} = 0.3\,\mathrm{M}_{\mathrm{Jup}} - 1\,\mathrm{M}_{\mathrm{Jup}}$) have zero detection probability within this survey. For the close-in Jupiter like planets ($M_{\mathrm{pl}} = 1\,\mathrm{M}_{\mathrm{Jup}} - 13\,\mathrm{M}_{\mathrm{Jup}}$) the sample completeness rises to 75 %. With this first study they can constrain the close-in massive planet frequency to less than 10.5 %.

A second attempt to find the true planet occurrence rate was made with the Spectrographe pour l'Observation des Phénomènes des Intérieurs stellaires et des Exoplanètes (SOPHIE) (Bouchy & Sophie Team 2006). The survey covered 125 main-sequence stars with spectral types from A0V to F9V (Borgniet et al. 2019). Both surveys combined give an upper limit on the A star close-in planet occurrence rate of 4.5 %. A comparison to the close-in giant planet occurrence in solar type stars needs tighter upper limits.

1.2.2 Transit-surveys

Transit surveys are much better suited for the challenge of detecting hot Jupiters around A-type stars. The geometric transit probability is $P_{\mathrm{transit}} =$

$\frac{R_\star}{a}$ ($R_\star$ is the stellar radius and a the distance from the host star). Thus, transits are more likely to occur around stars with larger radii and close-in planets are more likely to transit than those with longer periods. On the other hand, the transit depth is determined by the planet-to-star radius ratio. This ratio is smaller around A-type stars which makes the detection of planets more difficult.

Several ground-based and space telescopes are capable of detecting hot Jupiters around A-type stars. The 18 planets known so far were detected with *Kepler* (Borucki et al. 2010), the Kilodegree Extremely Little Telescope (KELT) (Pepper et al. 2007, 2012), the Multi-site All-Sky CAmeRA (MASCARA) (Talens et al. 2017), the Hungarian-made Auto-mated Telescope Network (HATN) and HATS (Bakos et al. 2004, 2013) and the Super Wide Angle Search for Planets (WASP) (Pollacco et al. 2006). There is even a first discovery from the TESS mission – a brown dwarf orbiting an A star (Šubjak et al. 2020).

Of those 18 detections, 17 are close-in or very close-in massive planets. This means that in contrast to what is observed in radial velocity surveys around evolved stars – close-in massive planets do exist around A-type stars. Several of those planets have been confirmed with radial velocity measurements but hundreds of RV-measurements were needed to obtain a mass of those planets, e.g. for WASP-33 (Lehmann et al. 2015). In addition to that, all of these transiting surveys can monitor a large number of stars at the same time. Thus, although the planet fraction is very low they are capable of finding some candidates. Even if the mass cannot be confirmed with RV measurements a transiting planet can count as a discovery after all other options (e.g. eclipsing background binary) are ruled out. Zhou et al. (2019b) presented a first statistical analysis of the TESS survey. With $0.25 \pm 0.11\,\%$ their derived close-in giant planet frequency is smaller around A-type stars than around G-type stars ($0.71 \pm 0.31\,\%$). I present an upper limit of the *Kepler* A-type stars hot Jupiter frequency in this thesis and in Sabotta et al. (2019).

1.2.3 Light curve variation of non-transiting planets

Loeb & Gaudi (2003) suggested that planets could be detected in light curves obtained by space telescopes even if they are non-transiting. Those light curve variations have three different origins:

1. the changing illumination of the planet with respect to the observer (reflection effect),
2. the brightness variations due to the planet's gravitational impact on the star (ellipsoidal variation) and
3. the changing number of photons that arrive on the detector due to the motion of the star towards the observer and away from the observer (Doppler beaming/boosting).

Mazeh & Faigler (2010) and Faigler & Mazeh (2011) modeled these effects with simple equations:

$$\frac{\Delta F_{\mathrm{refl}}(\hat{t})}{\bar{F}} = -A_{\mathrm{refl}} \cos\left(\frac{2\pi}{P_{\mathrm{pl}}}\hat{t}\right), \tag{1.1}$$

$$\frac{\Delta F_{\mathrm{ellip}}(\hat{t})}{\bar{F}} = -A_{\mathrm{ellip}} \cos\left(\frac{2\pi}{P_{\mathrm{pl}}/2}\hat{t}\right) \text{ and} \tag{1.2}$$

$$\frac{\Delta F_{\mathrm{beam}}(\hat{t})}{\bar{F}} = A_{\mathrm{beam}} \sin\left(\frac{2\pi}{P_{\mathrm{pl}}}\hat{t}\right). \tag{1.3}$$

Here $\hat{t} = t - t_{\mathrm{trans}}$ is the time difference with respect to the transit time, $\bar{F}$ is the averaged flux and A_{refl}, A_{ellip} and A_{beam} are the respective amplitudes. The shape of the expected signal in the light curve is shown in figure 1.1.

Several non-transiting planet candidates were already identified using the light curve modulation due to the three effects. E.g. Millholland & Laughlin (2017) identified sixty hot Jupiter candidates in *Kepler* FGK stars and Wong et al. (2020) presented the phase curve variations of three known planets observed with TESS. The method was recently extended to model eccentric orbits as well (Engel et al. 2020) and was proved capable of detecting non-eclipsing eccentric binary stars.

Due to the characteristic shape of the light curve modulations, it could be possible to identify these effects in Generalized Lomb-Scargle Periodograms

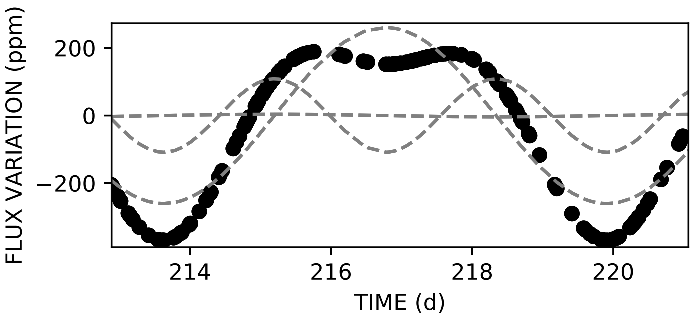

Figure 1.1: Model of ellipsoidal-, beaming- and reflection effect. Dashed lines: single effect, dotted line: combined effects

(GLS-periodograms) (Zechmeister & Kürster 2009). Balona (2013) and Balona (2014) studied the GLS-periodograms of *Kepler* A-type stars. Balona (2014) identified 166 light curves that show an interesting feature in their periodogram. Part of this feature could be interpreted as the signal of a non-transiting hot Jupiter. As other methods did not identify a large fraction of hot Jupiters around this stellar type (see sections above) these planet candidates need follow-up observations. 166 additional planets would significantly increase the A-star planet sample (see figure 1.2). The resulting hot Jupiter frequency would become 8.4 %. Such a large population of inner planets would challenge planet formation theories. The first time this hypothesis was tested was in Sabotta et al. (2019) and the analysis and conclusions are presented in this thesis.

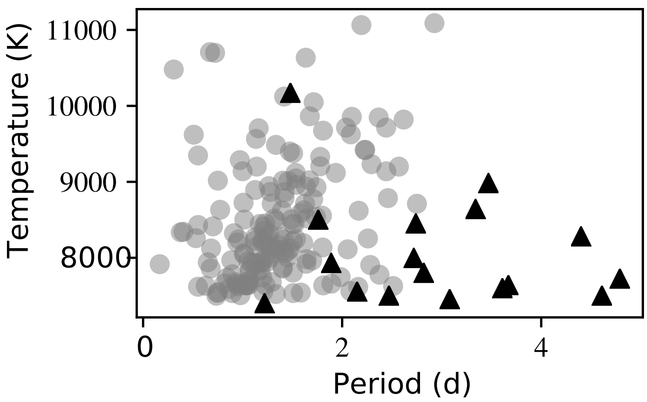

Figure 1.2: Known planets around A stars and suggested planet candidates. Black triangles: detected and confirmed close-in planets of A-type stars from `exoplanet.eu`. Gray circles: additional possible planets according to Balona (2014).

1.3 Small worlds around G-type stars

Small and low mass planets can have various densities, e.g. a system characterized by Guenther et al. (2017) hosts two low mass planets with densities of $13.1\,\mathrm{g\,cm^{-3}}$ and $2\,\mathrm{g\,cm^{-3}}$. Yet, several authors tried to establish a mass-radius relation for small exoplanets, e.g. Wolfgang et al. (2016), Chen et al. (2017), Ning et al. (2018) which could be used to compare transit and radial velocity surveys. Statistically, the planet radius range of $0.8\,\mathrm{R_\oplus}$ to $4\,\mathrm{R_\oplus}$ is equivalent with the mass range of $1\,\mathrm{M_\oplus}$ to $10\,\mathrm{M_\oplus}$.

The *Kepler* space mission observed more than 58 000 G- and K-type stars (Howard et al. 2012). For small planets with radii of $2\,\mathrm{R_\oplus}$ to $4\,\mathrm{R_\oplus}$ Howard et al. (2012) obtained a planet frequency of $2.5\,\%$ for small planets with periods $P_{\mathrm{pl}} < 10\,\mathrm{d}$ and $13\,\%$ for periods $P_{\mathrm{pl}} < 50\,\mathrm{d}$.

The radial velocity results can be better compared to Fressin et al. (2013), who extended the analysis to the radius range from $0.8\,R_\oplus$ to $4\,R_\oplus$. For periods of 0.8 d to 10 d the occurrence rate is 13.4 % and for periods up to 84 d it is as high as 64.9 %. Burke et al. (2015) claimed a small planet frequency of 77 % but they looked at longer periods of 50 d to 300 d.

Large radial velocity surveys measured the small mass planet occurrence rate as well. Howard et al. (2010) published data of 166 G-type stars from the instrument High Resolution Echelle Spectrometer (HIRES) at the Keck observatory. They determined a low mass ($3\,M_\oplus$ to $10\,M_\oplus$) planet occurrence rate of 11.8 % for periods up to 50 d. They did not use a classical injection-and-retrieval experiment (see section 3.2) to obtain their detection limits. For this reason their occurrence rates could be underestimated in the regions with low completeness (Sabotta et al. 2020, in prep.). Also they did not have the sensitivity to detect Earth mass planets. In combination those two effects could be the reason for their relatively low small mass planet frequency.

Mayor et al. (2011) evaluated the data from the HARPS and CORALIE survey with 822 non-active G-type stars in the same mass-period bins as Howard et al. (2010). They retrieved a frequency of 17 % in the same period-mass bin of $3\,M_\oplus$ to $10\,M_\oplus$ and a frequency of 41 % in the bin of $1\,M_\oplus$ to $10\,M_\oplus$. Those results are in agreement with those obtained with *Kepler* considering the fact that their period bin is larger.

1.4 M stars – giant and low mass planets

1.4.1 RV-surveys

M dwarfs are in principle ideal targets for searching for low mass planets with the radial velocity method. Due to the low mass of the host stars, the radial velocity amplitude of a planet with given mass and period increases in comparison to that of a G dwarf host star. On the other hand, M dwarfs are relatively faint and their cooler effective temperature shifts the peak emission to redder wavelengths. Detectors and spectrographs in the past were designed for the detection of planets around solar-like stars. In recent years, the interest increased in refining the planet population around the smaller M dwarfs. Newer spectrographs are designed to target this type of stars, with increased sensitivity of detector and spectrograph towards redder wavelengths, e.g. CARMENES (Quirrenbach et al. 2014), SPIRou (Donati et al. 2018), the Infrared Doppler (IRD) instrument (Kotani et al. 2018), The Habitable-zone Planet Finder (HPF) (Mahadevan et al. 2014), the Near Infra-Red Planet Searcher (NIRPS) (Wildi et al. 2017) and the CRyogenic high-resolution InfraRed Echelle Spectrograph (CRIRES)(Kaeufl et al. 2004).

The first statistical study of M dwarf occurrence rates was done by Endl et al. (2006). Until then only very few M dwarf planets were known. For this reason, they focused on close-in Jupiter like planets for which they determined an upper limit of 1.3 % from their 90 stars sample. The Keck Planet Search studied 110 M dwarfs but they found only two M dwarf planets in their sample (Cumming et al. 2008). They were unable to constrain the overall occurrence rates but they predicted a 3–10 times lower occurrence rate of gas giants for periods of 2000 d or shorter than for FGK stars (1–3 %). A search for companions around only 40 M dwarfs with Ultraviolet and Visual Echelle Spectrograph (UVES) at one of the Very Large Telescope (VLT) telescopes yielded similar results (Zechmeister et al. 2009).

Whereas those early studies had to rely on a very small planet sample, Bonfils et al. (2013) based their statistical analysis on 14 planets and 96 stars observed with HARPS. They also did not find a single close-in Jupiter-like planet but with their sample size they could only constrain the hot Jupiter frequency to be lower than 1 %. This low number could still be consistent with the lower end of the G-type star hot Jupiter rate. For super Earths with masses smaller than $10\,\mathrm{M}_\oplus$ in orbits up to 100 d they found an overall occurrence rate of almost 90 %, but their completeness in this regime is quite low. This high number is consistent with the G-type small planet occurrence rate which is determined in narrower period ranges of up to 84 d. For short periods up to 10 d Bonfils et al. (2013) obtain a small planet rate of 36 %, which is higher than that of 13.4 % found for G-type stars.

The largest and most extensive radial velocity survey of M dwarfs up to date is conducted by the CARMENES consortium (Quirrenbach et al.

2014). They observe over 300 stars and more than 28 planets were already published. A first analysis of a 125 star subsample is provided in this thesis and in Sabotta et al. (2020, in prep.).

1.4.2 Transit-surveys

The meager statistical data from RV-surveys evidently requires transit data for comparison. Transit surveys have the similar challenge of M dwarfs being comparatively cool and faint targets. On the other hand: the planet-to-star radius ratio of Earth-like planets is bigger than that of small planets orbiting solar like stars.

One of the most striking results of Howard et al. (2012) was that *Kepler* predicts an overabundance of small planets around cool stars. The frequency of those planets rises steadily the lower the effective temperature of the star. Mann et al. (2012) removed giant stars from the *Kepler* cool dwarf sample and obtained an even higher planet occurrence rate in the range $2\,R_\oplus$ to $32\,R_\oplus$ than Howard et al. (2012). The results of Howard et al. (2012) were questioned by Fressin et al. (2013) who cleaned the sample from false positives. After this procedure they no longer found a correlation of small planet frequency with stellar effective temperature.

Since then many more analyses of *Kepler* M dwarfs were published which utilized improved stellar or planetary parameters or a refined algorithm to determine detection probabilities. Dressing & Charbonneau (2013) evaluated the light curves of 3897 dwarfs hosting 95 planet candidates in 64 planetary systems. Their small planet ($1\,R_\oplus$ to $4\,R_\oplus$) frequency for periods less than 50 d is 0.9 planets per star. Gaidos et al. (2016) looked at 4216 *Kepler* M dwarfs. They revised the stellar parameters of Dressing & Charbonneau (2013) and typically retrieved larger radii and higher temperatures. From the new stellar sample, they concluded that a typical M dwarf hosts 2.2 planets with radii of $1\,R_\oplus$ to $4\,R_\oplus$ with orbital periods from 1.5 d to 180 d. Mulders et al. (2015) derived a small planet ($1\,R_\oplus$ to $4\,R_\oplus$) occurrence rate around M dwarfs in orbits up to 50 d to be twice that of G-type stars. They also found out that planets with orbital periods of 10 d or less are less frequent than planets with longer periods. Hardegree-Ullman et al. (2019) calculated a planet frequency as a function of stellar type from M3 to M5. Their size limits are $0.5\,\mathrm{R}_\oplus$ to $2.5\,\mathrm{R}_\oplus$. In this regime they determine an overall planet frequency of 1.2 planets per star and a steep increase from earlier to later type stars: 0.86 planets/star for M3 dwarfs to a ratio of 3.1 for M5 dwarfs. Their orbital constraint is 0.5 d to 10 d. A joint analysis of *Kepler* data release 25, Gaia data release 2 and data from 2MASS by Hsu et al. (2020), also confirmed that small planets ($R_p = 0.5\,\mathrm{R}_\oplus - 4\,\mathrm{R}_\oplus$) around M dwarfs are very common. The authors conclude that their results are consistent with every early M dwarf being a planet host.

All in all, the newer *Kepler* analyses give evidence to a very high small planet occurrence rate of at least 0.9 planets per M dwarf. A comparison of those results with radial velocity surveys will remain a challenge. A $0.5\,\mathrm{R}_\oplus$ planet of an M dwarf is still hardly detectable by state-of-the art instruments. Kanodia et al. (2019) investigated the mass-radius-relation of 24 fully characterized M dwarf exoplanets. According to their findings a $0.5\,\mathrm{R}_\oplus$ planet only has a mass of $0.1\,\mathrm{M}_\oplus$ whereas the $1\,\mathrm{R}_\oplus$ to $4\,\mathrm{R}_\oplus$ bin is consistent with the $1\,\mathrm{M}_\oplus$ to $10\,\mathrm{M}_\oplus$ bin of Bonfils et al. (2013) and Sabotta et al. (2020, in prep.). Following the results derived from data of the *Kepler* satellite, a low frequency of low mass planets around M dwarfs in the parameter space reachable by CARMENES and other instruments would be inconsistent with what we know from the *Kepler* transit search.

On the other side of the planet mass range there are the giant planets. Close-in giant planets are very rare around M dwarfs. Up to now not a single one has been detected by radial velocity surveys. Still those planets do exist. Bayliss et al. (2018) discovered a hot Jupiter with a mass of $0.8\,\mathrm{M}_{\mathrm{Jup}}$ around an early M-dwarf with $M_\star = 0.6\,\mathrm{M}_\odot$ with the Next-Generation Transit Survey (NGTS) in a 2.6 d orbit. With their sample of 20 000 early M dwarfs the NGTS team will be able in the future to set tight upper limits on the frequency of hot Jupiters.

Chapter 2

A stars

Balona (2014) published a list of 166 *Kepler* stars that could potentially be planet hosts. My study on the A star planet frequency focuses on this data set. It is a subset out of around 2000 A stars observed by the *Kepler* space mission. In the following I will refer to them as "Balona stars". If those "possible planets" exist, the planet frequency of close-in planets would be around 8.4 %. This is a much higher frequency than that of close-in giant planets around G-type stars (0.4 %–1.5 %).

All of those 166 stars show a peculiar feature in the periodogram of their light curves (see figure 2.1). Some of the stars in the sample are δ Scuti stars that pulsate. Those pulsations are typically within a few hours and therefore they cannot explain the features Balona (2014) found at periods of the order of a few days.

In each of those periodograms there is a broader feature (highlighted in blue in figure 2.1) which could be due to the brightness variation of spots on a differentially rotating star. The discovery of possible magnetic structures on A-type stars is relatively new and made possible by the *Kepler* satellite. A stars are believed to not have a convective zone that could lead to activity signatures similar to those on the Sun. Balona (2013) published a list of *Kepler* A stars that could be rotationally variable based on their periodograms. The amplitudes of those light curve variations are typically only several hundred parts per million. In the meantime Sikora et al. (2020) have

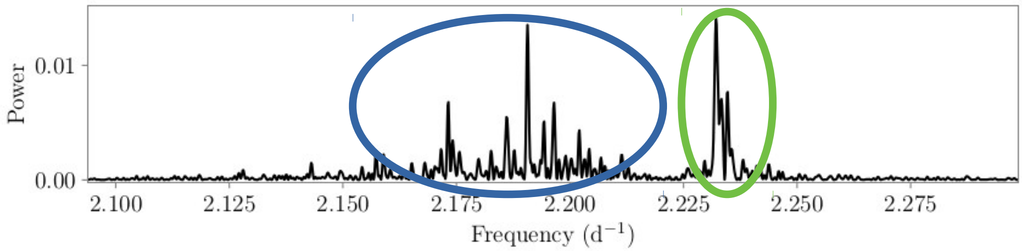

Figure 2.1: Peculiar feature observed by Balona (2014) in 166 *Kepler* light curve periodograms; blue: broad feature, maybe spots and differential rotation; green: sharp feature, maybe planet

obtained spectra of several of those stars and confirm that the variability is liked to the rotation period of more than 10 % of those stars. Böhm et al. (2015) discovered rotational modulation of the A0 standard star Vega. Even if there is evidence for spot like structures on A stars those studies did not test if A stars are rotating differentially. Nevertheless, within this thesis I will focus on the sample of possible planets as its aim is to study the planet frequencies around stars more massive than the Sun.

Very close to this broader feature there is a sharp feature (highlighted in green in figure 2.1). According to Balona (2014) that could be due to the reflection-, beaming and ellipsoidal effects caused by a potential Jupiter mass or brown dwarf companion (see section 1.2.3). Such high mass planets in short period orbits should be detectable with RV measurements although A stars are not very suitable for RV determination.

A high hot Jupiter frequency of 8.4 % around A stars would challenge planet formation theories and contradict results from transiting surveys. The first time this planet-hypothesis was tested was in Sabotta et al. (2019). In the following sections I describe in detail the methods and results presented in this paper.

2.1 Data

One way to test the planet-hypothesis is to search for radial-velocity variations. The planet candidates are of Jupiter size and mass (otherwise the

name other name	α (J2000.0)[1] δ (J2000.0)[1]	SpT[2]	m_v^3	parallax[1] (mas)
KIC 3766112 HD 225570	$19^\mathrm{h}44^\mathrm{m}1.9^\mathrm{s}$ $+38°52'58.5''$	A0	11.3	0.92 ± 0.04
KIC 4944828 HD 225856	$19^\mathrm{h}47^\mathrm{m}47.2^\mathrm{s}$ $+40°0'57.3''$	A5	9.9	2.04 ± 0.03
KIC 7352016 TYC 312925431	$19^\mathrm{h}13^\mathrm{m}14.2^\mathrm{s}$ $+42°54'49.5''$	A9	12.0	1.15 ± 0.02
KIC 7777435 HD 188874	$19^\mathrm{h}55^\mathrm{m}24.4^\mathrm{s}$ $+43°29'48.0''$	A2	10.7	1.39 ± 0.03
KIC 9222948 BD+45 2925	$19^\mathrm{h}34^\mathrm{m}46.7^\mathrm{s}$ $+45°37'11.8''$	A1	10.2	2.25 ± 0.05
KIC 9453452 TYC 354130011	$19^\mathrm{h}4^\mathrm{m}36.1^\mathrm{s}$ $+46°3'37.9''$	A4	10.6	1.57 ± 0.03

Table 2.1: Properties of the six *Kepler* stars observed with OES and TCES (Sabotta et al. 2019)
[1] Taken from Gaia DR2 (Gaia Collaboration et al. 2016, 2018)
[2] Taken from Frasca et al. (2016)
[3] Taken from Høg et al. (2000)

amplitudes of the ellipsoidal, beaming and reflection effect would be too low). Therefore they are good candidates for observations with a 2 m class telescope. Nevertheless it is not possible to observe all 166 "Balona stars" as they are relatively faint. If the hypothesis is true all of them have radial velocity variations due to a planetary companion. Therefore, I randomly chose a subset of six stars for follow-up observations. Their spectral type (SpT) ranges from A0 to A9 and they have magnitudes ranging from $9.9 - 12.0$ mag. All of them are located in the Kepler field in the Cygnus and Lyra constellations. They are visible from central Europe from May to September. Table 2.1 shows an overview of their characteristics.

In addition to that, we observed MASCARA 1 (Talens et al. 2017) as a reference. It is the host of a well known massive and short period planet. I use it as a test if I can detect a planet around an A8 star with radial velocity data from the telescopes in Tautenburg and Ondřejov. With the spectra of MASCARA 1, I also test how many spectra are needed to obtain the mass of such a planet candidate. The RV-amplitude of this star is $400\,\mathrm{ms}^{-1}$ corresponding to a mass of the planet of $2.7\,\mathrm{M_{Jup}}$. The orbital period of the planet MASCARA 1b is 2.15 d.

2.1.1 Kepler space mission

The *Kepler* satellite observed around 156 000 stars during the main mission from 2009 to 2013. Its main goal was to find the frequency of Earth like planets around solar type stars (Borucki et al. 2010). As *Kepler* focused on detecting planets in the habitable zone, they rejected stars earlier than F5 (Borucki 2020). For this reason the satellite observed only around 2000 A-type stars.

Most of the A stars were observed in long-cadence mode. The data was read out every 30 minutes for four years. It is divided in 90-days sections as the spacecraft was rotated every 90 days. The resolution of the observations is 4 arc seconds/pixel.

All *Kepler* data is publicly available from the Mikulski Archive for Space Telescopes at `https://archive.stsci.edu/` (MAST).

2.1.2 TCES - Tautenburg Coudé Échelle Spectrograph

The Alfred-Jensch telescope is located in Tautenburg near the city of Jena, Germany. It has a 2 m primary mirror and an échelle spectrograph called the Tautenburg Coudé Echelle Specrograph (TCES). The maximum resolving power of the TCES is $\lambda/\Delta\lambda = 67\,000$. For this study, I use a wider slit (1 mm slit corresponding to 2" on the sky) to obtain a higher signal-to-noise ratio (S/N) in shorter time, such that the spectral resolution is only $\lambda/\Delta\lambda = 35\,000$. The TCES is equipped with three different cross-dispersing grisms. For this study I use the grism that covers the visual wavelength range from 4700 Å to 7400 Å.

We took 164 spectra of the six "Balona stars" and 113 spectra of MASCARA 1. The typical S/N of the spectra near the H-alpha region around 6562.8 Å ranges from $25 - 120$ (see table 2.2).

star	S/N	star	S/N
KIC 3766112	25 – 45	KIC 7777435	30 – 60
KIC 4944828	40 – 80	KIC 9222948	40 – 75
KIC 7352016	30 – 35	KIC 9453452	30 – 60
MASCARA-1	80 – 120		

Table 2.2: Typical S/N for *Kepler* A star observations from Tautenburg (Sabotta et al. 2019)

2.1.3 OES - Ondřejov Échelle Spectrograph

Observing with telescopes at different sites increases the chance of having good observing conditions for at least one of them. Therefore, we observed the six "Balona stars" with a second similar 2 m telescope. The Perek telescope is located in Ondřejov which is about 40 km south east of Prague in Czech Republic. Observations were conducted with the Ondřejov Echelle Specrograph (OES). It has a resolving power $\lambda/\Delta\lambda = 44\,000$ for a slit width of 0.6 mm (2" on sky). The OES covers a wavelength range of 3870 Å to 7090 Å with several gaps between the orders at redder wavelengths. We describe the instrument in detail in Kabáth et al. (2019).

For this study, a total of 65 spectra of the six "Balona stars" and 38 spectra of MASCARA 1 were taken with the OES. Due to the low S/N of the spectra I co-added several spectra that were taken during the same night. We obtain only relative and not absolute radial velocities. Therefore, if I want to combine RV-values of both instruments, I need to have enough data points from each of them to get a zero point of each data set. Six of the combined spectra were discarded because the observed stars had too few measurements to obtain this offset between the two instruments. Correspondingly, 9 spectra of MASCARA 1 and a total of 18 spectra of three of the "Balona stars" were used in the final analysis. The spectra were reduced by the Ondřejov team. They used the usual data reduction steps (see section 2.2). The typical S/N near the H-alpha region of the spectra ranges from $15 - 30$ (see table 2.3).

star	S/N	star	S/N
KIC 4944828	20 – 30	KIC 9222948	20 – 40
KIC 9453452	15	MASCARA-1	35

Table 2.3: Typical S/N for *Kepler* A star observations from Ondřejov (Sabotta et al. 2019)

2.2 Method

2.2.1 The Tautenburg Spectroscopy Pipeline

To achieve homogeneous reduction results it is useful to perform the data reduction steps with an automated pipeline. I wrote the Tautenburg Spectroscopy Pipeline (τ-spline) and included a graphical user interface for ease of use.

The pipeline performs the usual data reduction steps: bias-subtraction, flat-fielding, removal of cosmic rays, scattered light subtraction, extraction, wavelength calibration and normalization. It makes use of standard IRAF[1] and PyRaf routines[2] and the cosmic ray code by Malte Tewes based on the method by Van Dokkum (2001). The pipeline is designed for the Tautenburg Coudé Échelle spectrograph. It is publicly available in my *github* repository: `https://github.com/ssabotta/tau-spline`.

In order to test if the pipeline is capable of producing well calibrated spectra for the RV-determination, I have reduced spectra of 51 Peg that were obtained during the 3rd Tautenburg observing school. The program RADIAL extracted the RVs using iodine absorption lines as a reference. This program follows the methods described in Valenti et al. (1995) and Butler et al. (1996) and was successfully used e.g. in Cochran & Hatzes (1994) and Cochran et al. (1997). 51 Peg b has a period of $P = 4.23\,\mathrm{d}$ and the RV-semiamplitude is $K = (56 \pm 1)\,\mathrm{ms}^{-1}$ (e.g. Marcy et al. 1997). We have obtained 32 RV-values and I can confirm those literature values. For comparison: Marcy et al. (1997) used a total of 110 spectra. My orbital solution has a relative error of around 2 % for the period and 15 % for the semi-

[1] IRAF is distributed by the National Optical Astronomy Observatories, which are operated by the Association of Universities for Research in Astronomy, Inc., under cooperative agreement with the National Science Foundation.

[2] PyRaf is a product of the Space Telescope Science Institute, which is operated by AURA for NASA

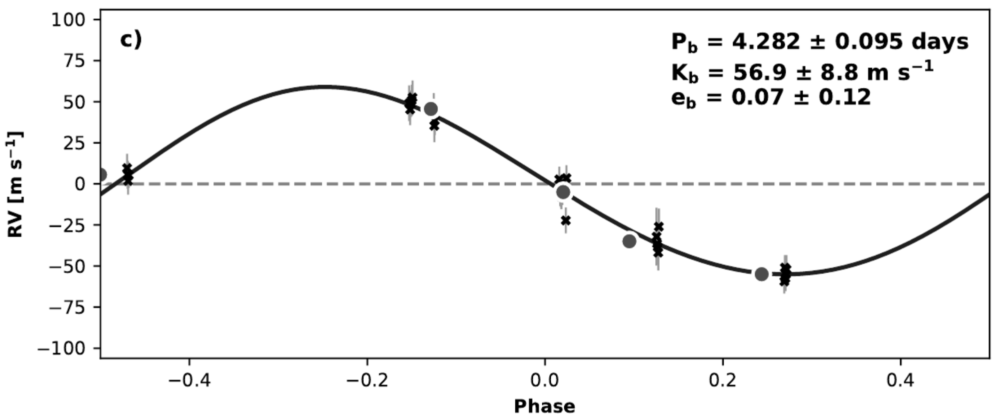

Figure 2.2: RV-curve of 51 Peg b (data from the TLS observing school). Crosses: individual RVs; big dots: binned RVs

amplitude (see figure 2.2). This proves that the pipeline is capable of producing well calibrated spectra for the RV-determination.

2.2.2 Radial velocities of A stars

Expected RV errors

Obtaining RVs of A stars is a challenging endeavor. The RV-precision depends heavily on the number of lines that can be used for determining the Doppler shift in our spectra. Also blended spectral lines or a low signal to noise that hides several lines can decrease the precision of the measurements. A high resolution of the spectrograph increases the precision of the RVs as it improves the sampling of the spectral lines. A high resolution spectrum requires more space on the Charge-coupled device (CCD) than a spectrum with a lower resolution. Therefore on a CCD with a given size there is an optimum of resolution and bandwidth that gives the best RV precision. With the error functions published in Hatzes (2016) and Hatzes (2019) I can get an estimate of the RV-error of the TCES A star spectra:

$$\frac{\sigma}{\mathrm{ms}^{-1}} = C(S/N)^{-1}R^{-3/2}B^{-1/2}(v\sin i/2)f(\mathrm{SpT}). \tag{2.1}$$

In this function there are the instrument dependent factors C – instrument specific coefficient, $R^{-3/2}$ – resolution of the spectrograph, $B^{-1/2}$ – bandwidth of the spectrograph in Angstroms and the observation dependent factor $(S/N)^{-1}$ –

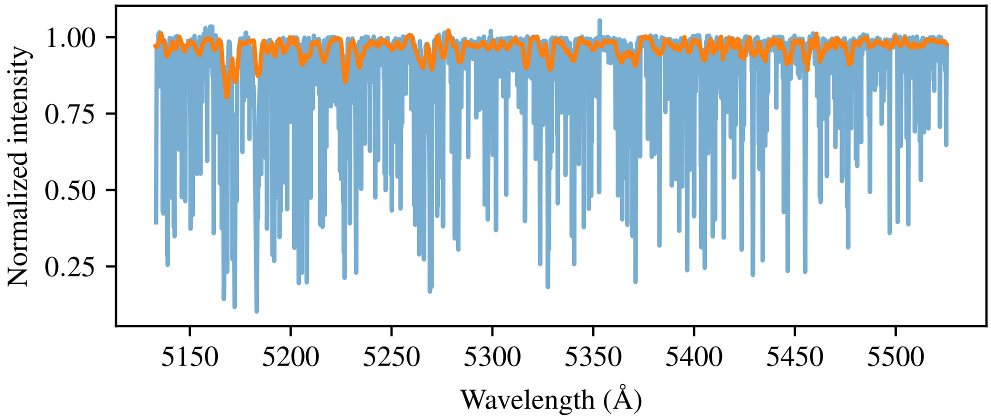

Figure 2.3: Comparison of A star and G star spectra: G-type star in blue, A-type star in orange

signal to noise ratio – and the star dependent factors $v \sin i/2$ – rotational velocity and $f(\mathrm{SpT})$ – spectral type factor.

The SpT dependent factor $f(\mathrm{SpT})$ takes into account that A-type stars have fewer spectral lines than G-type stars. The rotational velocity is included in the function because of rotational broadening. Figure 2.3 shows examples of A and G star spectra. The line number and line width for A-type stars are very different from those of G-type stars.

For a quantitative estimate I take the RV-errors of the 51 Peg example. These are calculated by RADIAL with the standard deviation of the RVs in the different chunks: $\sigma_{51\,\mathrm{Peg}} = 9\,\mathrm{ms}^{-1}$. I use the same spectrograph and telescope for the A star measurements. Therefore, equation 2.1 becomes:

$$\frac{\sigma}{\mathrm{ms}^{-1}} = \frac{(S/N)_{51\,\mathrm{Peg}}}{(S/N)_{\mathrm{A\ star}}} \frac{(v \sin i)_{\mathrm{A\ star}}}{(v \sin i)_{51\,\mathrm{Peg}}} \frac{f(\mathrm{SpT})_{\mathrm{A\ star}}}{f(\mathrm{SpT})_{51\,\mathrm{Peg}}} \sigma_{51\,\mathrm{Peg}} \tag{2.2}$$

- The typical signal to noise of the 51 Peg spectra is 100 and that of our A star measurements is around 50.
- The $(v \sin i)_{\mathrm{A\ star}}$ of a typical A-type star is $\approx 80\,\mathrm{kms}^{-1}$ (Hatzes 2019).
- The Rotational Period of 51 Peg is 22 d (Simpson et al. 2010) and its radius is $R_\star = 1.2 R_\odot$ (Fuhrmann et al. 1997). Therefore, the $(v \sin i)_{51\,\mathrm{Peg}} \approx 2.8\,\mathrm{kms}^{-1}$.

- I calculate $f(\mathrm{SpT})$ with the formula from (Hatzes 2019):

$$f(\mathrm{SpT}) = f(T_{\mathrm{eff}}) = 0.16e^{1.79\left(\frac{T_{\mathrm{eff}}}{5000}\right)}. \tag{2.3}$$

- The effective temperature of 51 Peg is 5793 K (Fuhrmann et al. 1997) such that $f(\mathrm{SpT})_{51\ \mathrm{Peg}} \approx 1.3$.
- The typical A star effective temperature is 8000 K such that $f(\mathrm{SpT})_{\mathrm{A\ star}} \approx 2.8$.

Accordingly, the expected RV-error of the A star spectra is:

$$\frac{\sigma}{\mathrm{ms}^{-1}} = 2 \cdot 28.5 \cdot 2.2 \cdot 9\,\mathrm{ms}^{-1} \approx 1100\,\mathrm{ms}^{-1} \tag{2.4}$$

The cross-correlation method

The RVs are obtained with the cross-correlation method. I do not use the iodine cells in Tautenburg and Ondřejov as a reference, because the RV precision is not limited by the instrumental drift but by the low number of spectral lines of the stars and rotational broadening. The S/N is another limiting factor and the iodine cell takes away flux from the specta.

As a template for the cross-correlation I use the stellar spectra themselves. Following the example set by Anglada-Escudé & Butler (2012), the template-construction is an iterative process. First I determine the RV-shift of each spectrum based on the highest S/N spectrum as a template. As a next step I shift all spectra with this RV-shift such that all lines overlap. The final template is then a combination of all those shifted spectra. It has a much higher signal to noise than the single stellar spectra.

The cross-correlation function can be influenced by the telluric lines, which in A stars are much narrower than the stellar lines. I therefore avoided those échelle orders that are contaminated by telluric lines. Additionally, I excluded orders with no visible lines in the template spectrum. From the useful orders I took only the middle part with the highest S/N.

The telluric method

The instrumental drift of the TCES within one night is roughly $200\,\mathrm{ms}^{-1}$ as measured using a time series of white light (flat-field) observations taken through the

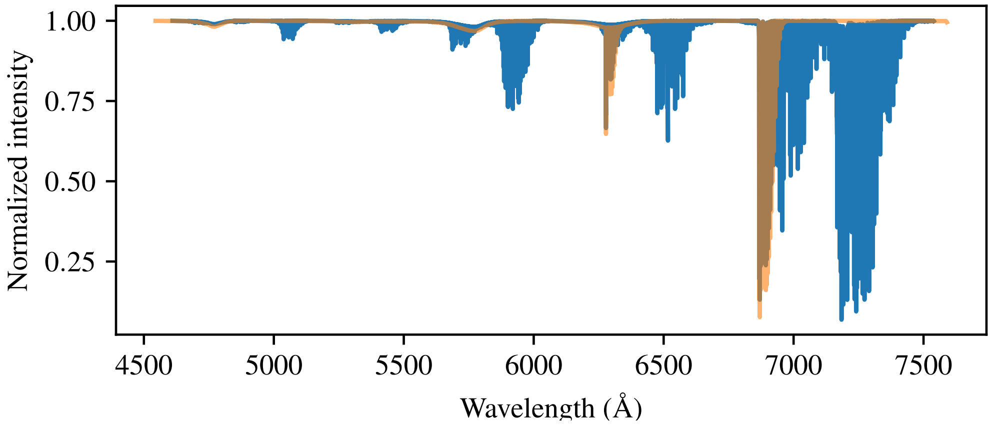

Figure 2.4: Telluric template with telluric lines from O_2 and H_2O. Blue: O_2 and H_2O, orange: only O_2

iodine cell (Hatzes 2019). I reduced the errors due to the instrumental drifts by correcting my RVs with the telluric shift as originally suggested by Griffin (1973). The telluric lines (mainly O_2 and H_2O) in our spectra are fixed to certain wavelengths. Therefore, I can measure the wavelength shift of the telluric lines and trace down the instrumental instabilities. I extracted the telluric lines with the ESO Program MOLECFIT (Smette et al. 2015; Kausch et al. 2015) and used cross-correlation to obtain the corresponding RV-shifts. Figure 2.4 shows the telluric O_2 and H_2O lines in Tautenburg. Figueira et al. (2010) determined a RV stability of $10\,\mathrm{ms}^{-1}$ of the O_2 lines. Lehmann et al. (2013) claim that with the TCES we can typically reach an accuracy of $50\,\mathrm{ms}^{-1}$ with this method. In Figueira et al. (2010) they did not analyze the H_2O lines. I took only the O_2 lines of the telluric reference for the determination of the instrumental drifts. The line depth of the H_2O lines is highly variable in comparison to the O_2 lines because of the changing water content in the atmosphere at both telescope sites. The O_2 lines from 6275 - 6325 Å served as reference for the spectra of the OES and the lines from 6865 - 6945 Å served as reference for the spectra of the TCES.

2.2.3 Transit search and modeling

The geometrical transit probability is $P_{\mathrm{transit}} = \frac{R_\star}{a}$ (where a is the distance of the planet to its host star). From Balona (2014) we know that the planet candidates on average have a semi-major axis of $a \approx 0.02\,\mathrm{AU}$. The average stellar radius

star	Period (d)	R_{star} ($R_\odot$)	Transit depth if $R_p \approx R_{Jup}$
KIC 3766112	0.45 d	2.320[1]	0.19 %
KIC 4944828	0.93 d	2.457[1]	0.17 %
KIC 7352016	0.93 d	2.073[1]	0.23 %
KIC 7777435	0.68 d	2.572[1]	0.15 %
KIC 9222948	1.29 d	1.821[1]	0.30 %
KIC 9453452	0.61 d	2.166[1]	0.21 %

Table 2.4: Transit depths of giant planets in close orbits of *Kepler* A stars (Sabotta et al. 2019)
[1] Taken from Berger et al. (2018)

in the Balona (2014) sample is $R_\star \approx 2.3\,R_\odot$. The transit depth of a Jupiter-size planet is therefore 0.2 %. The individual transit probability of the 166 stars is around 53 %. The probability that none of the possible planets is transiting is as low as 10^{-55}. Hence, I scanned the sample for transiting events in collaboration with Judith Korth and Sascha Grziwa in Cologne. We used their transit finding pipeline EXOTRANS (Grziwa et al. 2012; Korth et al. 2019).

Balona (2014) claimed that the transits could be hidden in the data. This could happen as the transits of very close-in planets cover a large part of the planetary orbit. To double-check if this could happen to the transit finding algorithm, I conducted a blind test. I merged the *Kepler* light curves with a transit model. I used the transit model code by Parviainen (2015) with the limb darkening coefficients in Sing (2010). The used transit depths are listed in table 2.4. We searched for those model transits again with EXOTRANS.

2.2.4 Transit simulation

Among the 2000 A-type stars observed with *Kepler*, the *Kepler*-pipeline found only four transiting planets (see table 2.5). Only one of them, namely Kepler-13 A b, can be classified as hot Jupiter.

A simulation can be used to obtain an estimate of the underlying planet frequency that would lead to only one transiting hot Jupiter among 2000 observed stars. The number of planets in each simulation run is drawn from a binomial

planet	orbital period	radius
Kepler-13 A b	1.76 d	2.042 R_{Jup}
Kepler-340 b	22.9 d	3.36 $R_{\oplus}$
Kepler-340 c	14.8 d	2.49 $R_{\oplus}$
Kepler-1115 b	23.5 d	1.7 $R_{\oplus}$

Table 2.5: *Kepler* discoveries of transiting planets around A type stars

distribution:

$$P_{\mathrm{k,planets}}(k) = \binom{2000}{k} f_{\mathrm{planet}}^{k}(1 - f_{\mathrm{planet}})^{(2000-k)}. \tag{2.5}$$

The geometric transit probability $P_{\mathrm{transit}} = \frac{R_\star}{a}$ can be calculated from the actual radii of the Kepler A stars published in Berger et al. (2018). For the purpose of the simulation, the semimajor axis a is randomly distributed from 0.01–0.1 AU.

For a particular planet–distance combination, I count a transit with the probability P_{transit}. I ran 7000 simulations in this way to find out how many transits are expected in the *Kepler* sample of A stars for various planet frequencies.

2.3 Results

2.3.1 RV results

With the Tautenburg spectroscopy pipeline and cross-correlation I obtained RV time series for all six sample stars. Additionally, I used spectra of MASCARA 1 (Talens et al. 2017) as a general test if I can get a mass estimate of an A star with my analysis method.

RV errors of Tautenburg and Ondřejov spectra

From the cross-correlation with my self-template I obtain RVs for each of the spectral orders. I remove outliers with a sigma-clipping algorithm. The median of the remaining RVs is the RV value and the standard deviation provides the corresponding RV-error. The average RV-error of the MASCARA 1 spectra is 990 $\mathrm{m\,s^{-1}}$ which is very close to the expected error. All RVs and corresponding errors as published in Sabotta et al. (2019) are documented in the appendix.

RV curves

I have analysed the RV curves with the Radial Velocity Modeling Toolkit – RadVel – by Fulton et al. (2018). As a first step a maximum log-likelihood fit was performed. This fit can be used as an initial fit for a Markov-Chain Monte Carlo (MCMC) exploration. The result of the MCMC test can be used as error of the K-amplitude and period of the planet candidate.

The fit requires initial masses, periods and eccentricities. MASCARA 1 hosts a transiting planet with a well-known period (Talens et al. 2017). The periods of the planet candidates around the six *Kepler* stars are given by Balona (2014). I fix the eccentricities to zero because most close-in Jupiters are in circular orbits due to the rapid tidal circulation of any eccentric orbits.

For MASCARA 1 there are enough RV-measurements to perform an MCMC analysis. It results in a K-amplitude of $K = (390 \pm 130)\,\mathrm{ms}^{-1}$ which is consistent with the literature value: $K = (400 \pm 100)\,\mathrm{ms}^{-1}$ (Talens et al. 2017). For the "Balona stars" I have obtained only 30 RV-values to determine the upper limits. This number of RV-values is enough to obtain upper limits in the planetary mass regime. Therefore, I have also checked the outcome of the RV-analysis for the case of having only 30 spectra of MASCARA 1. I randomly deleted some of the RV-values until only 30 RVs were left. A maximum log-likelihood fit results in a K-amplitude of $570\,\mathrm{ms}^{-1}$. Therefore, the method of using a maximum log-likelihood fit for obtaining the one σ upper limit is plausible. Both RV-curves are shown in figure 2.5.

The fits of the six RV-curves of the *Kepler* stars are displayed in figures 2.6 and 2.7. K-amplitudes of the log-likelihood fits range from $(150 - 450)\,\mathrm{ms}^{-1}$. The MCMC analysis of all six of them leads to a most probable K-amplitude of zero.

Upper limits for the companion masses

The maximum log-likelihood fit to the RV-curves serves as the one σ upper limit for the K-amplitude. The companion mass is given by:

$$\left(\frac{M_{\mathrm{pl}}\sin i}{M_{\mathrm{Jup}}}\right) = 28.4^{-1}\left(\frac{K}{\mathrm{ms}^{-1}}\right)\left(\frac{P}{1\,\mathrm{yr}}\right)^{1/3}\left(\frac{M_\star}{\mathrm{M}_\odot}\right)^{2/3} \tag{2.6}$$

I show upper limits with 99 % confidence and one σ confidence. They range from $3.8\,\mathrm{M_{Jup}}$ to $7.3\,\mathrm{M_{Jup}}$ or $1.5\,\mathrm{M_{Jup}}$ to $2.9\,\mathrm{M_{Jup}}$ respectively (see table 2.6). All

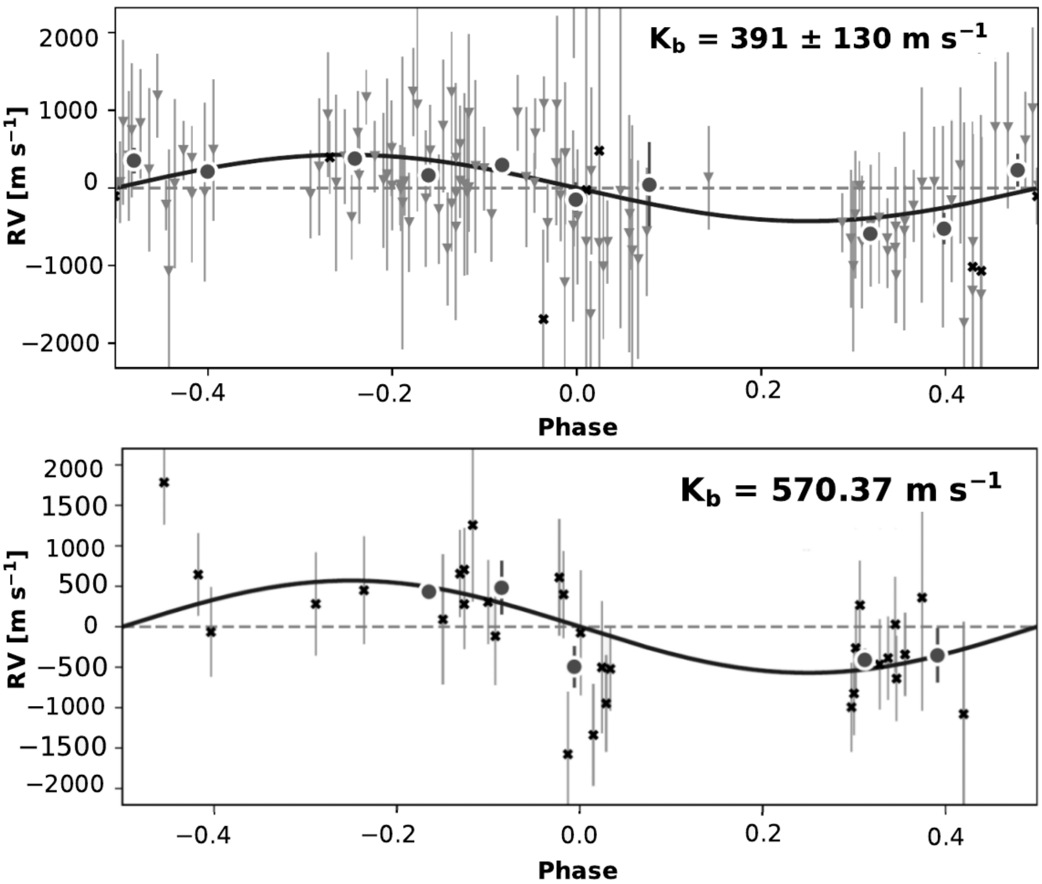

Figure 2.5: Upper panel: RV curve for MASCARA-1 b. X: the Ondřejov values; Triangles: the Tautenburg values; Circles: Binned radial velocities; lower panel: Example of upper limit for MASCARA-1 b with only 30 data points from Tautenburg, black curve is the maximum-likelihood fit (Sabotta et al. 2019)

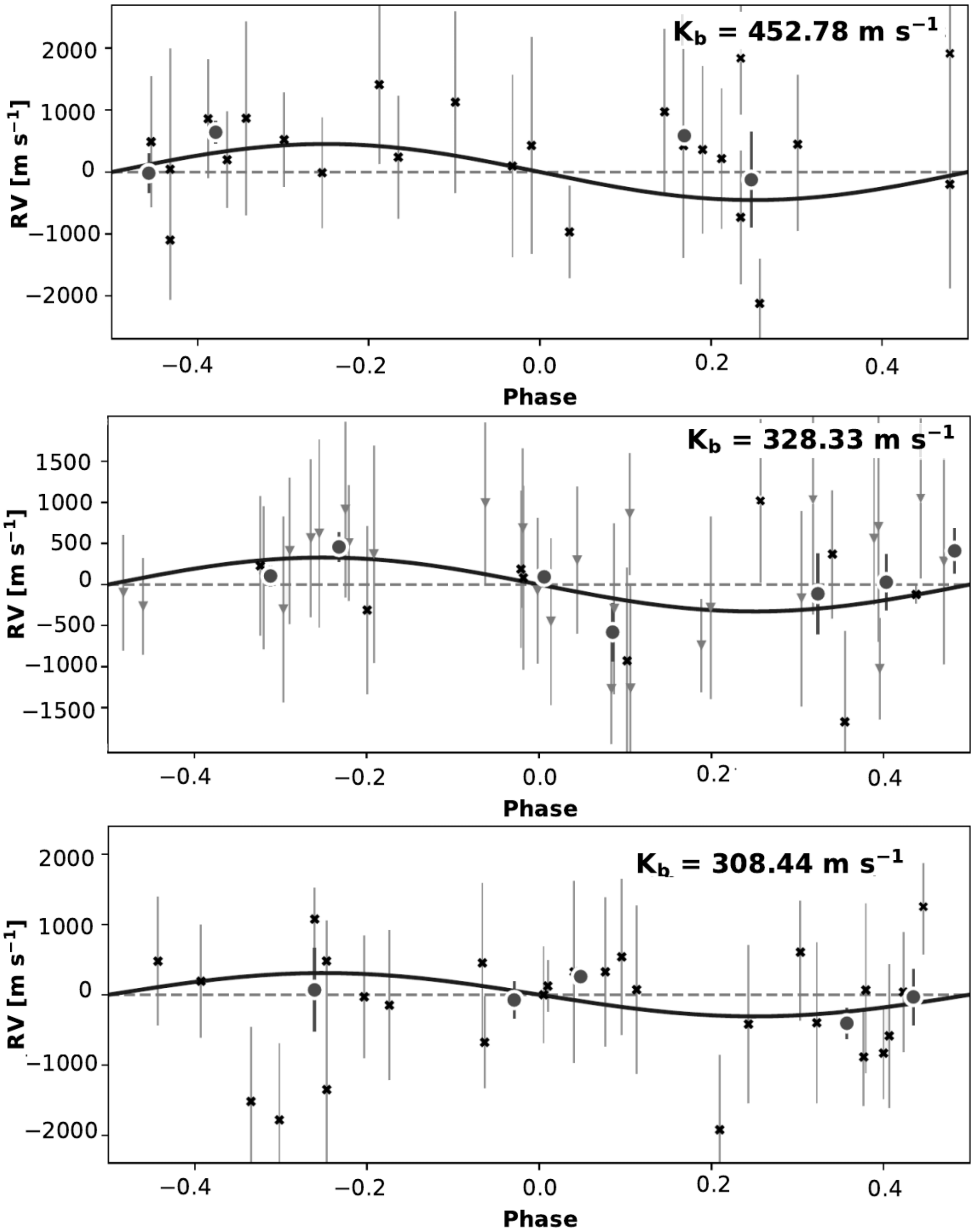

Figure 2.6: RV-curves of (1) KIC 3766112, (2) KIC 4944828, (3) KIC 7352016. A simple maximum log-likelihood fit gives the $1\,\sigma$ upper limit. The most probable solution after an MCMC exploration is a K-amplitude of zero (Sabotta et al. 2019).

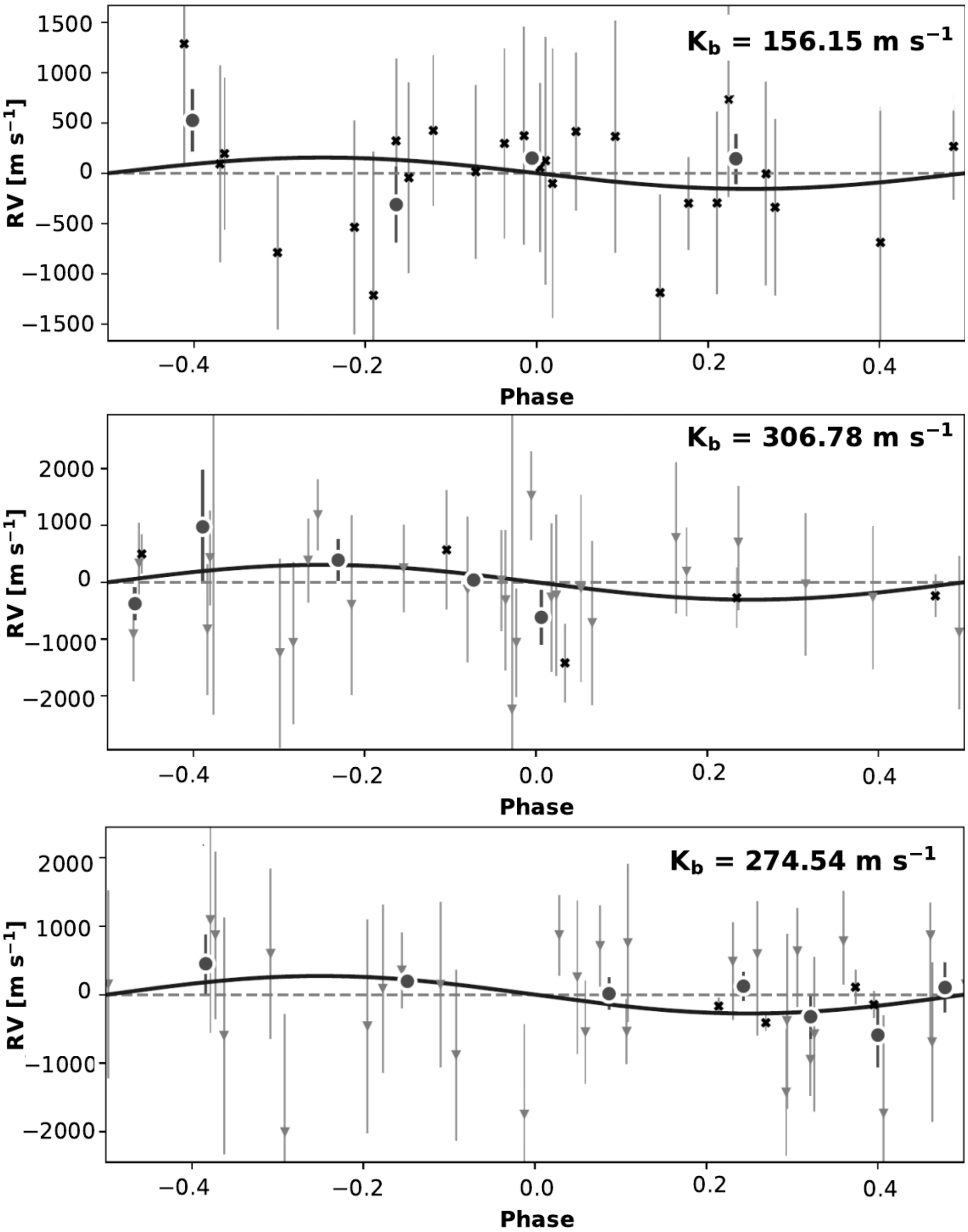

Figure 2.7: RV-curves of (1) KIC 7777535, (2) KIC 9222948, (3) KIC 9453452. A simple maximum log-likelihood fit gives the $1\,\sigma$ upper limit. The most probable solution after an MCMC exploration is a K-amplitude of zero (Sabotta et al. 2019).

star	star mass	max. K	period	upper limit 99 %	upper limit 1 σ
	($M_\odot$)	(ms^{-1})	(d)	(M_{Jup})	(M_{Jup})
KIC 3766112	2.2	450	0.45	7.3	2.9
KIC 4944828	2.0	330	0.93	6.3	2.5
KIC 7352016	3.0	290	0.93	7.3	2.9
KIC 7777435	2.1	210	0.68	3.8	1.5
KIC 9222948	2.3	310	1.29	7.3	2.9
KIC 9453452	2.1	270	0.61	4.5	1.9

Table 2.6: Mass upper limits of possible companions to *Kepler* A stars (Sabotta et al. 2019)

upper limits lie in the planetary mass regime.

2.3.2 Results of the transit search and modeling

In addition to the results from RV-determination, I have searched the data for transit signals. I conducted a blind test to prove that we would find a transit of a Jupiter-like planet in a close orbit around an A-type star. Figure 2.8 shows a typical example of a transit model. The transit does cover a large part of the orbit but due to the high transit depth it is still clearly visible in the light curve and GLS-periodogram. The transit finding algorithm EXOTRANS correspondingly finds all the modeled transits.

We used the algorithm on the actual data of the 166 "Balona stars" and could not find any transits of Jupiter-like planets. Several smaller signals were detected but they are most likely due to activity. Also they were much too small for a transiting Jupiter-sized planet.

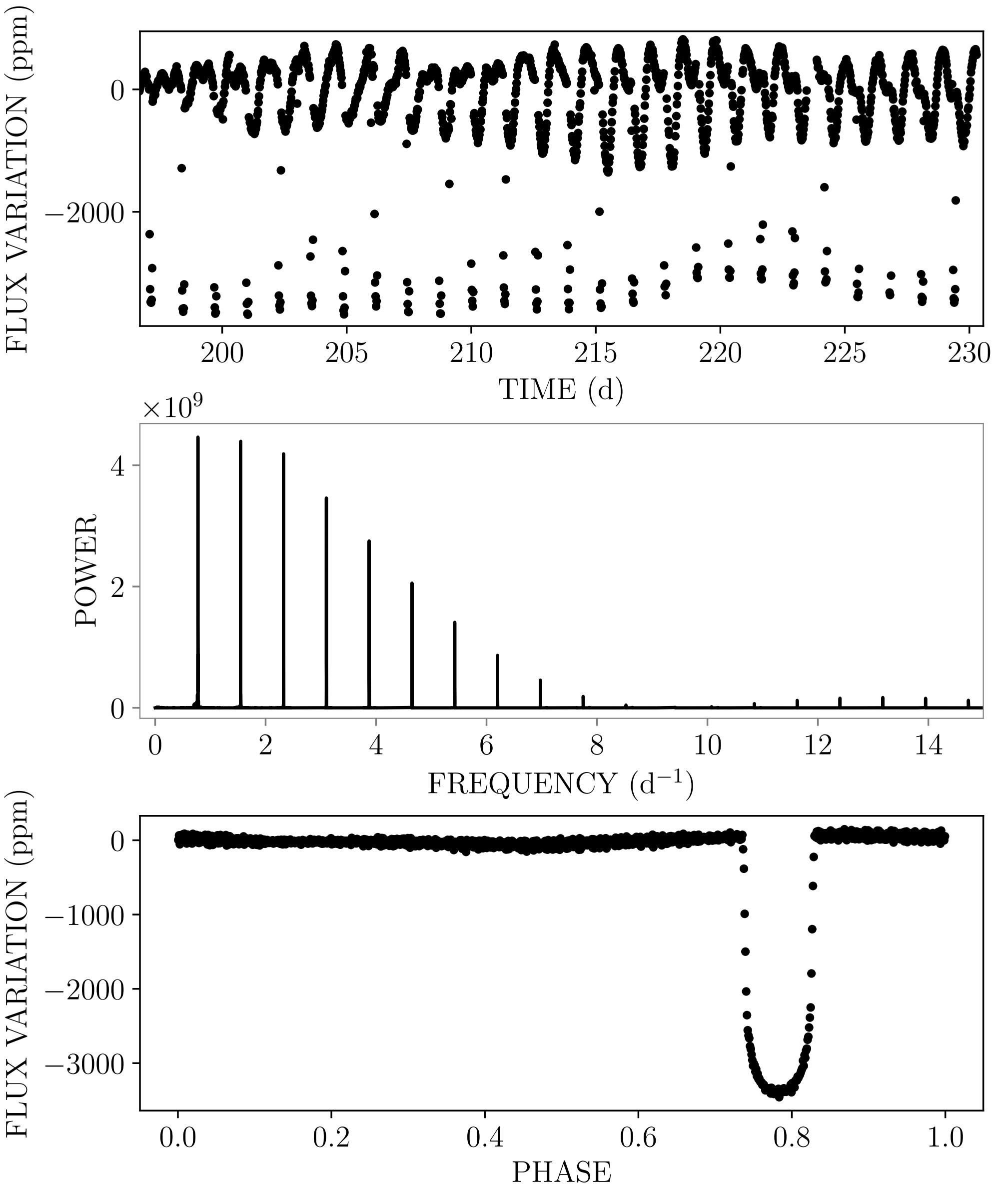

Figure 2.8: Transit model of a Jupiter size object in *Kepler* light curve of KIC 9222948; top panel: 30 d section of the time series, middle panel: GLS-periodogram of the light curve, lower panel: phase-folded and binned light curve (Sabotta et al. 2019)

2.3.3 Results of the transit simulation

I ran two transit simulations with close-in giant planet frequencies 0.15 % and 1.2 % from planet formation theories (see Sabotta et al. 2019). I also ran one simulation with the planet frequency of 8.4 % as suggested by Balona (2014). The last one I ran to find the upper limit corresponding to exactly one transit with $2\,\sigma$ confidence.

For the $2\,\sigma$ error, 95 % of the simulation outcomes have to lie in this interval around the median value; for the $1\,\sigma$ error 68 % of the simulation outcomes have to fulfill this criterion.

The simulation results were the following (see figures 2.9 and 2.10):

1. The first simulation used an underlying planet frequency of 0.15 %. Within the $2\,\sigma$ interval 0-3 transits would have occurred and 0-2 transits within the $1\,\sigma$ interval.
2. The second simulation predicted 4-15 transits (two σ) or 6-12 transits (one σ) for the 1.2 % planet frequency.
3. The third simulation used a planet frequency of 8.4 % as suggested by Balona (2014). The lowest number of transits within the two σ interval would be 49 transits.
4. For the fourth simulation I slowly increased the planet frequency until in the two σ interval at least two transits are expected. This resulted in an upper limit for the underlying planet frequency in the *Kepler* A star sample of 0.75 %.

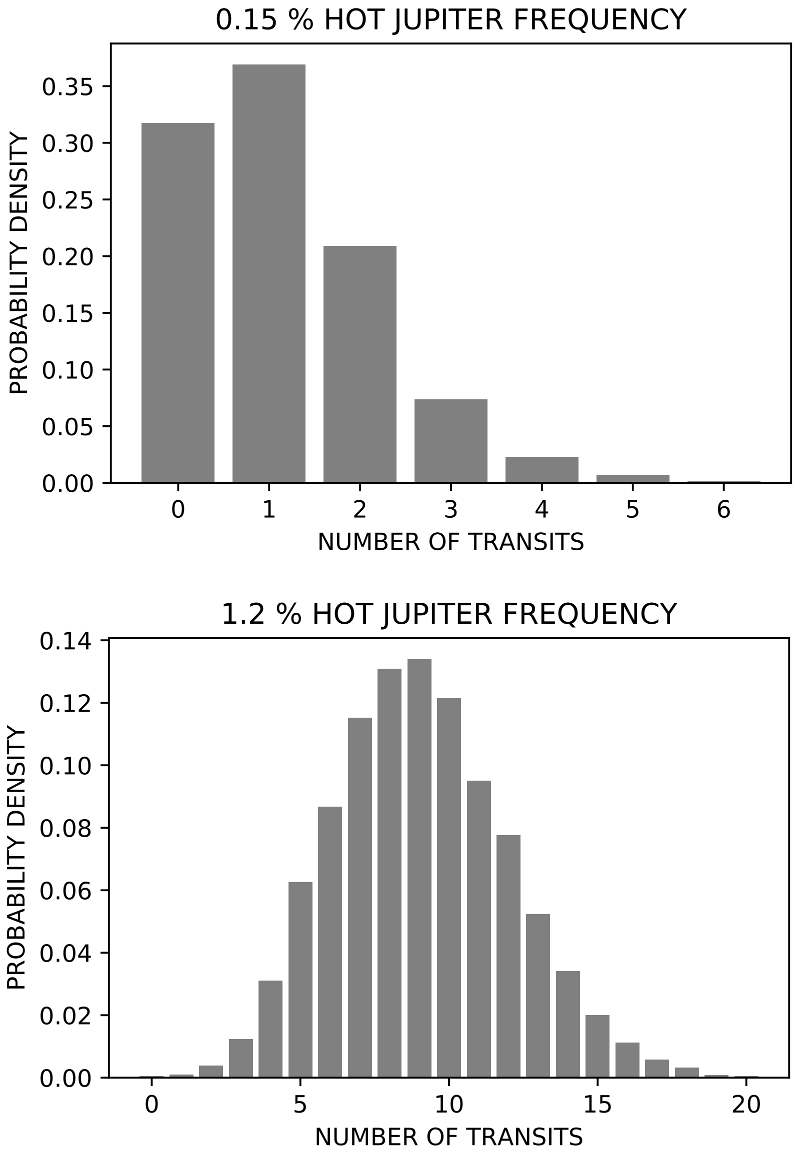

Figure 2.9: Transiting objects expected for different planet frequencies with $2\,\sigma$; Part 1: 0.15 per cent 0-3 transits ($1\,\sigma$: 0-2 transits), 1.2 per cent 4-15 transits ($1\,\sigma$: 6-12 transits) (Sabotta et al. 2019)

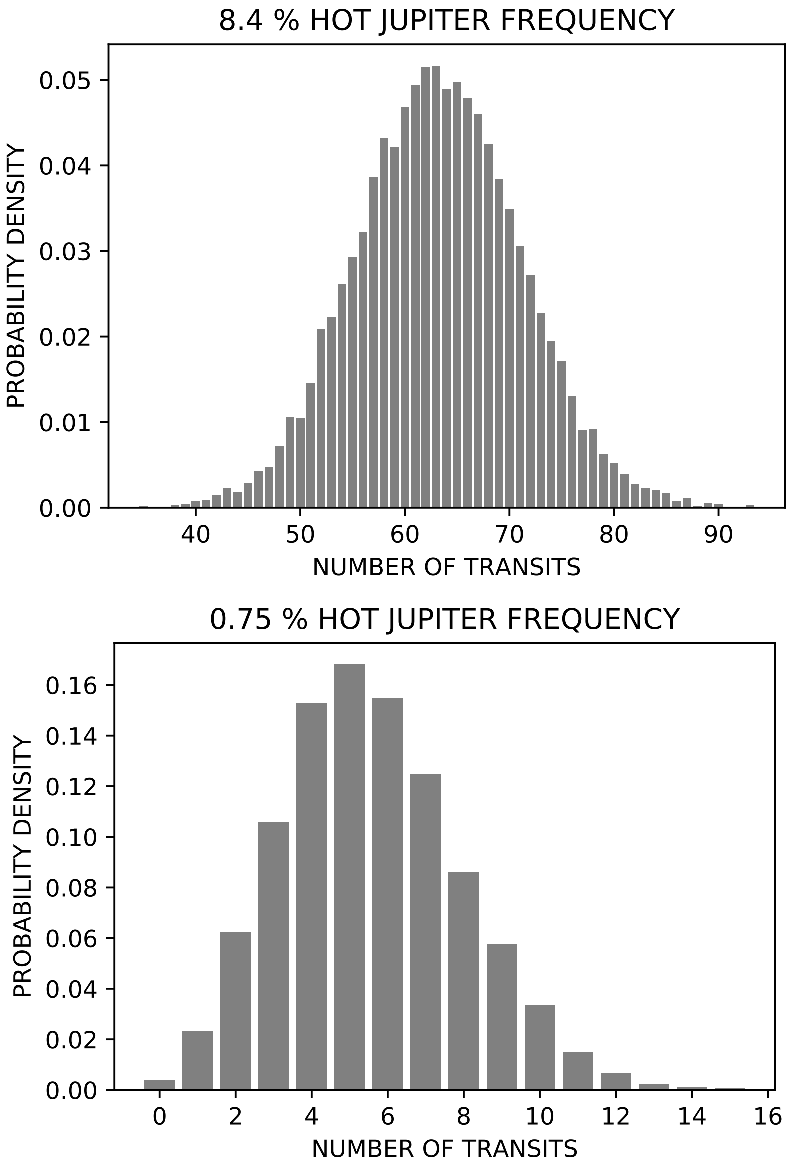

Figure 2.10: Transiting objects expected for different planet frequencies with $2\,\sigma$; Part 2: 8.4 per cent 49-78 transits ($1\,\sigma$: 55-71 transits), 0.75 per cent 2-10 transits ($1\,\sigma$: 3-8 transits) (Sabotta et al. 2019)

2.4 Discussion

Balona (2014) claimed that 8.4 % of the *Kepler* main-sequence A-type stars are hosts to a massive close-in planet with a period of only several days. A frequency of 8.4 % would indicate a much higher frequency of such planets around A-type stars than around G-type stars (see section 1.1). The aim of the analysis above was to test this hypothesis of a very high hot Jupiter frequency around A-type stars.

One valid explanation that would contradict the hot Jupiter hypothesis is that the peculiar periodicities observed by Balona (2013) are caused by non-eclipsing stellar companions. I measured upper limits for six of the "Balona stars". All upper limits indicate that the mass of a possible companion has to be in the planetary regime. This is supported by the fact that there is only one eclipsing binary, namely KIC 6147122, flagged by the *Kepler* pipeline in the sample of 166 stars. Its orbital period is 15.5 d, which is longer than the periods found by Balona (2014).

The question remains if the *Kepler* pipeline could have missed a large fraction of transiting hot Jupiters around A stars. Transits occur periodically. If they cover a large enough fraction of the planetary orbit they could be obvious in the periodogram. Therefore, I have analyzed the periodogram of the light curve of Kepler-13 A which is the only *Kepler* A star with a known planet. The orbital period and the aliases of this period clearly show up in the periodogram with a very high significance (see figure 2.11). I did the same analysis on my artificial blind test data with the same result (see figure 2.8). I conclude that it is highly unlikely that the *Kepler* pipeline, Balona (2014) or the EXOTRANS pipeline would have missed such a transit event.

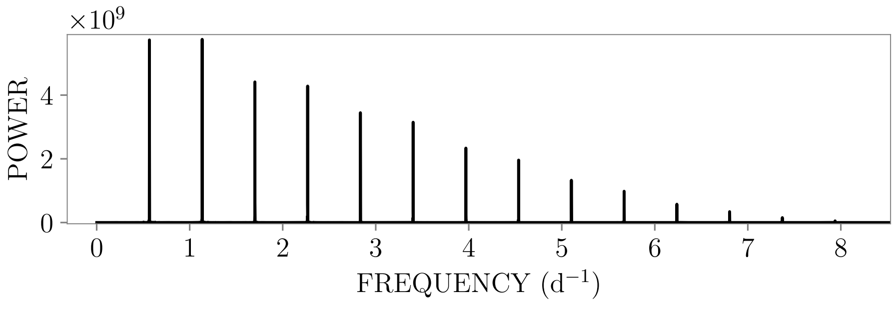

Figure 2.11: Periodogram of Kepler-13 A b (Sabotta et al. 2019)

Even if one or two transits were missed: a close-in planet fraction as high as 8.4 % would still be excluded by my results. At this planet fraction at least 49 transiting planets are expected with a $2\,\sigma$ significance. My results provide more evidence for a very low number of close-in massive planets around A stars. The upper limit I found is as low as 0.75 % and the most probable frequency is around 0.15 %.

What we know from other RV or transit surveys (more in section 1.2) is that a close-in giant planet fraction of more than 4.5 % is deemed unlikely as well. In comparison to the G star hot Jupiter occurrence rate (0.4 %–1.5 %), my results indicate a lower hot Jupiter frequency ($0.15^{+0.60}_{-0.15}$ %) around main-sequence A stars.

This study clearly shows that the planet hypothesis is most likely not the origin for the peculiar features in 166 periodograms published by Balona (2014). In the meantime Saio et al. (2018) proposed a different explanation for them. They call the subgroup of stars “hump & spike” stars. The “hump” is the broad feature. Saio et al. (2018) propose that this broad feature could be caused by Rossby waves. The hypothesis is supported by the fact that those kind of waves are linked to the rotational frequency of those stars. The “spikes” or the sharp features could be a result of spots on the star. Therefore they are linked to the star’s rotational period. Sikora et al. (2018) proposed that the broad and sharp peaks could be caused by a region near a convective-radiative boundary and inhomogeneities near the surface. This demonstrates that the planet-hypothesis is not the only possible explanation for the peculiar features.

Chapter 3

M stars

3.1 Data

Most of the previous exoplanet surveys focused on solar type stars (e.g. Mayor et al. 2011; Howard et al. 2012). This is due to the assumption that life could prevail better on a planet that is very similar to our Earth. In addition to that, solar type stars are brighter in the visual band than M stars. Nevertheless it is of great interest to detect planets around the cooler and lighter M dwarfs. They are smaller and the transit probability of earth-like planets in the habitable zone is much higher. Due to the more favorable planet-to-star radius ratio, it is easier to use transmission spectroscopy to determine the planet's atmospheres. In addition to that, M stars have masses of only 0.1 – 0.6 $M_\odot$ and are therefore good targets for radial velocity measurements of low-mass planets. The frequency of M-stars that are near to our solar system is around 70 % (e.g. Henry et al. 2006, 2018) – our next neighbor, Proxima centauri is an M dwarf. A further plus in observing earth-like planets in the habitable zone around M-stars is that shorter periods can be observed and confirmed in much shorter time.

This change in priorities lead to the need of an instrument that is designed especially to determine radial velocities of M-stars. The peak emission of M stars is shifted to longer wavelengths in comparison to G stars due to their lower effective temperature. Most state-of-the-art high precision spectrographs do not cover this redder wavelength regime; e.g. HARPS covers a wavelength range of 378 nm to 691 nm (Pepe et al. 2002).

3.1.1 CARMENES

The M dwarf planet frequency is still an open question. I describe what is known about the M star planet frequency from transit surveys and HARPS in section 1.4. The CARMENES consortium was founded to find the occurrence rate of rocky planets in the habitable zone around M dwarfs. It consists of 11 institutions from Spain and Germany – the Thuringian State observatory is one of them. The task was to build a high resolution spectrograph that is capable of finding the M dwarf planet population. It is mounted at the 3.5 m telesope at the Calar Alto Observatory in Spain. The Calar Alto is located near Almeria in the Spanish region Andalucía. The weather conditions there are such that about 2/3 of all night hours can be used for obervations (`http://www.caha.es/CAHA/MISC/weather.html`). CARMENES consists of two spectrographs in the wavelength ranges 0.55 – 1.05 µm (visual arm) and 0.97 – 1.7 µm (near infrared arm) with spectral resolutions of $R = 94\,600$ and $R = 80\,400$ respectively.

To avoid instrumental shifts, a temperature stability of the instrument of ± 0.01 K is achieved. This is done by putting the spectrographs into an isolated vacuum tank. Additionally the infrared spectrograph is cooled down to 140 K to avoid thermal emission that disturbs the observation at this wavelength regime. CARMENES is equipped with hollow-cathode lamps and a Fabry-Pérot-Interferometer which are used as wavelength reference (Quirrenbach et al. 2014). The radial velocities of the spectra are extracted with the Spectrum radial velocity analyser (SERVAL) by Zechmeister et al. (2018). From a drift in the Fabry-Pérot-Interferometer, we know that the temperature is not stable enough to maintain the required precision of $1\,\mathrm{ms}^{-1}$ at different nights. For this reason, all signals are corrected with a nightly zero point (NZP), that makes use of a set of pre-defined RV-standard stars (Trifonov et al. 2018). With those corrections CARMENES and SERVAL reach down to a $1\,\mathrm{ms}^{-1}$ precision in the visual channel and $5\,\mathrm{ms}^{-1}$ in the near infrared channel. In the infrared region the spectra are contaminated by telluric lines and the line density decreases. Although the near infrared arm does not reach the same precision for RV measurements as the visual arm, it is very effective in detecting exoplanet atmospheres in wavelength regions that other spectrographs cannot probe (e.g. Nortmann et al. 2018). Reiners et al. (2018b) found out that the highest RV precision is achievable in the wavelength range from 700 nm to 900 nm. This wavelength range is covered by the visual channel of CARMENES. Thus, I base my analysis on the visual channel observations.

Among the Guaranteed Time Observations (GTO) targets there are active and less active stars. Observations of more active stars can be useful to extract information on the influence of activity on RV measurements. Star spots can mimic a planetary signal because they distort the line profiles of the absorption lines. This distortion can be measured as an RV shift. A well known example is the G-type star HD 166435. The RVs of the stellar activity measured for this star are similar to the RVs we would expect from a planet (Queloz et al. 2001). Therefore we need to monitor the activity of our stars in order to distinguish planetary from activity signals. The CARMENES activity indicators (see section 3.1.3) are automatically extracted by SERVAL.

3.1.2 The stellar sample

During the GTO of the CARMENES consortium, about 340 stars are monitored for planetary signals. The stars are selected from the input catalogue CARMEN(ES) Cool dwarf Information and daTa Archive (Carmencita) (Caballero et al. 2016). As the survey is still ongoing, I limit my analysis to those 125 stars for which we finished observations. This is is the case if we have obtained 50 RV-values for a star and do not see any periodic signal of planetary nature or if we have found and published a planet. The maximum observable K-amplitude to Root Mean Square (RMS) ratio improves rapidly within the first few measurements and with more numbers of observations it decreases more slowly (see figure 3.12). The number of nights that can be used during the CARMENES GTO time is limited. The cutoff at 50 RV-measurements is a trade off between the number of stars that are included in the survey and the maximum number of measurements the team can obtain per star.

Some of the target stars show a large RV scatter of more than $10\,\mathrm{ms}^{-1}$ that is most probably caused by activity. Those target stars are called "active RV loud" and we terminated observations of most of them after 11–13 RV values were taken (Tal-Or et al. 2018). Furthermore, I did not include in this list 9 spectroscopic binaries, we ceased to observe after a short time. All the targets that were added to the CARMENES GTO sample later, were not included in the analysis as well. They were added because we wanted to confirm a transiting planet. Therefore, including them would lead to an overestimation of the planet occurrence rate. The full list of all 125 included CARMENES stars and their masses can be found in the appendix (tables B.1 and B.2). In the following, I will call this sample the "completed sample".

A histogram of the masses of the CARMENES GTO sample (see figure 3.1) shows that they are almost equally distributed from 0.1 to 0.6 solar masses. Almost all of the stellar masses are from Schweitzer et al. (2019) with a typical error 3–5 %. Very few stellar masses are calculated with the mass-luminosity-metallicity relation from Mann et al. (2019). There are a few targets in the mass bin $0.6\,\mathrm{M}_\odot$ to $0.7\,\mathrm{M}_\odot$ and all of them are in our reduced sample. The earlier and later M dwarfs are a little bit over represented in the reduced sample but overall the "completed sample" is a good representation of the whole sample. The median mass of the whole CARMENES sample is $0.348\,\mathrm{M}_\odot$ and that of the reduced sample is $0.35\,\mathrm{M}_\odot$.

I also compared the RMS of the observations and the numbers of observations of the "completed sample" to the whole sample. It can be noted that almost all of the high RMS targets are in the "completed sample". I expect that the completeness of this sample will be affected by this. As a consequence the median RMS of the "completed sample" is higher ($5.3\,\mathrm{ms}^{-1}$) than that of the whole sample ($3.9\,\mathrm{ms}^{-1}$). A higher RMS of a time series can either be introduced by activity or by planets that increase the RV scatter. To check what is the reason for the difference in RMS, I divide the time series in active and less active stars. The active stars are the stars that have stronger H-alpha emission than 84 % of the sample stars. If I calculate the RMS only

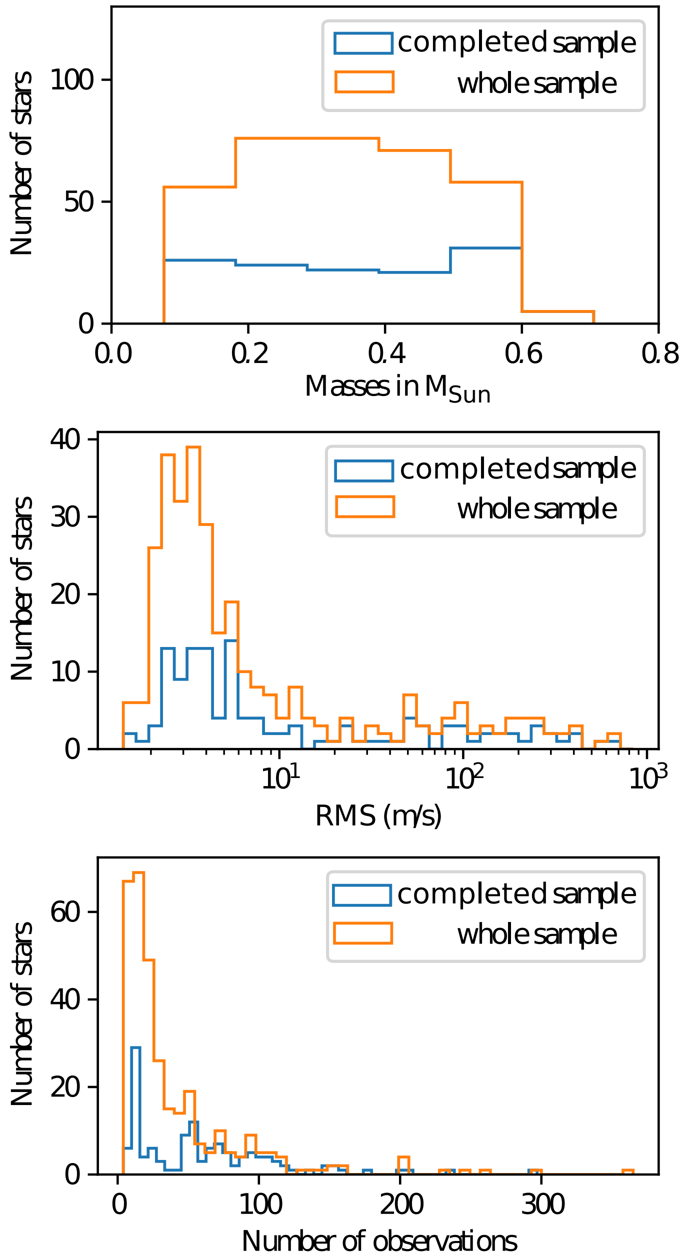

Figure 3.1: Comparison of (a) upper panel: the masses, (b) middle panel: the RMS of the observations and (c) lower panel: the number of observations throughout the CARMENES sample and the reduced sample from Sabotta et al. (2020, in prep.)

from the less active stars, the difference of RMS between the reduced and the whole sample is lower – $4.0\,\mathrm{m\,s^{-1}}$ to $3.4\,\mathrm{m\,s^{-1}}$ respectively.

The histogram of the number of observations shows a peak at 50 measurements for both samples. Observations are complete if after 50 measurements there is no clear planetary signal. There is another peak at 13 numbers of observations which is caused by the "active RV loud" sample. Observations were terminated earlier for this kind of stars. Most of the stars with a high number of observations are also in our "completed sample". This is because observations are terminated after the publication of a planet signal. This will change as the survey progresses. A big number of stars still has less than 50 numbers of observations. The median number of observations of the whole sample is only 23 whereas that of the "completed sample" is 52.

3.1.3 CARMENES planets

Several CARMENES planets were published in combination with other instruments like HARPS or HIRES – e.g. Barnard's star b (Ribas et al. 2018). Therefore, it is not sufficient to include all published CARMENES planets in our occurrence rate statistics. It is necessary to obtain a clean planet sample that does not rely on observations from other RV or transit surveys. In order to obtain that, I reviewed the GLS-periodograms of the RV data of all the 125 subsample stars. I looked for signals with a false alarm probability (FAP) of 1 % or less. The idea is that a signal with FAP of 1 % would be considered a planet candidate and more RV measurements would be taken.

I modeled these signals with a Keplarian fit. If a periodic signal remained present in the residuals, I modeled both the signals with a two planet fit. I repeated this procedure up to a maximum of three signals. Usually, one would repeat removing signals until no signals with FAP $< 1\,\%$ remain in the data. In the case of our data set, there are several signals that cannot be removed with a Keplarian model. The aim of this process is to identify those stars with interesting RV signals. Therefore, a fourth or fifth planet would show up in the more thorough analysis that should follow. The models were calculated with the Python package *PyAstronomy* (Czesla et al. 2019).

CARMENES uses several activity indicators. For this study, I incorporate four of them, namely H-alpha, the differential line width, the chromatic index and the calcium infrared triplet. The H-alpha and the calcium infrared lines are sensitive to chromospheric activity and are linked to the rotation period of a star or to a longer underlying activity cycle. Both indices are computed by SERVAL with the formula $I = \frac{F_0}{0.5 \cdot (F_1 + F_2)}$ from Kürster et al. (2003) (F_0 is the average flux around the line center and F_1 and F_2 are median fluxes in a reference region). Zechmeister & Kürster (2009) showed that this formula is similar to the pseudo equivalent width that is calculated by integrating over the flux in the line core. The chromatic index measures the wavelength dependence of the RV signal and the differential line width is similar to the Full width at half maximum (FWHM) of the spectral lines.

If one of the activity indicators has a significant (FAP $< 10\,\%$) periodogram peak in the vicinity ($10\,\%$) of an interesting RV period, I flag the RV period as activity. I also use rotation periods that were obtained from photometry by Díez Alonso et al. (2019). The rotation period can be detected in photometry if there is one spot or spot group corotating with the star. If a second spot or spot group is present, the photometry signal gives half the rotation period. The same works for three spots (one third of the rotation period) and so on. Therefore, I flag the rotation period and its first harmonic of the known rotational period as false positive automatically.

If a star is very active (median H-alpha index higher than in $84\,\%$ of the sample stars), the periodogram peak has to have a FAP of $0.1\,\%$ such that this period is flagged as a candidate. To confirm the periodicity of a signal, at least two orbits of the planet candidate are observed. Accordingly, I excluded all periods that are longer than half the time baseline.

With this procedure I obtain the signals of 28 known planets and 28 planet candidates that cannot be directly linked to activity indicators or the photometric rotational period. Of those 28 candidates, all but two can be vetted as activity signal manually (see tables 3.1 and 3.2). Some of them show the RV signal in higher harmonics of the rotation period – those are flagged as "rotation period harmonics". If a planet candidate signal is not stable in amplitude or phase over time it is flagged as "unstable period". The two remaining candidates cannot be distinguished with the number of RV observations and the photometry data we have. The whole list of periodic signals is shown in the appendix (tables B.3 to B.3). From this list it becomes clear that there is not a single activity indicator that could be used to find all the RV signals that originate from stellar activity. Sometimes only one activity indicator shows the same periodicity as the RV data. Therefore, all four activity indicators are needed to flag false positive detections.

Table 3.1: Output of the periodicity search program, known planets and unclear signals, part 1

CARM. ID	period	FAP	remark
J00067-075	21.17	0.5206 %	Planet candidate?
J01125-169	3.06	0.0047 %	Known planet[1]
J01125-169	4.7	0.0349 %	Known planet[1]
J02530+168	4.91	$< 10^{-6}$	Known planet[2]
J02530+168	11.41	$< 10^{-6}$	Known planet[2]
J03133+047	2.29	$< 10^{-6}$	Known planet[3]
J03133+047	67.91	0.3438 %	Rotation period[4]
J04376+528	7.9	0.1966 %	Rotation period harmonic
J04376+528	422.79	0.2191 %	Unstable period
J04588+498	8.97	0.0081%	Probably activity
J06011+595	44.1	0.3726 %	Rotation period harmonic
J06011+595	21.52	0.6634 %	Rotation period harmonic
J06548+332	14.21	$< 10^{-6}$	Known planet[5]
J06548+332	67.59	10^{-6}	Rotation period harmonic[5]
J06548+332	119.48	0.0003 %	Rotation period[5]
J08413+594	206.39	$< 10^{-6}$	Known planet[6]
J08413+594	39.3	0.0383 %	Probably activity
J09144+526	24.4	0.0012 %	Known planet[7]
J09561+627	8.93	0.0282 %	Unstable period
J10289+008	305.89	0.0166 %	Unstable period
J11026+219	4.54	0.0409 %	Activity signal
J11033+359	12.94	$< 10^{-6}$	Known planet[5]
J11417+427	41.28	$< 10^{-6}$	Known planet[8]
J11417+427	514.72	$< 10^{-6}$	Known planet[8]
J11421+267	2.64	$< 10^{-6}$	Known planet[8]
J11421+267	56.29	0.9319 %	Unstable period
J11511+352	25.5	0.5200%	Rotation period
J12123+544S	13.68	$< 10^{-6}$	Known planet[5]
J12123+544S	107.28	0.4552 %	Activity period[5]

[1] Stock et al. (2020) [2] Zechmeister et al. (2019)
[3] Bauer et al. (2020) [4] Newton et al. (2016)
[5] Stock et al. (2020, submitted) [6] Morales et al. (2019)
[7] González-Álvarez et al. (2020) [8] Trifonov et al. (2018)

Table 3.2: Output of the periodicity search program, known planets and unclear signals, part 2

CARMENES ID	period	FAP	remark
J12479+097	1.47	0.0012 %	Known planet[9]
J13229+244	3.02	$< 10^{-6}$	Known planet[10]
J14307-086	249.07	0.3527 %	Unstable period
J15194-077	5.37	0.0003 %	Known planet[8]
J15194-077	2.65	0.4592 %	Activity period
J15194-077	9.62	0.7188 %	Activity period
J16167+672S	86.9	$< 10^{-6}$	Known planet[11]
J16303-126	4.83	0.7732 %	Known planet[12]
J16303-126	17.88	0.0011 %	Known planet[12]
J16581+257	11.29	0.2735 %	Rotation period
J17378+185	15.52	0.0007 %	Known planet[13]
J17378+185	480.52	0.0073 %	Activity period[13]
J19169+051N	104.24	$< 10^{-6}$	Known planet[14]
J19169+051N	174.48	0.0008%	Activity signal[14]
J20533+621	183.37	0.1655%	Planet? Period is 1/2 year
J21164+025	14.45	$< 10^{-6}$	Known planet[13]
J21466+668	8.05	$< 10^{-6}$	Known planet[15]
J21466+668	2.31	$< 10^{-6}$	Known planet[15]
J22021+014	10.96	0.0405 %	Planet candidate?
J22115+184	381.86	0.0001 %	Unstable period
J22137-176	3.65	$< 10^{-6}$	Known planet[10]
J22252+594	13.35	$< 10^{-6}$	Known planet[16]
J22532-142	61.17	$< 10^{-6}$	Known planet[8]
J22532-142	30.09	$< 10^{-6}$	Known planet[8]
J23113+085	141.09	$< 10^{-6}$	Double star
J23419+441	178.74	0.0001%	Unstable period

[8] Trifonov et al. (2018) [9] Trifonov et al. (2020, submitted)
[10] Luque et al. (2018) [11] Reiners et al. (2018a)
[12] Wright et al. (2016) [13] Lalitha et al. (2019)
[14] Kaminski et al. (2018) [15] Amado et al. (2020, in prep.)
[16] Nagel et al. (2019)

3.2 Method

Most planet surveys publish the detection of planets but an important result of a survey is also the determination of the detection limits, which combined with the detections then gives the frequency of planets. To determine the frequency of planets in our sample, we need to identify possible planets we missed due to our detection limit. Our method and occurrence rates were published in Sabotta et al. (2020, in prep.).

3.2.1 Pre-whitening

Before I run my injection-and-retrieval experiment, I remove all signals I presented in section 3.1.3. This is necessary as periodic signals in the data from activity or from a planet lower the probability to recover injected artificial planets. If I would not remove those signals the detection limits would be higher and would not represent the true probabilities of detecting a planet. Higher mass upper limits lead to higher planet occurrence rates. Therefore, pre-whitening of the time series is important if I do not want to overestimate the planet occurrence rates.

3.2.2 Determining the detection probabilities

Injection-and-retrieval experiments to determine detection limits were used widely in the literature, e.g. Cumming et al. (1999), Zechmeister et al. (2009), Meunier et al. (2012) or Bonfils et al. (2013). They all inject simulated planet signals to the data and check if they can retrieve those signals. Differences of the methods are mainly in the way how measurement errors and stellar variability are treated and in the way the planet signals are retrieved. A method suitable for the CARMENES survey should make very few assumptions on the stellar variability as this is not very well studied for M dwarfs up to now. The retrieval process should follow the way of retrieving planet candidates in CARMENES the closest (see section 3.1.3). Therefore, my approach follows most closely the one from Bonfils et al. (2013).

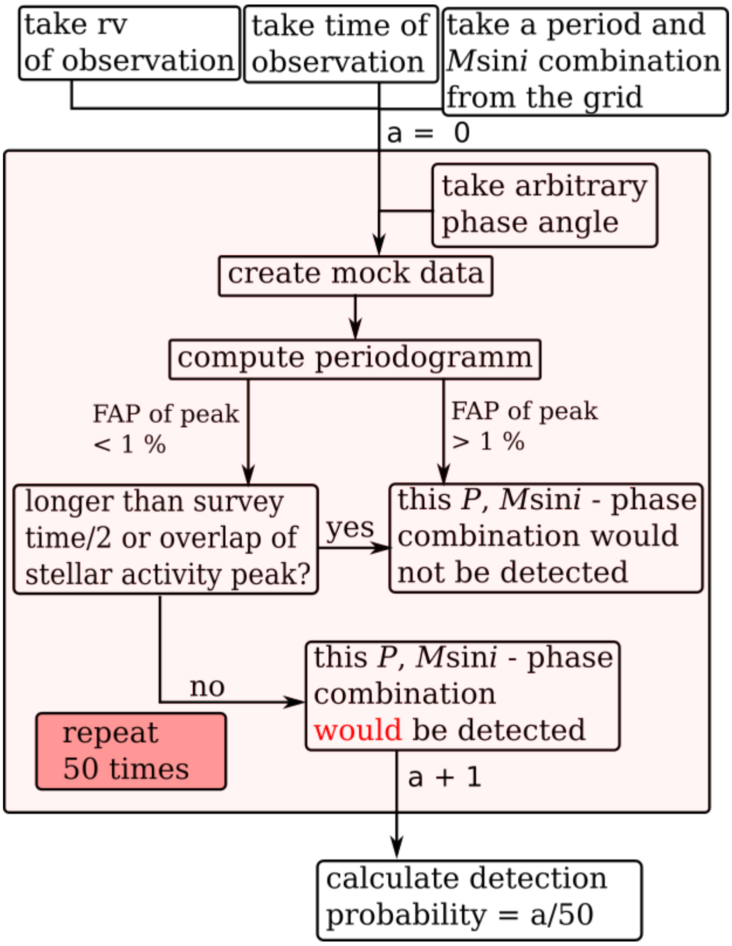

Figure 3.2: Illustration of the injection-and-retrieval experiment work flow

I start by creating a simulated planet signal with the time stamps of our observations. I compute a grid of possible $M \sin i$ and periods. Our grid has 3600 points and is logarithmically spaced such that lower masses and shorter periods have smaller spacing. The masses range from $1\,\mathrm{M}_{\oplus}$ to $100\,\mathrm{M}_{\mathrm{Jup}}$ and periods range from 1 d to 10000 d. Planet mass and period are taken from this grid. As in Endl et al. (2000), I add the measured radial velocities, RV_{observed}, as error to our simulated data. In that way I include activity induced RV variations and our intrinsic errors. I compute a periodogram and check if I can find the injected period in the simulated data. If the FAP is below 1 % this object would be considered a planet candidate and observed more frequently. Hence, I expect that this planet would have been detected.

This process is repeated several times with arbitrary phases (see figure 3.2). The detection probabilities are calculated for circular orbits and single planet systems. In section 3.4.3 I discuss why this simplification is reasonable.

For circular orbits the amplitude of the simulated data is computed by:

$$A = 28.4 \left(\frac{P}{1\,\mathrm{year}}\right)^{-1/3} \left(\frac{M_{\mathrm{pl}} \sin i}{\mathrm{M_{Jup}}}\right) \left(\frac{M_\star}{M_\odot}\right)^{-2/3} . \tag{3.1}$$

The radial velocity of the simulated time series is:

$$RV = A \sin\left(\frac{2\pi t}{P} + \phi\right) + RV_{\mathrm{observed}}. \tag{3.2}$$

I assign a detection probability of zero percent to those periods with a significant peak in the periodogramm of an activity indicator. Up to now it is not possible to disentangle a possible planet period from an activity signal at the same period.

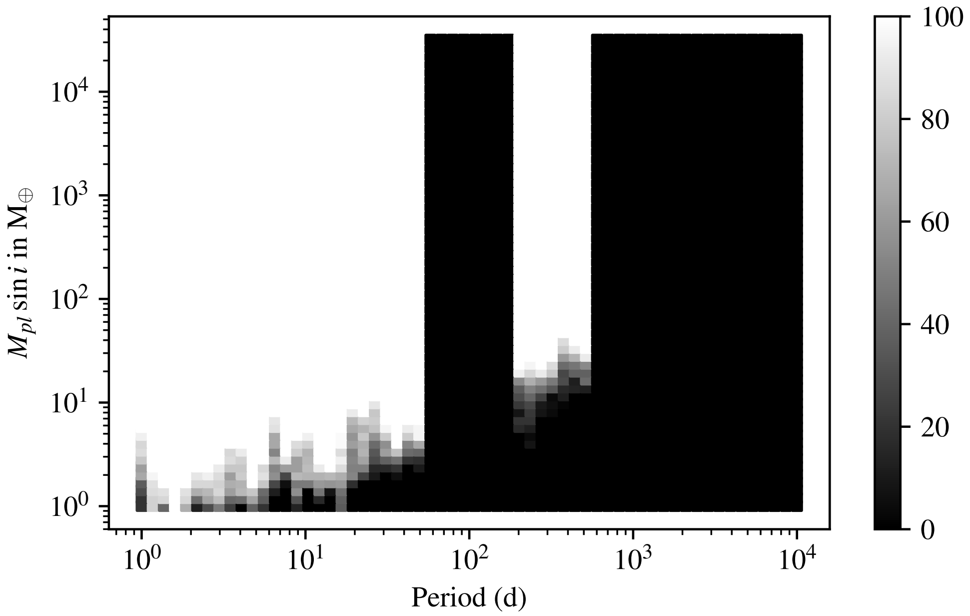

Figure 3.3: Example of a detection map with activity periods excluded. The detection probability of each grid point is given in gray scales: black grid points have a detection probability of zero and white corresponds to a detection probability of 100 %.

Figure 3.3 shows an example of a resulting detection map. The detection probability of each grid point is displayed in gray scales. In this example we would have been able to detect a $2\,M_\oplus$ planet at a period of 10 d.

3.2.3 From detection probability to occurrence rates

In the literature there are several methods that were used to calculate the planet occurrence rates from detection probabilities (e.g. Bonfils et al. 2013; Wittenmyer et al. 2016). I use two of the most frequently used methods.

Method 1 – period-mass bins

The only other large RV survey around M stars with published occurrence rates is Bonfils et al. (2013) who analyzed data from the HARPS spectrograph. In order to compare our results to that of Bonfils et al. (2013) we used a very similar method to obtain the occurrence rates. Basically, one finds an average number of stars N_{eff} in a period-mass bin around which the planets in this period-mass regime would have been detected. The other stars are not included in the occurrence rate analysis. To obtain N_{eff}, Bonfils et al. (2013) randomly chose points in their log uniform period-mass grid. Through their injection-and-retrieval experiment, they know how many stars have a detection probability of 50 % or more for planets with this period and mass. This number of stars is N_{eff}. They randomly pick a high number of grid points and report a median number of stars N_{eff} that have enough measurements to detect a planet in this period-mass bin. The scatter in N_{eff} and a binomial distribution give the error bars.

The difference in my method is that I calculate an expected number of planets for a certain planet frequency directly. Measurement errors due to a binomial distribution of planets are included from the beginning. In addition to that, I use the detection probability of each individual grid point directly. The equivalent to the Bonfils et al. (2013) method would be to assign zero probability to all grid points with detection probabilities of 50 % or less and 100 % to all grid points with detection probability of 50 % or more. This is not as precise as using the detection probabilities directly but statistically both methods lead to very similar results. Furthermore, my method has the advantage that measurement errors do not have to be recalculated if the number of detected planets N_{D} has to be revised.

I create a log uniform grid of possible planet frequencies. For every frequency in this grid, I calculate a number of expected planets as follows:

1. I randomly draw a number of planets that correspond to this frequency from a binomial distribution.
2. I randomly (uniform logarithmic) assign a period and mass within the period and mass range of the bin to each of those test planets.
3. To each planet, I randomly assign a star. The detection probability for this simulated planet is taken from the detection map of this star.
4. The test planet is counted as a detection with this probability.
5. The number of planets that are counted as a detection is the number of planets that should be detected if this frequency is the true underlying planet frequency.

This process is repeated 1000 times. The error bar to the planet frequency is derived by using the 16 % and 84 % percentiles of the 1000 numbers of planets obtained in this way. Table 3.3 shows the outcome of this simulation for the $1-10\,\mathrm{d}$ and $1-10\,\mathrm{M}_\oplus$ period-mass bin. In this bin the number of detected planets N_D is 8–10. This corresponds to a planet frequency of $26^{+13}_{-9}\,\%$.

I also present a number P_{det} which is the percentage of planets that can be retrieved. It is calculated from the 100 % planet frequency and it is equivalent to the N_{eff} of the Bonfils et al. (2013) method.

Method 2 – missed planets approach

With the second method the number of planets that are missed due to the detection limits is calculated. Each of the detected exoplanets of the survey is assigned a number of planets with same period and mass that could still be hidden around the non-planet hosts of the survey. If such a planet could be detected around all the other survey stars, the number of missing planets is zero and it is high if such a planet is not observable.

Table 3.3: Planet frequencies and corresponding number of expected planets for the $1-10\,\mathrm{d}$ and $1-10\,\mathrm{M}_{\oplus}$ period-mass bin. The number of CARMENES discoveries is highlighted in boldface.

planet frequency	lower limit	median	upper limit
0.067	1	2	4
0.079	1	3	4
0.092	1	3	5
0.108	2	4	6
0.127	2	4	7
0.149	3	5	7
0.174	4	6	**8**
0.204	5	7	9
0.240	6	**8**	11
0.281	7	**10**	13
0.329	8	11	14
0.386	**10**	13	16
0.452	12	15	19
0.530	14	18	22
0.621	17	21	25
0.728	21	25	29
0.853	25	29	34
1	29	34	39

The method is described in detail in Wittenmyer et al. (2020). They calculate the completeness fraction $f_C(P, M)$ of the non-hosts in the sample with this equation:

$$f_C(P, M) = \frac{1}{N_{\text{stars}}} \sum_{i=1}^{N_{\text{stars}}} f_{R,i}(P, M). \tag{3.3}$$

$f_R(P, M)$ is the recovery rate – the probability to find a planet at this specific mass-period combination and N_{stars} is the number of stars in the sample. To obtain this completeness fraction, I calculate detection maps of all the stars in our sample with only 28 grid points that correspond to the masses and periods from the planet sample. The detection limits are equivalent to the recovery rate $f_R(P, M)$. The completeness fraction $f_C(P, M)$ is a measure of how many other stars have enough RV measurements to detect a planet with the same period and mass. To obtain it, I average all the detection probabilities of this grid point.

The inverse of the individual recovery rate/detection probability $f_{R,i}$ of a survey planet multiplied with the completeness fraction $f_C(P, M)$ at this period and mass, is the number the number of missed planets assigned to a single survey planet $N_{\text{missed, i}}$:

$$N_{\text{missed, i}} = \frac{1}{f_{R,i}(P_i, M_i) f_c(P_i, M_i)}. \tag{3.4}$$

The total number of missed planets N_{missed} can then be derived with this equation:

$$N_{\text{missed}} = \sum_{i=1}^{N_{\text{planets}}} N_{\text{missed, i}} - N_{\text{planets}}, \tag{3.5}$$

where N_{planets} is the number of planets. The number of detected planets is subtracted from the sum of all missing planets.

The number of missed planets can then be used to correct the planet occurrence rate $f = \frac{N_{\text{detected}}}{N_{\text{stars}}}$ (N_{planets} is the number of detected planets). The corrected occurrence rate is:

$$f_{\text{corrected}} = \frac{N_{\text{missed}} + N_{\text{planets}}}{N_{\text{stars}}} = \frac{N_{\text{missed}} + N_{\text{planets}}}{N_{\text{planets}}} \cdot \frac{N_{\text{planets}}}{N_{\text{stars}}}, \tag{3.6}$$

with the correction factor $\left(\frac{N_{\text{missed}}+N_{\text{planets}}}{N_{\text{planets}}}\right)$.

In Wittenmyer et al. (2020) they use only the non-planet hosts to calculate the completeness fraction $f_C(P, M)$ of the survey at a certain mass and period. I modify the method and calculate the completeness fraction of all stars, including the 30 planet hosts. My pre-whitening procedure subtracts all significant periodic signals from the data, such that our time series are free of detectable planet signals. The reason for this change of methods is that the completeness fraction can be underestimated by using only the non-hosts if we have a very inhomogeneous sample. With our distribution of numbers of observations (see figure 3.1) this is the case.

The mean value and error bars of this method are given by the binomial distribution:

$$P(N_{\text{planets}}) = \binom{125}{N_{\text{planets}}} f_{\text{planet}}^{N_{\text{planets}}} (1 - f_{\text{planet}})^{(125 - N_{\text{planets}})}, \tag{3.7}$$

where $P(N_{\text{planets}})$ is the probability to obtain a certain number of planets, N_{planets} is the number of detected planets and f_{planet} is the underlying planet frequency. The distribution is used with the uncorrected number of planets. I obtain a cumulative binomial distribution with a lot of values f_{planet}. The 16 %, 50 % and 84 % level of the distribution serve as the lower error, mean value and higher error respectively. As a last step, I apply the frequency correction factor to those values.

3.3 Results

3.3.1 Completeness

I average the detection probability of each grid point to obtain a completeness map for our survey. The map is shown in figure 3.4. Each point of the map represents a period-mass combination. Color coded is the overall detection probability of the 125 stars subsample for the specific grid point. The planets, detected by CARMENES, that are listed in section 3.1.3 are overplotted as yellow stars.

It shows that at a 10 d orbit we can detect a planet of 7 $M_\oplus$ around half of our stars. Around 20 % of our stars even a 3 $M_\oplus$ planet can be detected at a 10 d orbit. I limit my analysis to half the time baseline as two orbital periods are needed to confirm the periodic nature of a planet candidate signal. For this reason, I obtain a zero detection probability starting from a 600 d period.

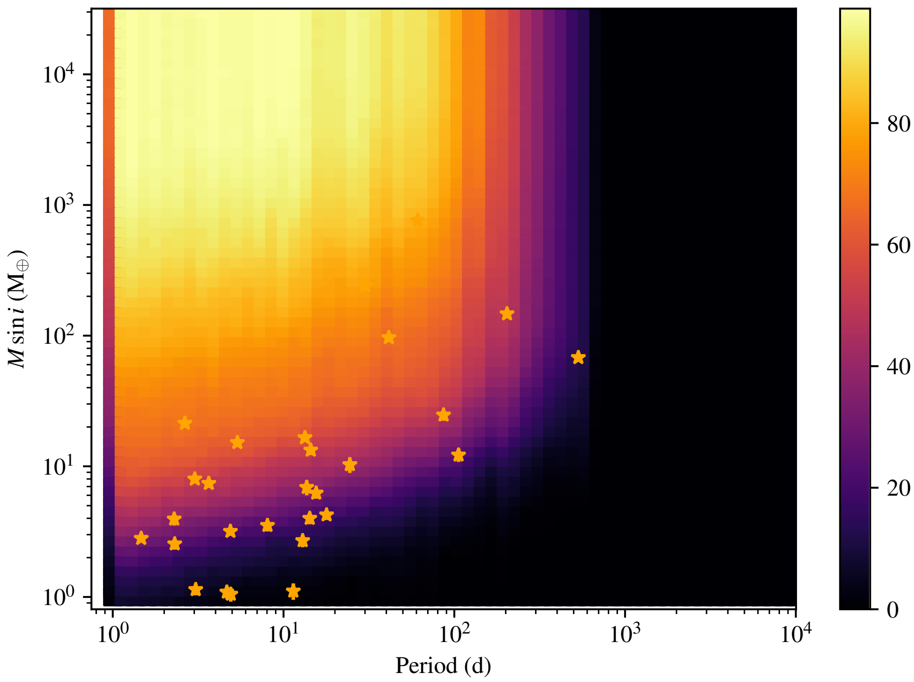

Figure 3.4: CARMENES completeness - color map: average detection probability of the 125 stars in our stopped subsample; yellow stars: planets with independent significant periodic signal from CARMENES (Sabotta et al. 2020, in prep.)

Another way to display the survey completeness is by the survey sensitivity. To obtain the average survey sensitivity, I average the detection probability along the rows or columns of the mass-period grid. I take the mass range from 1 $M_\oplus$ to 13 M_{Jup} and periods from 1 d to 240 d (which is the average of half the time baseline). In addition to the average survey sensitivity, I split the sample to higher ($M_\star > 0.337\mathrm{M}_\odot$) and lower mass stars ($M_\star < 0.337\mathrm{M}_\odot$). The result is shown in figure 3.5. The mass sensitivity is dampened for the lower mass stars. This is most probably because the "RV-loud" sample consists entirely of stars out of the low mass sample.

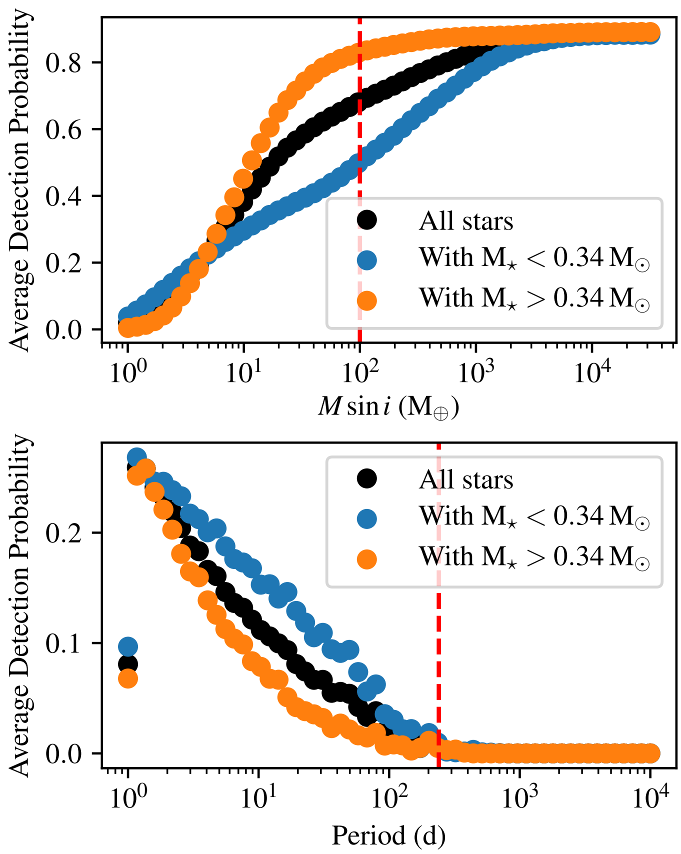

Figure 3.5: Upper panel: Average detection probability for periods 1–240 d vs. mass of the test planet; lower panel: average detection probability for masses 1–4000 $\mathrm{M}_\oplus$ vs. orbital period of the test planet

3.3.2 Occurrence rate

Method 1 – period-mass bins

I computed the occurrence rates of the different period-mass bins as described in section 3.2.3. The result is displayed in table 3.4. In addition to that, I

Table 3.4: Planet occurrence rates f, N_d is the number of planets detected, P_{det} is the fraction of planets we can detect in the period-mass bin (Sabotta et al. 2020, in prep.)

	Period (d)		
m sin i ($M_\oplus$)	1–10	10–10^2	10^2–10^3
10^3–10^4	$N_d = 0$	$N_d = 0$	$N_d = 0$
	$f < 0.014$	$f < 0.016$	$f < 0.04$
	$P_{\text{det}} = (97 \pm 2)\,\%$	$P_{\text{det}} = (91 \pm 2)\,\%$	$P_{\text{det}} = (37 \pm 5)\,\%$
10^2–10^3	$N_d = 0$	$N_d = 2$	$N_d = 1$
	$f < 0.014$	$f = 0.02^{+0.03}_{-0.02}$	$f = 0.03^{+0.06}_{-0.03}$
	$P_{\text{det}} = (88 \pm 3)\,\%$	$P_{\text{det}} = (79 \pm 4)\,\%$	$P_{\text{det}} = (32 \pm 5)\,\%$
10–10^2	$N_d = 2$	$N_d = 4 - 5$	$N_d = 2$
	$f = 0.025^{+0.03}_{-0.025}$	$f = 0.06^{+0.05}_{-0.03}$	$f = 0.085^{+0.11}_{-0.06}$
	$P_{\text{det}} = (70 \pm 5)\,\%$	$P_{\text{det}} = (57 \pm 4)\,\%$	$P_{\text{det}} = (19 \pm 4)\,\%$
1–10	$N_d = 8 - 10$	$N_d = 5 - 7$	$N_d = 0$
	$f = 0.26^{+0.16}_{-0.09}$	$f = 0.40^{+0.25}_{-0.20}$	–
	$P_{\text{det}} = (27 \pm 4)\,\%$	$P_{\text{det}} = (13 \pm 3)\,\%$	$P_{\text{det}} = \left(1.6^{+1.5}_{-0.8}\right)\,\%$

split the sample in two host star mass bins. The occurrence rates for earlier M dwarfs (higher mass) are displayed in table 3.5 and those for the later M dwarfs (lower mass) in table 3.6.

Method 2 – missed planets approach

With the missed planets approach I determine an overall planet occurrence rate of $1.85^{+0.36}_{-0.26}$ planets per star. There are 204 missed planets which gives an occurrence rate correction factor of 8.3. In table 3.7 I list the CARMENES planet detections and the associated number of "missed planets".

In order to be able to compare the results of the two methods, I also computed the occurrence rates in the same period-mass bins as above. Table 3.8 shows the results.

Table 3.5: Occurrence rates f of the earlier M dwarfs (higher mass), N_d is the number of planets detected, P_{det} is the fraction of planets we can detect in the period-mass bin (Sabotta et al. 2020, in prep.)

	Period (d)		
m sin i ($M_{\oplus}$)	1–10	10–10^2	10^2–10^3
10^3–10^4	$N_d = 0$	$N_d = 0$	$N_d = 0$
	$f < 0.03$	$f < 0.035$	$f < 0.09$
	$P_{\mathrm{det}} = (97 \pm 2)\,\%$	$P_{\mathrm{det}} = (93 \pm 3)\,\%$	$P_{\mathrm{det}} = (32 \pm 6)\,\%$
10^2–10^3	$N_d = 0$	$N_d = 2$	$N_d = 0$
	$f < 0.03$	$f = 0.033^{+0.045}_{-0.023}$	$f < 0.08$
	$P_{\mathrm{det}} = (96 \pm 3)\,\%$	$P_{\mathrm{det}} = (90 \pm 4)\,\%$	$P_{\mathrm{det}} = (41 \pm 6)\,\%$
10–10^2	$N_d = 1$	$N_d = 4 - 5$	$N_d = 2$
	$f = 0.015^{+0.04}_{-0.015}$	$f = 0.09^{+0.08}_{-0.055}$	$f = 0.13^{+0.15}_{-0.095}$
	$P_{\mathrm{det}} = (87 \pm 4)\,\%$	$P_{\mathrm{det}} = (73 \pm 6)\,\%$	$P_{\mathrm{det}} = (19 \pm 4)\,\%$
1–10	$N_d = 0$	$N_d = 4 - 5$	$N_d = 0$
	$f < 0.09$	$f = 0.60^{+0.40}_{-0.30}$	–
	$P_{\mathrm{det}} = (29 \pm 6)\,\%$	$P_{\mathrm{det}} = (10 \pm 4)\,\%$	$P_{\mathrm{det}} = (1.4 \pm 1.4)\,\%$

Table 3.6: Occurrence rates f of the later M stars (lower mass), N_d is the number of planets detected, P_{det} is the fraction of planets we can detect in the period-mass bin (Sabotta et al. 2020, in prep.)

	Period (d)		
m sin i ($M_{\oplus}$)	1–10	10–10^2	10^2–10^3
10^3–10^4	$N_d = 0$	$N_d = 0$	$N_d = 0$
	$f < 0.036$	$f < 0.04$	$f < 0.11$
	$P_{\mathrm{det}} = (96 \pm 4)\,\%$	$P_{\mathrm{det}} = (89 \pm 5)\,\%$	$P_{\mathrm{det}} = (32 \pm 5)\,\%$
10^2–10^3	$N_d = 0$	$N_d = 0$	$N_d = 1$
	$f < 0.04$	$f < 0.06$	$f = 0.07^{+0.21}_{-0.06}$
	$P_{\mathrm{det}} = (79 \pm 5)\,\%$	$P_{\mathrm{det}} = (64 \pm 7)\,\%$	$P_{\mathrm{det}} = (25 \pm 5)\,\%$
10–10^2	$N_d = 1$	$N_d = 0$	$N_d = 0$
	$f = 0.04^{+0.09}_{-0.04}$	$f < 0.09$	$f < 0.2$
	$P_{\mathrm{det}} = (48 \pm 7)\,\%$	$P_{\mathrm{det}} = (39 \pm 5)\,\%$	$P_{\mathrm{det}} = (14 \pm 5)\,\%$
1–10	$N_d = 8 - 10$	$N_d = 1 - 2$	$N_d = 0$
	$f = 0.60^{+0.35}_{-0.25}$	$f = 0.20^{+0.40}_{-0.18}$	–
	$P_{\mathrm{det}} = (25 \pm 5)\,\%$	$P_{\mathrm{det}} = (15 \pm 4)\,\%$	$P_{\mathrm{det}} = (1.8 \pm 1.8)\,\%$

Table 3.7: Table of all planets in the sample with the weights for missed planets

CARM. ID	period (d)	$M \sin i$ $M_\oplus$	$f_C(P, M)$ in %	$f_R(P, M)$ in %	missed planets
J01125-169	3.06	1.14	8	36	34
J01125-169	4.66	1.09	5	34	58
J02530+168	4.91	1.05	4	100	23
J02530+168	11.41	1.11	2	100	49
J03133+047	2.29	3.95	44	100	1
J06548+332	14.24	4	25	100	3
J08413+594	203.6	147	66	100	1
J09144+526	24.45	10.3	48	100	1
J11033+35	12.95	2.7	16	100	5
J11417+427	514.7	68	32	96	2
J11417+427	41.38	96.7	75	100	0
J11421+267	2.64	21.36	69	100	0
J12123+544S	13.67	6.9	43	100	1
J12479+097	1.47	2.81	37	100	2
J13229+244	3.02	8	58	100	1
J15194-077	5.37	15.2	64	100	1
J16167+672S	86.54	24.7	56	100	1
J16303-126	4.83	3.18	24	100	3
J16303-126	17.88	4.25	25	100	3
J17378+185	15.53	6.24	36	100	2
J19169+051N	105.9	12.2	38	100	2
J21164+025	14.44	13.3	57	100	1
J21466+668	2.31	2.55	28	100	3
J21466+668	8.05	3.53	26	54	6
J22137-176	3.65	7.4	55	100	1
J22252+594	13.35	16.57	61	100	1
J22532-142	30.13	241.5	80	100	0
J22532-142	61.08	760.9	87	100	0

Table 3.8: Planet occurrence rates f, N_d is the number of planets detected, $P_{\rm det}$ is the fraction of planets we can detect in the period-mass bin (Sabotta et al. 2020, in prep.)

	Period (d)		
m sin i ($M_\oplus$)	1–10	10–10^2	10^2–10^3
10^2–10^3	$N_d = 0$	$N_d = 2$	$N_d = 1$
	–	$N_{miss} = 0.4$	$N_{miss} = 0.5$
	–	$c_{corr} = 1.2$	$c_{corr} = 1.5$
	–	$f = 0.025^{+0.019}_{-0.012}$	$f = 0.02^{+0.02}_{-0.01}$
10–10^2	$N_d = 2$	$N_d = 4$	$N_d = 2$
	$N_{miss} = 1$	$N_{miss} = 3$	$N_{miss} = 4$
	$c_{corr} = 1.5$	$c_{corr} = 1.7$	$c_{corr} = 3.0$
	$f = 0.024^{+0.023}_{-0.015}$	$f = 0.064^{+0.033}_{-0.024}$	$f = 0.062^{+0.046}_{-0.030}$
1–10	$N_d = 10$	$N_d = 7$	$N_d = 0$
	$N_{miss} = 141$	$N_{miss} = 65$	–
	$c_{corr} = 15$	$c_{corr} = 11.8$	–
	$f = 1.20^{+0.38}_{-0.31}$	$f = 0.63^{+0.26}_{-0.20}$	–

3.4 Discussion

3.4.1 Comparison of the two occurrence rate methods

I have derived the occurrence rate from the sample completeness with two different methods. With the first method – the "period-mass-bin" method – I basically average the detection limits in several period-mass bins to derive a percentage of planets that can be detected in this bin. This percentage of planets is used to correct the planet occurrence rate. With the second method – the "missed-planets" method – I look at the detection probability that is related to every single CARMENES planet detection. This is used to derive a number of planets with same mass and periods we could have missed in the rest of the sample. The number of "missed planets" is used to correct the planet occurrence rates. In table 3.9, I show a direct comparison of the two results.

In the period-mass bins with masses higher than $10\,\mathrm{M}_{\oplus}$, the two methods are consistent within the error bars. For this thesis, I have analyzed a subsample of 125 stars out of over 300 CARMENES GTO stars. Therefore the occurrence rates in those bins are probably overestimated. I included all of the already published CARMENES planets with signals in CARMENES data only. The higher mass planets need fewer numbers of observations to show up in the periodogramm. It is probable that we have already found most or all of the higher mass planets with periods less than 600 d in our GTO sample. This bias can boast the occurrence rates in general but it cannot explain a relative increase of planet frequencies towards longer periods.

For the period-mass bins below masses of $10\,\mathrm{M}_{\oplus}$, the "missed planets" approach gives a significantly higher planet occurrence rate than the "period-mass-bin" method. Furthermore, with the "missed planets" method I find a higher planet fraction for shorter periods than for longer periods but with the "period-mass-bin" method the opposite is the case.

Table 3.9: Planet occurrence rates f obtained with the "period-mass bin" approach (method 1) in black and the "missed planet" approach (method 2) in red.

	Period (d)		
m sin i ($M_\oplus$)	1–10	10–10^2	10^2–10^3
10^2–10^3	$f < 0.014$	$f = 0.02^{+0.03}_{-0.02}$	$f = 0.03^{+0.06}_{-0.03}$
	–	$f = 0.025^{+0.019}_{-0.012}$	$f = 0.02^{+0.02}_{-0.01}$
10–10^2	$f = 0.025^{+0.03}_{-0.025}$	$f = 0.06^{+0.05}_{-0.03}$	$f = 0.085^{+0.11}_{-0.06}$
	$f = 0.024^{+0.023}_{-0.015}$	$f = 0.064^{+0.033}_{-0.024}$	$f = 0.062^{+0.046}_{-0.03}$
1–10	$f = 0.26^{+0.16}_{-0.09}$	$f = 0.40^{+0.25}_{-0.20}$	–
	$f = 1.20^{+0.38}_{-0.31}$	$f = 0.63^{+0.26}_{-0.20}$	–

If I split the sample into earlier and later M stars at $M_\star = 0.337\,M_\odot$, I observe something similar. The results of the "period-mass-bin" method suggest that the early M dwarfs host their low-mass planets at longer periods than the later M dwarfs (see tables 3.5 and 3.6). I calculate the "missed-planets" for the same stellar mass bins with the second method and obtain occurrence rates of $f = 1.56^{+0.45}_{-0.40}$ and $f = 0.67^{+0.49}_{-0.32}$ for the 1–10 d and the 10–100 d bin respectively. This result differs from the results obtained by *Kepler*. Mulders et al. (2015) found that the occurrence rates of planets around all kinds of main-sequence stars are lower at short periods but reach a plateau for longer periods. The sample completeness in the 1–10 $M_\oplus$ and 10–100 d bin is very low. Only 13 % of planets are detectable in this bin. Nevertheless, with the current completeness and both methods, this drop of occurrence rate of lower mass planets around stars with $M_\star < 0.337\,M_\odot$ towards longer periods is significant.

Both occurrence rate methods have their strengths. The "missed planets" method probes only the parameter space of the planets that were detected. With the "period-mass bin" approach, we can probe the whole parameter space and give upper limits where we did not find any planets.

Within the "missed planets" method, some planets clearly dominate the statistics – especially Teegarden b and c and the two included planets of YZ Ceti. Their host stars have masses $0.132\,M_\odot$ and $0.094\,M_\odot$ respectively, so both of them belong to the lower mass sample. If I remove only YZ Ceti d from the statistics, the frequency of planets in the 1-10 d and 1-10 $M_\oplus$ bin changes from $f = 1.20^{+0.38}_{-0.31}$ to $f = 0.71^{+0.24}_{-0.19}$. Therefore, a single false positive could lead to a wrong occurrence rate estimate. The correction factors in the low mass bins are $c_{corr} = 15$ and $c_{corr} = 11.8$. A high correction factor also leads to a higher uncertainty as a slight deviation would result in a significantly different value.

In figure 3.4 the planets used for this study are shown. It is clear that in the 10–100 d low mass bin, the detected planets are not well distributed over the whole bin. As the "missed planets" method relies on the planet detections it is possible that the occurrence rate in this bin is significantly too low. A single detection in the region with longer period and lower mass would boast the occurrence rates. As the survey completeness is low in this region, the probability to find such a planet is also low although the occurrence rate could be very high.

The risk of the period-mass-bin method on the other hand is that if I choose the bin size too large, the occurrence rates can be underestimated. This is the case especially if the detection limits in this bins are very inhomogeneous. This is the case in the bins with $M \sin i < 10\,M_\oplus$.

I calculate the occurrence rates by distributing the planets in a log-uniform fashion in the period-mass bins. I use the survey sensitivity shown in figure 3.5 to find out if this is reasonable. In figure 3.6, I plot a histogram of the detected planets per mass. I use six logarithmic histogram bins with masses from $1\,M_\oplus$ to $1000\,M_\oplus$. I correct the planet number in each bin with the average survey sensitivity. The resulting planet number is decreasing with increasing planet mass. In the $1\,M_\oplus$ to $10\,M_\oplus$ bin the lower mass planets are three times as frequent as the higher mass planets. The survey completeness is lower for lower mass planets. Therefore, if I distribute the test planets in a log-uniform way, I underestimate the planet frequency.

(a) Number of planet detections vs. planet mass for the whole sample of 125 stars,

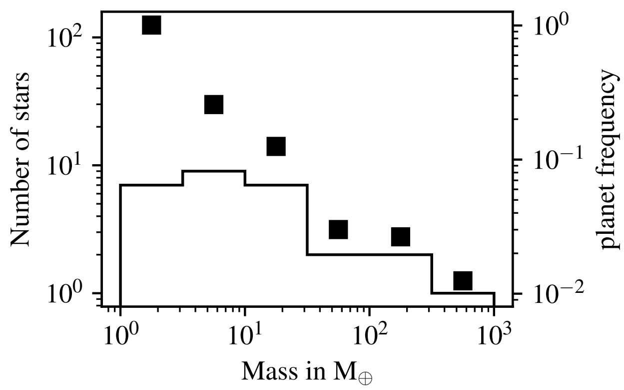

(b) for the earlier M dwarfs ($M_\star > 0.337\,\mathrm{M}_\odot$) and

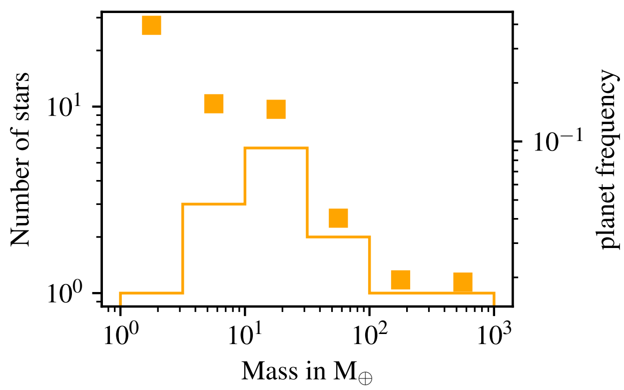

(c) for the later M dwarfs ($M_\star < 0.337\,\mathrm{M}_\odot$).

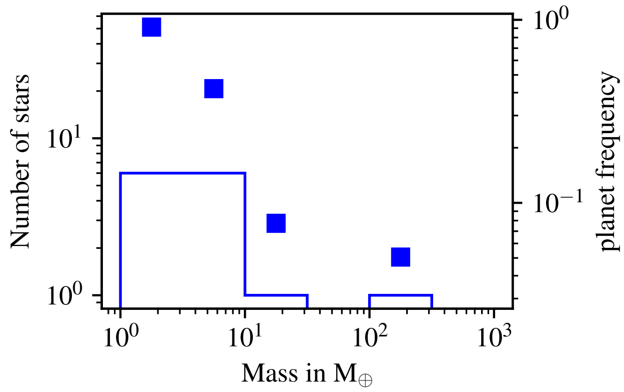

Figure 3.6: Number of CARMENES planet detections as a function of planet mass for various stellar masses. Histogram: number of CARMENES planet detections; Squares: number of planets corrected for observation bias.

The question is if a very high low mass planet occurrence rate of 1.6 planets in periods of 1–10 d is realistic from what we know about planets around stars with $M_\star < 0.337\,M_\odot$. We know at least one example with no planet detections in this mass-period range. Recently, Ribas et al. (2018) published the discovery of a $3.2\,M_\oplus$ planet around Barnard's star in a 233 d orbit. With more than 700 measurements they do not find such a planet with mass in the range of $1\,M_\oplus$ to $10\,M_\oplus$ at shorter periods. The used RV measurements exclude such a companion. Hence, to get such a high number as 1.6 planets per star, most planet hosts should have at least a second companion. The Extrasolar Planets Encyclopaedia lists 17 planets in 13 planetary systems with those parameters. This corresponds to a multiplicity of only 1.3 planets per star – this is without counting stars that do not have any planet detections in this regime. The exoplanets known today therefore support a high occurrence rate of 1 planet per star or higher but do not support a very high number of 1.6 planets per star.

In the 10–100 d bin the same exercise leads to a multiplicity of 1.4 planets per star with planet mass of $1\,M_\oplus$ to $10\,M_\oplus$. This is twice the number of 0.7 determined with the "missed planets" method or seven times the number of 0.2 planets per star determined with the "period-mass bin" method.

For these reasons I think that the true occurrence rate in the 1–10 d low mass bin is somewhere in between the ones determined by the two methods but most likely closer to the "missed-planets" results. In the 10–100 d bin, the occurrence rate could be significantly underestimated by both methods. With the future CARMENES legacy program the true planet frequencies in those bins can be determined (see section 3.4.6.

3.4.2 Comparison to HARPS (Bonfils et al. 2013)

The largest previous radial velocity study of M dwarfs was the HARPS M dwarf survey (Bonfils et al. 2013). It included 102 stars and 14 planets. A direct comparison of their occurrence rates with mine is presented in table 3.10. The results are consistent in all but one period-mass bin. In the 10–100 d and 10–100 $M_\oplus$ bin they deviate from the HARPS upper limit.

Table 3.10: Planet occurrence rates f from the HARPS survey (Bonfils et al. 2013) in blue and CARMENES results in black.

	Period (d)		
m sin i ($M_\oplus$)	1–10	10–10^2	10^2–10^3
10^2–10^3	$f < 0.01$	$f = 0.02^{+0.03}_{-0.01}$	$f < 0.01$
	$f < 0.014$	$f = 0.02^{+0.03}_{-0.02}$	$f = 0.03^{+0.06}_{-0.03}$
10–10^2	$f = 0.03^{+0.04}_{-0.01}$	$f < 0.02$	$f < 0.04$
	$f = 0.025^{+0.03}_{-0.025}$	$f = 0.06^{+0.05}_{-0.03}$	$f = 0.085^{+0.11}_{-0.06}$
1–10	$f = 0.36^{+0.24}_{-0.10}$	$f = 0.52^{+0.50}_{-0.16}$	–
	$f = 0.26^{+0.16}_{-0.09}$	$f = 0.40^{+0.25}_{-0.20}$	–

In the low mass bins I obtain lower planet occurrence rates. This is partly due to a better completeness of our sample in this area. The HARPS completeness over the two low mass bins is roughly 14 % (1–10 d) and 6 % (10–100 d) whereas ours is 27 % and 13 % respectively. This leads to smaller correction factors.

Another reason for the discrepancy could be observational bias. The five planets included in the HARPS statistics of the 1–10 d and 1–10 $M_\oplus$ period-mass bin are Gl 876 d, Gl 581 e, Gl 433 b, Gl 176 b and Gl 667 Cb. Three of those stars were in the original CARMENES GTO sample but they were stopped after 20–30 RV-measurements, because the planet discoveries were already published by the HARPS team. The CARMENES measurements were published in Trifonov et al. (2018). This introduces an observational bias. As those signals are not confirmed by CARMENES data alone, those planets are not included in the planet sample of this thesis.

Including two more planets in our earlier M dwarf sample and one in our later M dwarf sample would alter the occurrence rates as follows:

- the overall occurrence rate in this bin would increase from $f = 0.26^{+0.16}_{-0.09}$ to $f = 0.33^{+0.15}_{-0.10}$,
- the occurrence rate of the earlier M dwarf sample would increase from $f < 0.09$ to $f = 0.10^{+0.10}_{-0.065}$,
- the occurrence rate of the later M dwarf sample would increase from $f = 0.60^{+0.35}_{-0.25}$ to $f = 0.73^{+0.35}_{-0.30}$.

The three planets included in the HARPS statistics of the 10–100 d and 1–10 $\mathrm{M}_\oplus$ bin are Gl 581 c and d and Gl 667 Cc. Both planet hosts are in our low mass planet sample but with 0.33 $\mathrm{M}_\odot$ (in CARMENES) and 0.32 $\mathrm{M}_\odot$ (Anglada-Escudé et al. 2013) they are still three times as heavy as our very low mass planet hosts. Our results suggest that early M stars have a low planet occurrence rate of less than 9 % in the 1–10 d and 1–10 $\mathrm{M}_\oplus$ period-mass bin (see table 3.5). The HARPS results suggest the exact opposite. This could mean that the fraction of low mass planets close to their star increases for lighter stars than 0.33 $\mathrm{M}_\odot$.

I find a similar discrepancy of the results for planets with $M \sin i > 10\,\mathrm{M}_\oplus$. The HARPS results suggest a higher planet frequency closer to the host star but CARMENES results suggest the opposite.

One possibility could be that we have already detected all planets with $M \sin i > 10\,\mathrm{M}_\oplus$ in the CARMENES sample such that an occurrence rate study of the whole sample will lead to a lower occurrence rate in the 10–100 d bin. Therefore I ran the occurrence rate study on the whole sample. The result in the 10 to 100 d and 10 to 100 $\mathrm{M}_\oplus$ bin is $f = 0.025^{+0.02}_{-0.015}$ and in the 1 to 10 d bin it is $f = 0.008^{+0.005}_{-0.008}$. This means that the frequency increase towards longer periods persists.

As we find all of the planets in this bin around our earlier M dwarf (higher mass) sample, the mass distribution of the host stars cannot explain this. A future study of combined HARPS and CARMENES occurrence rate could resolve this issue.

3.4.3 The effect of eccentricity and multiplicity

Most of the detection probability analyses for RV-surveys assume circular orbits of single planets. In the following sections I will show why this is a reasonable simplification.

In order to include eccentricity and multiplicity in our injection-and-retrieval experiment I would have to make some strong assumptions on the underlying distributions. The problem is the following: our knowledge on the eccentricity distribution is limited as highly eccentric orbits reduce the detectability in transiting and RV-surveys.

Multi planet systems

Multi planet systems can have an impact on the planet detectability. It is thus necessary to find out what the impact of the assumption of single planets is and how it affects the results. Garcia-Piquer et al. (2017) retrieved only around 3 % of their simulated multi-planet systems completely. A lot of planets in their simulation had such a low mass that they cannot be detected by current RV surveys. For this reason the probability to detect all planets of a multi-planet system is very low. Hatzes (2019) ran a simulation with the TRAPPIST-1 system as an example. It shows that at an RMS value of $3\,\mathrm{ms}^{-1}$ around 500 numbers of observations are needed to find all the seven planets but the first planet can already be identified with 60 numbers of observations.

The results of Tremaine & Dong (2012) on the other hand imply that it is mostly valid to approximate multi-planet systems as several single planet systems ("approximation of separability").

To estimate the effect of multi-planetary systems in our survey I use an artificial planet population (Burn et al. 2020). The accuracy of the model is not crucial to the success of this test as I only need several input planets in realistic orbit and mass configurations. The artificial sample consists of around 4x700 planet systems. The artificial host stars have stellar masses of $0.1\,\mathrm{M}_\odot$, $0.3\,\mathrm{M}_\odot$, $0.5\,\mathrm{M}_\odot$ and $0.7\,\mathrm{M}_\odot$. Almost every star of the artificial population is the host of a multi-planet system. I randomly draw 125 planet

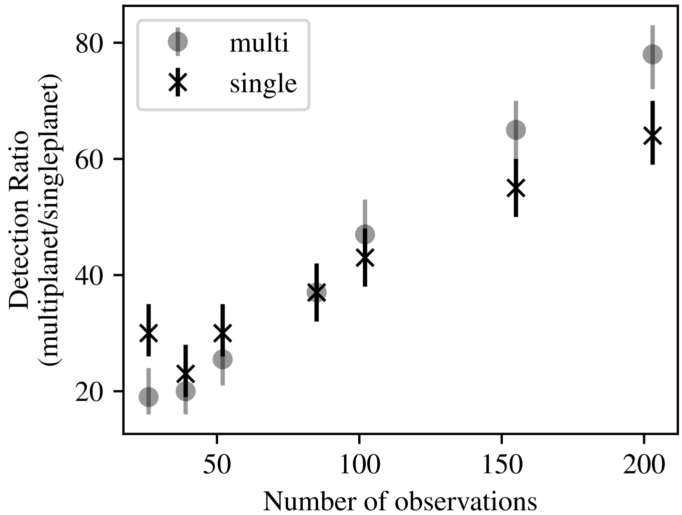

Figure 3.7: absolute number of retrieved planet hosts from artificial sample out of 130

hosts in the same mass distribution as in the real CARMENES sample. I use this as the first population. I construct a second population consisting of only the single planet with the highest RV-amplitude out of the first population. To obtain realistic measurement errors and time stamps I randomly pick CARMENES time series with 26, 39, 52, 85, 102, 155 and 203 number of observations. On top of these time series I insert the artificial planets with 50 random inclinations, phase angles and orientation of the ellipse in the orbital plane. The mutual inclinations are taken from the planet population.

In the multi-planet mode I detected significant signals (i.e. FAP $< 1\,\%$) in the periodogram of $7\,\%-49\,\%$ of the planet hosts in comparison to $11.6\,\%-41\,\%$ in the single planet mode. The ratio of significant signals detected in the multi-planet mode to those detected in the single planet mode depends on the number of observations (see figure 3.7). With 26 RV measurements around $60\,\%$ of multi-planet hosts can still be identified in comparison to single planet hosts. Starting from around 80 RV measurements multi-planet systems begin to be more likely to be detected than the corresponding single planet system. At the level of 50 observations $80\,\%$ of the multi-planet hosts can be identified.

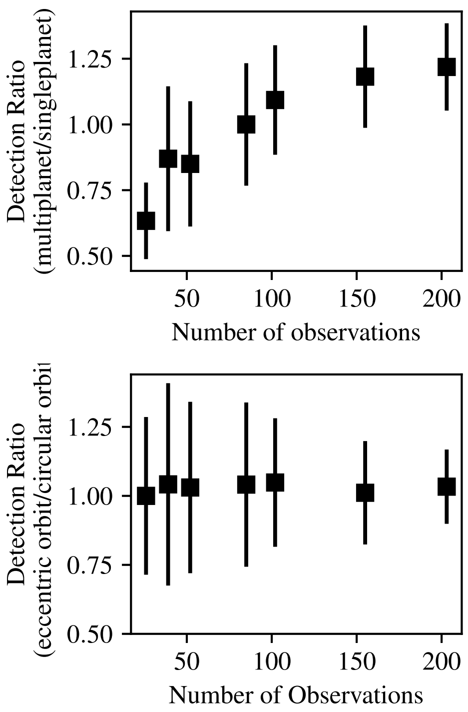

Figure 3.8: fraction of retrieved planets – Nobs

With data from the Kepler satellite a statistics for multi-planet systems can be derived. The geometrics that limit transit surveys lead to a slight underestimation of multiplicity (Garcia-Piquer et al. 2017). Nevertheless I adopt the multiplicity from Garcia-Piquer et al. (2017) for an estimate its effect on the true exoplanet frequency. With data from the *Kepler* satellite the authors derived a frequency of 58.9 % for single planet systems, 26.5 % for double planet systems, 8.6 % for triple, 4.3 % for quadruple, 1.3 % for quintuple 0.2 % for sextuple, and 0.2 % for heptuple planet systems.

I estimate how many planets we might "lose" with the "approximation of separability". For this estimate, I assume that all of the stars in our sample host planets. In this case roughly 60 % are single planet host which means that 75 multi-planet hosts remain. Half of our stars have 53 or less observations. Roughly 75 % of multi-planet hosts can be identified among them, which means, we "lose" only 25 %. In this case only 9 multi-planet hosts are lost (7 % of the planet hosts we put in originally). Considering that the uncorrected planet occurrence rate is 28/125 = 22.4 %, this number of lost multi-planet hosts shrinks to 2.

Therefore, I conclude that missed multi-planet systems have a very low influence on the planet occurrence rate. Therefore, treating multi-planet systems as several single planet systems is a reasonable simplification used in occurrence rate studies.

Eccentric orbits

Cumming (2004) stated that the periodogram itself is sensitive for most eccentric orbits with $e < 0.4$. The observed eccentricity distribution parameterized as described in Kipping (2013) (see figure 3.9) shows that around 80 % of the detected planets fall under this criterion. If I include eccentricity in our injection and retrieval experiment, consequently I do not see much of a difference on the 90 % detection threshold. The difference occurs in the 90–100 % detection probability area where some of the orbits cannot be detected with our sampling. To calculate the completeness map I count every grid point with a detection probability of more than 90 % as a detection. Therefore the effect of eccentric orbits is negligible.

To double check this effect I ran a similar test as for the multi-planet systems. I took the same data set with 26, 39, 52, 85, 102, 155 and 203 number of observations. Using the the artificial planet population I compared the single planet systems with the same set of single planet systems with eccentricities set to zero. The resulting correction factor is close to one for all numbers of observations (see figure 3.8). In the artificial population high eccentricities are very rare as well.

With either the observed eccentricity distribution or the artificial population as a test I therefore conclude that using circular orbits for our completeness map is reasonable. Therefore neither eccentric orbits nor multiple planets significantly alter the planet statistics.

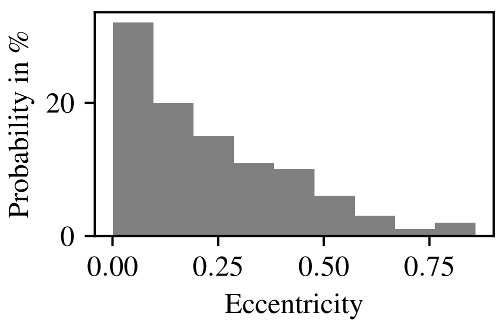

Figure 3.9: Observed eccentricity distribution as in (Kipping 2013)

3.4.4 Number of observations needed

The detection probability of Earth like planets in our sample is quite low. Figure 3.5 implies that it is zero on average for periods up to 240 d for planets around our early M dwarfs and close to zero for planets around our later M dwarfs. For this reason, it is of interest how many observations are needed to find a planet of this mass around an M dwarf.

I selected three example stars with masses $M_{star} = 0.17\ M_{\odot}$; $M_{star} = 0.315\ M_{\odot}$ and $M_{star} = 0.51\ M_{\odot}$, of which more than 200 RV values were obtained with CARMENES. I sequentially removed RV measurements to find out how this affects the detection probability. As the phase coverage of the RV data typically got better towards later observing times, I deleted points starting from the beginning until only 20 RV measurements remained. For each data set I computed detection maps. I identified the lowest mass synthetic planet that could be retrieved with a 50 % detection probability. The same was done for the 16 % and 84 % detection probability level. The results are shown in figures 3.10 and 3.11. In the figures the $1\,M_{\oplus}$ level is indicated with a dashed gray line. The 50 numbers of observations threshold is highlighted as well, as CARMENES observations are completed at this amount of measurements if no interesting signal is present.

With 50 measurements I could not detect an Earth mass planet in a 10 d orbit around the three stars with different masses. In the low mass case I could see the signal of a $1.8\,M_{\oplus}$ planet. Starting from around 80 numbers of observations I get a detection probability of 14 % and starting from 100 numbers of observations it increases to 50 %. To get an Earth like planet at a 10 d period with 84 % detection probability at least 400 RV-measurements are required.

In the case of the $M_{star} = 0.315\ M_{\odot}$ star an Earth like planet could be detected in a 1.4 d period orbit with 200 observations. A similar longer period planet would be undetected even with 200 RV measurements. With 50 RV-values we could find a $2\,M_{\oplus}$ planet at a 1.4 d orbit and a $3.5\,M_{\oplus}$ planet at a 10 d orbit.

Around the early M dwarf with $M_{star} = 0.51\ M_{\odot}$ an Earth mass planet cannot be detected although there are 370 observations. The lowest mass planet, that could be detected in a 10 d orbit has a mass of around $3\,M_{\oplus}$. With 50 observations we could see the signal of a $5\,M_{\oplus}$ planet.

Keeping this result in mind, it is obvious, why the four low mass planets

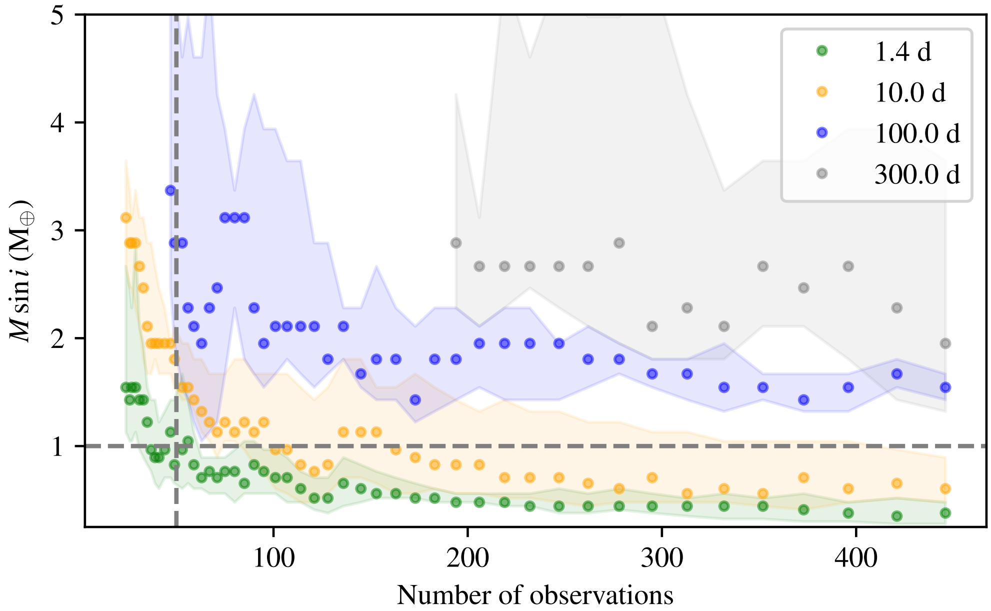

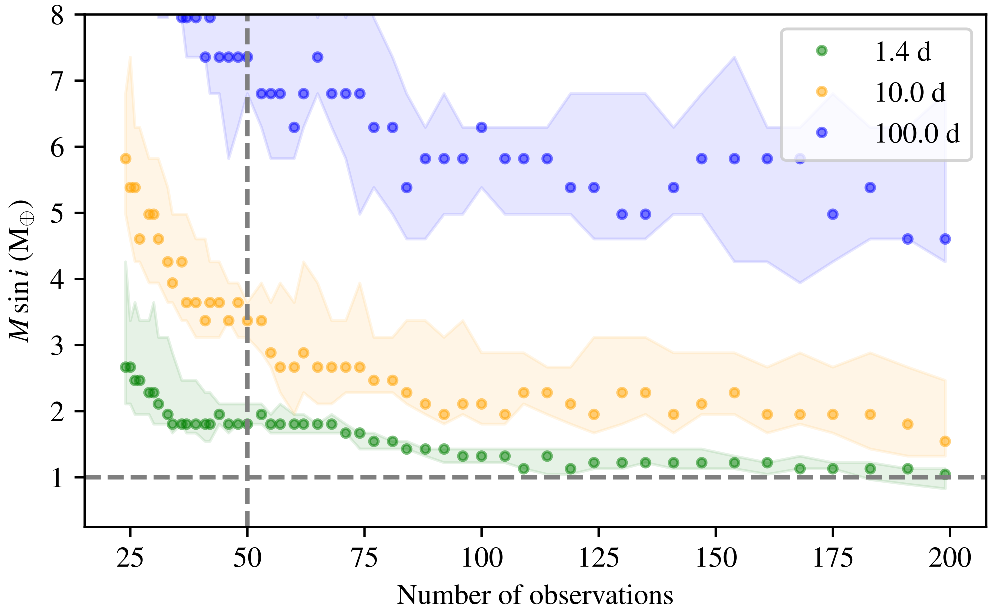

Figure 3.10: Upper limit for masses at different numbers of observations; dots are at 50 % detection probability, filled area is 16 % and 84 % detection probability; upper panel: late M dwarf with $M_{star} = 0.17\ M_{\odot}$; lower panel: earlier M dwarf with $M_{star} = 0.315\ M_{\odot}$

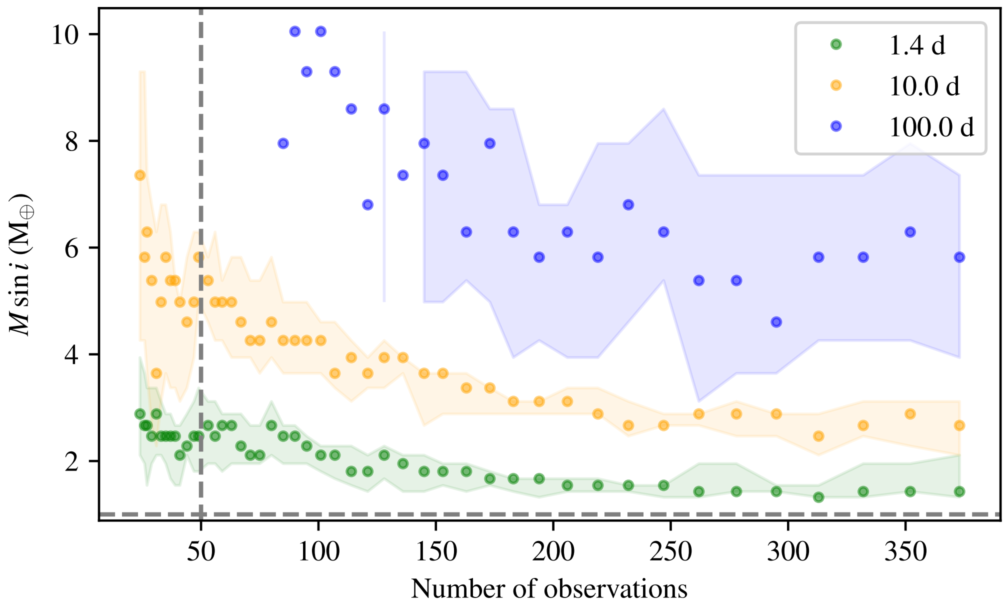

Figure 3.11: Upper limit for masses at different numbers of observations; dots are at 50 % detection probability, filled area is 16 % and 84 % detection probability; earlier M dwarf with M_{star}= 0.51 $M_\odot$ and strong activity signal at the rotation period

in our sample are orbiting very low mass stars. This does not mean that higher mass M stars do not host very low mass planets of less than $2\,M_\oplus$ but with CARMENES we cannot determine their frequency. In this simulation I included the activity of the stars by using the actual RV-values. Most M stars are active stars and even a perfect instrument could not detect such planets if the RV-jitter due to activity is not mitigated.

The upper limit of planets that we can detect depends not only on the stellar mass, but also on the intrinsic RMS scatter of the observations. Our three stars have RMS of $2.6\,\mathrm{ms}^{-1}$ ($M_{\mathrm{star}} = 0.17\ M_\odot$), $2.9\,\mathrm{ms}^{-1}$ ($M_{\mathrm{star}} = 0.315\ M_\odot$) and $2.98\,\mathrm{ms}^{-1}$ ($M_{\mathrm{star}} = 0.51\ M_\odot$). The RMS scatter of these stars are lower than the median value of the CARMENES sample, but there are stars that show even lower scatter. For this reason, I plot the 50 % upper limits in K-amplitude normalized to the RMS (figure 3.12).

I fit the result with a power law:

$$f(x) = a \cdot x^{-b} + c. \tag{3.8}$$

From the result of the fit I conclude that for our sample $\frac{K}{\sigma} \propto \frac{1}{n_{obs}}$ – at least at a period of 10 d. The plot shows that there is a significant improvement in $\frac{K}{\sigma}$ from 50 to 200 numbers of observations but more observations do not significantly improve the K to RMS ratio.

(a) K amplitude/RMS for a star with M_{star}= 0.17 $M_\odot$

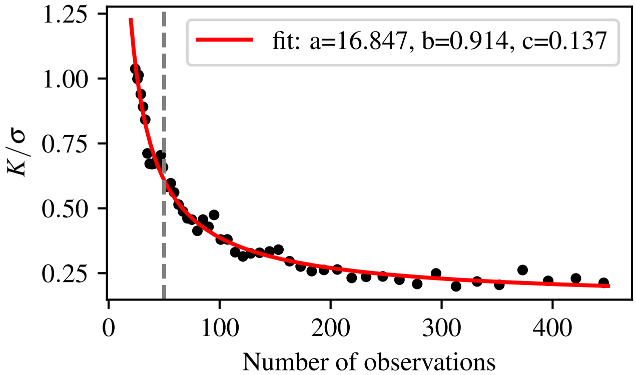

(b) K amplitude/RMS for a star with M_{star}= 0.315 $M_\odot$

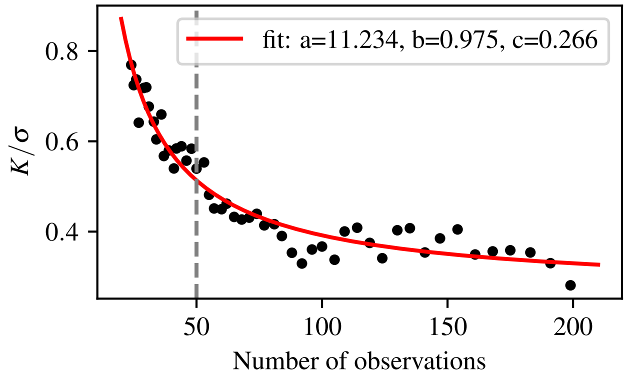

(c) K amplitude/RMS for a star with M_{star}= 0.51 $M_\odot$

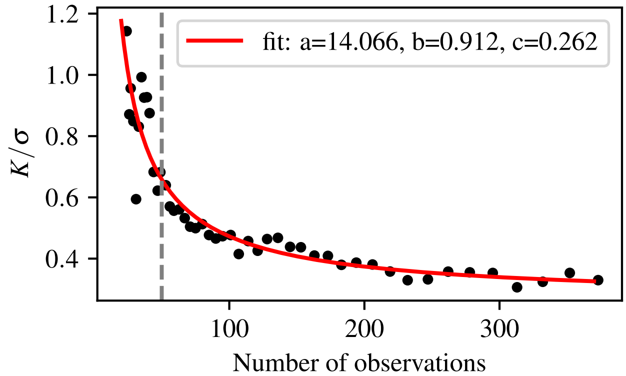

Figure 3.12: K amplitude/RMS of the time series vs. number of observations for three different stars with masses of (a) M_{star}= 0.17 $M_\odot$, (b) M_{star}= 0.315 $M_\odot$ and (c) M_{star}= 0.51 $M_\odot$ at the period of 10 d. A power law fit is plotted in red.

3.4.5 Comparison with planet population synthesis

I compare our results to the artificial planet population from planet population synthesis models (see section 3.4.3). The artificial planets are from the next generation Bern models that form large amounts of artificial planet systems with the core accretion planet formation mechanism (e.g. Mordasini et al. 2012; Emsenhuber et al. 2020a; Schlecker et al. 2020). These models are currently extended to low mass stars (Burn et al. 2020). From such a preliminary artificial population, I plot a subset of the population that is comparable in host star mass distribution into the completeness map (see figure 3.13).

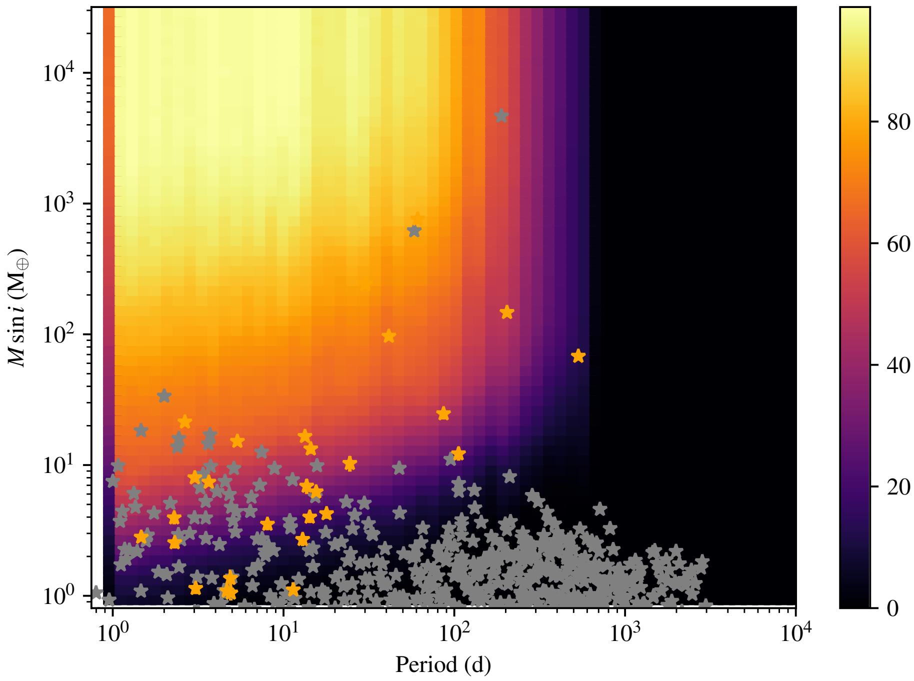

Figure 3.13: CARMENES completeness with artificial planet population overplotted in gray (CARMENES planets in orange)

It becomes obvious that most artificial planets have periods and masses that are not detectable with CARMENES. My results from section 3.4.4 imply that the vast majority of the synthetic planets cannot be detected even with a very high amount of measurements. In a future project I want to assign CARMENES time series to the synthetic populations and assign

Table 3.11: Planet occurrence rates f from planet population synthesis in red, from the HARPS survey (Bonfils et al. 2013) in blue and CARMENES results in black.

	Period (d)	
m sin i ($M_\oplus$)	1–10	10–10^2
10–10^2	$f = 0.07 \pm 0.03$	$f = 0.01 \pm 0.01$
	$f = 0.03^{+0.04}_{-0.01}$	$f < 0.02$
	$f = 0.025^{+0.03}_{-0.025}$	$f = 0.06^{+0.05}_{-0.03}$
1–10	$f = 0.52 \pm 0.10$	$f = 0.74 \pm 0.11$
	$f = 0.36^{+0.24}_{-0.10}$	$f = 0.52^{+0.50}_{-0.16}$
	$f = 0.26^{+0.26}_{-0.09}$	$f = 0.40^{+0.25}_{-0.20}$

detection probabilities to each planet in collaboration with Martin Schlecker at the MPIA in Heidelberg. The goal is to obtain an observable population that can be directly compared to the real planet sample.

Nevertheless, I can already compare the occurrence rates in four of the period-mass bins obtained from theory, HARPS and from our sample (see table 3.11). The theoretical sample is consistent with the HARPS and CARMENES occurrence rates in the sense that most artificial planets are in the 10–100 d and 1–10 $M_\oplus$ period-mass bin. It is also consistent with HARPS in the sense that the least amount of planets is expected in the 10–100 d and 10–100 d period-mass bin. In this bin it is inconsistent with our results from CARMENES. For that reason it is of importance to resolve the true exoplanet frequency of that bin in the future. It can give helpful clues on where the planet population synthesis models have to be better adapted to low mass stars. The overall higher frequencies are expected due to the fact that by construction of the models multi-planet systems with a lot of planets are favored.

3.4.6 Implications for the CARMENES legacy program

The CARMENES data that has been obtained up to now allows to determine the frequency of planets with $M_{\rm pl} > 10 M_\oplus$ in orbits shorter than 100 d. With more data we could additionally resolve the frequencies of long-period planets and of low-mass planets with masses from $1\,\mathrm{M}_\oplus$ to $10\,\mathrm{M}_\oplus$:

1. As shown in figures 3.10 and 3.11 we know that with 50 observations, we can detect planets with masses of $3\,\mathrm{M}_\oplus$ to $10\,\mathrm{M}_\oplus$ in a 100 d orbit depending on the host star mass. In this thesis, I analyze only orbital periods until half of the time baseline. If you do not apply this strict criterion, the occurrence rates of this bin become smaller than those in the shorter period bin (see master theses of Juan Carlos Muños and Iván Muños). The current theoretical planet population models also predict a lack of planets with masses of $10\,\mathrm{M}_\oplus$ or more for periods longer than 10 d. Therefore, we should aim for obtaining the same number of measurements spread over a longer period of time in order to obtain a longer time baseline of the observations. In this way we can probe the 100-1000 d bin for this mass range in the future.
2. Secondly, and maybe more importantly, we should aim at resolving the discrepancy of planet occurrence rates of planets less massive than $10\,\mathrm{M}_\oplus$ in short period orbits around our sample of stars with lower mass (stars with $M_\star < 0.337\,\mathrm{M}_\odot$). The stars with lower mass are ideal for observations with CARMENES as they mostly emit in a wavelength region that cannot be observed as well with most other instruments. Out of this sample we should randomly select 10 inactive stars for which we increase the amount of RV-measurements to 200. However, one could argue that this will introduce a bias towards inactive stars. This is the case only if the planet population of active stars is different from that of inactive stars. Up to now planet formation models do not include stellar activity. Therefore, the RV quiet sample in fact is a better test sample for those theories than the whole sample. In addition to that we have to avoid active stars as it is more difficult to detect small mass planets around them.

   The aim of this strategy is to get a more homogeneous sample that can be probed down to lower mass stars. The different results of the two occurrence rate methods are mainly due to a very large range of upper limits of the 125 star sample. The occurrence rate of this highly observed sample will have large error bars but the number of stars is sufficient to distinguish between 1.6 planets per star or 0.6 planets per star. In the first case, we expect around 16^{+4}_{-3} planet discoveries and in the second case only 6^{+3}_{-3}. In the 10–100 d bin this strategy will also significantly improve the statistics. My results suggest that the planet frequency is lower in this bin than that of the short period bin. If future observations support those results, this would challenge planet formation theories.

Chapter 4

Conclusion

The aim of this thesis is to study the frequencies of planet around A and M type stars. As A stars are heavier and M stars are lighter than the stars typically studied, my results can be used to test planet formation theories as a function of stellar mass. To this end, I have analyzed radial velocity data from the OES and TCES spectrographs in Ondřejov and Tautenburg, radial velocity data from the CARMENES spectrograph and photometric data from the *Kepler* space mission.

I have tested the hypothesis of a very high close-in giant planet occurrence rate of 8.4 % around main-sequence A-type stars. The hypothesis was formulated by Balona (2014) based on periodic variations in *Kepler* light curves that could originate from a sub-stellar companion. I have studied the radial velocities of six stars out of a sample of the 166 A-type stars with a proposed planetary companion. I have obtained upper limits that are clearly in the planetary regime such that I can rule out a close-in stellar companion as a cause of the observed light curve variations.

From the sample of roughly 2000 Kepler A stars I can statistically rule out such a very high frequency of giant planets. I have derived an upper limit of 0.75 % with the most probable frequency being much lower with about 0.15 %. This is further evidence that close-in giant planets are very rare around A-type stars and probably even rarer than around G-type stars.

This is expected from theory and protoplanetary disk observations. Giant planets in total are expected to be more frequent around this type of stars, as the protoplanetary disk is observed to have a higher mass. Therefore it has more material to form planets. On the other hand this also results in a shorter disk lifetime and consequently in a shorter migration timescale. For this reason giant planets maybe do not have enough time to migrate inwards such that their periods are in general longer. This leads to a lower number of close-in giant planets as compared to giant planets at longer periods.

Considering the lower protoplanetary disk mass of M stars, we expect a generally lower giant planet occurrence rate. I have studied a subset of 125 stars out of the 300 stars in the CARMENES M dwarf survey. From this sample I have obtained planet frequencies for different mass and period bins. My results support a lower giant planet frequency in orbits longer than 10 d and they also support a similar or lower frequency of close-in giant planets as compared to G-type stars. In fact, the planet with the highest mass in short period orbits detected with CARMENES has a mass of only $14\,\mathrm{M}_\oplus$. My upper limits for the close-in giant planet occurrence are higher than the frequencies published for G-type stars. For this reason a much larger sample of stars needs to be observed in order to obtain tighter upper limits.

In the intermediate mass range of 10–$100\,\mathrm{M}_\oplus$ my CARMENES results indicate an increased frequency towards longer periods in contradiction to earlier results from HARPS and planet population synthesis. The HARPS M dwarf planet statistics includes no planet detections, whereas I include four or five planet detections in this mass-period range. The planet frequency, I determined in this thesis, increases from $2.5^{+3}_{-2.5}\,\%$ in the 1–10 d bin to $6^{+5}_{-3}\,\%$ in the 10–100 d bin. A bias could be introduced by the selection of 125 out of over 300 target stars. Even if this was the case, the frequency increase towards higher periods would be supported by the large data set as well.

Planets with masses lower than $10\,\mathrm{M}_\oplus$ are very numerous around G-type stars. Results from the *Kepler* mission hint towards an even higher number of small mass planets around low mass stars. I have retrieved occurrence rates from my detection limits with two different methods. For higher masses those methods produce similar results. In the lower mass regime the completeness is inhomogeneous across the period-mass bins. As a consequence I have obtained very different low mass planet frequencies. With the first method of essentially averaging the detection limits throughout the period-mass bin I have obtained a frequency of 66 % for periods up to 100 d. This is consistent with small mass planet frequencies known for G-type stars. The second method assigns a number of missed planets associated with every planet detection. With this method I have found an occurrence rate of 1.8 planets per star. This is a lot higher than the number of planets around solar like stars. Nevertheless, this number is consistent with some of the *Kepler* frequencies of low mass planets around M dwarfs. In order to unify the results of both methods, we need to gather a higher number of observations per star. My results suggest that this number should be around 200 for 10 quiet low-mass stars. This could be the aim of an extended CARMENES legacy program.

Bibliography

Alibert, Y., Mordasini, C., & Benz, W. 2011, A&A, 526, A63

Alibert, Y., Mordasini, C., Benz, W., & Winisdoerffer, C. 2005, A&A, 434, 343

Amado, P., Bauer, F., Rodriguez Lopez, C., Rodriguez, E., & Lopez-Gonzales, M. 2020, in prep., A&A

Anderson, D., Temple, L., Nielsen, L., et al. 2018, arXiv preprint arXiv:1809.04897

Andrews, S. M., Rosenfeld, K. A., Kraus, A. L., & Wilner, D. J. 2013, ApJ, 771, 129

Anglada-Escudé, G. & Butler, R. P. 2012, ApJS, 200, 15

Anglada-Escudé, G., Tuomi, M., Gerlach, E., et al. 2013, A&A, 556, A126

Bakos, G., Noyes, R. W., Kovács, G., et al. 2004, PASP, 116, 266

Bakos, G. Á., Csubry, Z., Penev, K., et al. 2013, PASP, 125, 154

Balona, L. 2013, MNRAS, 431, 2240

Balona, L. 2014, MNRAS, 441, 3543

Bashi, D., Helled, R., Zucker, S., & Mordasini, C. 2017, A&A, 604, A83

Bauer, F. F., Zechmeister, M., Kaminski, A., et al. 2020, arXiv e-prints, arXiv:2006.01684

Bayliss, D., Gillen, E., Eigmüller, P., et al. 2018, MNRAS, 475, 4467

Berger, T. A., Huber, D., Gaidos, E., & van Saders, J. L. 2018, ApJ, 866, 99

Bodenheimer, P., Hubickyj, O., & Lissauer, J. J. 2000, Icarus, 143, 2

Böhm, T., Holschneider, M., Lignières, F., et al. 2015, A&A, 577, A64

Bonfils, X., Delfosse, X., Udry, S., et al. 2013, Astronomy & Astrophysics, 549, A109

Borgniet, S., Lagrange, A. M., Meunier, N., & Galland , F. 2017, A&A, 599, A57

Borgniet, S., Lagrange, A. M., Meunier, N., et al. 2019, A&A, 621, A87

Borsa, F., Rainer, M., Bonomo, A. S., et al. 2019, A&A, 631, A34

Borucki, W. J. 2020, arXiv e-prints, arXiv:2005.07831

Borucki, W. J., Koch, D., Basri, G.,

et al. 2010, Science, 327, 977

Borucki, W. J., Koch, D. G., Basri, G., et al. 2011, ApJ, 736, 19

Boss, A. P. 1995, Science, 267, 360

Boss, A. P. 2006, ApJ, 643, 501

Boss, A. P., Butler, R. P., Hubbard, W. B., et al. 2007, Transactions of the International Astronomical Union, Series A, 26A, 183

Bouchy, F. & Sophie Team. 2006, in Tenth Anniversary of 51 Peg-b: Status of and prospects for hot Jupiter studies, ed. L. Arnold, F. Bouchy, & C. Moutou, 319–325

Burke, C. J., Christiansen, J. L., Mullally, F., et al. 2015, ApJ, 809, 8

Burkert, A. & Ida, S. 2007, ApJ, 660, 845

Burn, R., Schlecker, M., Mordasini, C., et al. 2020, in American Astronomical Society Meeting Abstracts, Vol. 236, American Astronomical Society Meeting Abstracts #236, 222.06

Butler, R. P., Marcy, G. W., Williams, E., et al. 1996, PASP, 108, 500

Caballero, J. A., Cortés-Contreras, M., Alonso-Floriano, F. J., et al. 2016, in 19th Cambridge Workshop on Cool Stars, Stellar Systems, and the Sun (CS19), Cambridge Workshop on Cool Stars, Stellar Systems, and the Sun, 148

Chen, G., Guenther, E. W., Pallé, E., et al. 2017, A&A, 600, A138

Cochran, W. D. & Hatzes, A. P. 1994, Ap&SS, 212, 281

Cochran, W. D., Hatzes, A. P., Butler, R. P., & Marcy, G. W. 1997, ApJ, 483, 457

Collier Cameron, A., Guenther, E., Smalley, B., et al. 2010, MNRAS, 407, 507

Cumming, A. 2004, MNRAS, 354, 1165

Cumming, A., Butler, R. P., Marcy, G. W., et al. 2008, PASP, 120, 531

Cumming, A., Marcy, G. W., & Butler, R. P. 1999, APJ, 526, 890

Currie, T. 2009, ApJ, 694, L171

Czesla, S., Schröter, S., Schneider, C. P., et al. 2019, PyA: Python astronomy-related packages

Deleuil, M., Aigrain, S., Moutou, C., et al. 2018, A&A, 619, A97

Díez Alonso, E., Caballero, J. A., Montes, D., et al. 2019, A&A, 621, A126

Donati, J.-F., Kouach, D., Lacombe, M., et al. 2018, SPIRou: A NIR Spectropolarimeter/High-Precision Velocimeter for the CFHT, 107

Dorval, P., Talens, G. J. J., Otten, G. P. P. L., et al. 2020, A&A, 635, A60

Dressing, C. D. & Charbonneau, D. 2013, The Astrophysical Journal, 767, 95

Emsenhuber, A., Mordasini, C.,

Burn, R., et al. 2020a, arXiv e-prints, arXiv:2007.05561

Emsenhuber, A., Mordasini, C., Burn, R., et al. 2020b, arXiv e-prints, arXiv:2007.05562

Endl, M., Cochran, W. D., Kürster, M., et al. 2006, ApJ, 649, 436

Endl, M., Kürster, M., & Els, S. 2000, Astronomy and Astrophysics, 362, 585

Engel, M., Faigler, S., Shahaf, S., & Mazeh, T. 2020, arXiv e-prints, arXiv:2007.13773

Faigler, S. & Mazeh, T. 2011, MNRAS, 415, 3921

Figueira, P., Pepe, F., Lovis, C., & Mayor, M. 2010, A&A, 515, A106

Fischer, D. A. & Valenti, J. 2005, ApJ, 622, 1102

Frasca, A., Molenda-Żakowicz, J., De Cat, P., et al. 2016, Astronomy & Astrophysics, 594, A39

Fressin, F., Torres, G., Charbonneau, D., et al. 2013, ApJ, 766, 81

Fuhrmann, K., Pfeiffer, M. J., & Bernkopf, J. 1997, A&A, 326, 1081

Fulton, B. J., Petigura, E. A., Blunt, S., & Sinukoff, E. 2018, PASP, 130, 044504

Gaia Collaboration, Brown, A. G. A., Vallenari, A., et al. 2018, A&A, 616, A1

Gaia Collaboration, Prusti, T., De Bruijne, J., et al. 2016, Astronomy & Astrophysics, 595, A1

Gaidos, E., Mann, A. W., Kraus, A. L., & Ireland, M. 2016, MNRAS, 457, 2877

Garcia-Piquer, A., Morales, J. C., Ribas, I., et al. 2017, A&A, 604, A87

Gaudi, B. S., Stassun, K. G., Collins, K. A., et al. 2017, Nature, 546, 514

González-Álvarez, E., Zapatero Osorio, M. R., Caballero, J. A., et al. 2020, arXiv e-prints, arXiv:2003.13052

Griffin, R. 1973, MNRAS, 162, 243

Grziwa, S., Pätzold, M., & Carone, L. 2012, MNRAS, 420, 1045

Guenther, E. W., Barragán, O., Dai, F., et al. 2017, A&A, 608, A93

Hardegree-Ullman, K. K., Cushing, M. C., Muirhead, P. S., & Christiansen, J. L. 2019, AJ, 158, 75

Hartman, J. D., Bakos, G. Á., Buchhave, L. A., et al. 2015, AJ, 150, 197

Hatzes, A. 2019, The Doppler Method for the Detection of Exoplanets (IOP Astronomy)

Hatzes, A. P. 2016, in Methods of Detecting Exoplanets (Springer), 3–86

Hatzes, A. P., Endl, M., Cochran, W. D., et al. 2018, AJ, 155, 120

Hatzes, A. P. & Rauer, H. 2015, ApJ, 810, L25

Hellier, C., Anderson, D. R.,

Barkaoui, K., et al. 2019, MNRAS, 490, 1479

Henry, T. J., Jao, W.-C., Subasavage, J. P., et al. 2006, AJ, 132, 2360

Henry, T. J., Jao, W.-C., Winters, J. G., et al. 2018, AJ, 155, 265

Høg, E., Fabricius, C., Makarov, V., et al. 2000, Astron. Astrophys, 355, L27

Howard, A. W., Marcy, G. W., Bryson, S. T., et al. 2012, ApJS, 201, 15

Howard, A. W., Marcy, G. W., Johnson, J. A., et al. 2010, Science, 330, 653

Hsu, D. C., Ford, E. B., & Terrien, R. 2020, arXiv e-prints, arXiv:2002.02573

Ida, S. & Lin, D. N. C. 2005, ApJ, 626, 1045

Ida, S. & Lin, D. N. C. 2008, ApJ, 685, 584

Jackman, J. A. G., Wheatley, P. J., Bayliss, D., et al. 2019, MNRAS, 489, 5146

Johnson, J. A., Fischer, D. A., Marcy, G. W., et al. 2007, ApJ, 665, 785

Johnson, M. C., Rodriguez, J. E., Zhou, G., et al. 2018, AJ, 155, 100

Kabáth, P., Skarka, M., Sabotta, S., & Guenther, E. 2019, Contrib. Astron. Obs. Skalnaté Pleso, 49, 462

Kaeufl, H.-U., Ballester, P., Biereichel, P., et al. 2004, in Society of Photo-Optical Instrumentation Engineers (SPIE) Conference Series, Vol. 5492, Ground-based Instrumentation for Astronomy, ed. A. F. M. Moorwood & M. Iye, 1218–1227

Kaminski, A., Trifonov, T., Caballero, J. A., et al. 2018, A&A, 618, A115

Kanodia, S., Wolfgang, A., Stefansson, G. K., Ning, B., & Mahadevan, S. 2019, ApJ, 882, 38

Kausch, W., Noll, S., Smette, A., et al. 2015, A&A, 576, A78

Kennedy, G. M. & Kenyon, S. J. 2008, ApJ, 673, 502

Kipping, D. M. 2013, MNRAS: Letters, 434, L51

Korth, J., Csizmadia, S., Gandolfi, D., et al. 2019, MNRAS, 482, 1807

Kotani, T., Tamura, M., Nishikawa, J., et al. 2018, in Society of Photo-Optical Instrumentation Engineers (SPIE) Conference Series, Vol. 10702, Ground-based and Airborne Instrumentation for Astronomy VII, 1070211

Kürster, M., Endl, M., Rouesnel, F., et al. 2003, A&A, 403, 1077

Lalitha, S., Baroch, D., Morales, J. C., et al. 2019, A&A, 627, A116

Lambrechts, M. & Johansen, A. 2012, A&A, 544, A32

Lehmann, H., Guenther, E., Sebastian, D., et al. 2015, A&A, 578, L4

Lehmann, H., Southworth, J.,

Tkachenko, A., & Pavlovski, K. 2013, A&A, 557, A79

Lin, D. N. C., Bodenheimer, P., & Richardson, D. C. 1996, Nature, 380, 606

Loeb, A. & Gaudi, B. S. 2003, ApJ, 588, L117

Lund, M. B., Rodriguez, J. E., Zhou, G., et al. 2017, AJ, 154, 194

Luque, R., Nowak, G., Pallé, E., et al. 2018, A&A, 620, A171

Mahadevan, S., Ramsey, L. W., Terrien, R., et al. 2014, in Society of Photo-Optical Instrumentation Engineers (SPIE) Conference Series, Vol. 9147, Ground-based and Airborne Instrumentation for Astronomy V, 91471G

Mann, A. W., Dupuy, T., Kraus, A. L., et al. 2019, ApJ, 871, 63

Mann, A. W., Gaidos, E., Lépine, S., & Hilton, E. J. 2012, ApJ, 753, 90

Marcy, G. W., Butler, R. P., Williams, E., et al. 1997, ApJ, 481, 926

Marois, C., Macintosh, B., Barman, T., et al. 2008, Science, 322, 1348

Marois, C., Zuckerman, B., Konopacky, Q. M., Macintosh, B., & Barman, T. 2010, Nature, 468, 1080

Mayor, M., Marmier, M., Lovis, C., et al. 2011, arXiv e-prints, arXiv:1109.2497

Mayor, M. & Queloz, D. 1995, Nature, 378, 355

Mazeh, T. & Faigler, S. 2010, A&A, 521, L59

Meunier, N., Lagrange, A. M., & De Bondt, K. 2012, A&A, 545, A87

Millholland, S. & Laughlin, G. 2017, AJ, 154, 83

Morales, J. C., Mustill, A. J., Ribas, I., et al. 2019, Science, 365, 1441

Mordasini, C., Alibert, Y., Benz, W., Klahr, H., & Henning, T. 2012, Astronomy & Astrophysics, 541, A97

Mulders, G. D., Pascucci, I., & Apai, D. 2015, ApJ, 798, 112

Nagel, E., Czesla, S., Schmitt, J. H. M. M., et al. 2019, A&A, 622, A153

Newton, E. R., Irwin, J., Charbonneau, D., et al. 2016, ApJ, 821, 93

Nielsen, L. D., Brahm, R., Bouchy, F., et al. 2020, A&A, 639, A76

Ning, B., Wolfgang, A., & Ghosh, S. 2018, ApJ, 869, 5

Nortmann, L., Pallé, E., Salz, M., et al. 2018, Science, 362, 1388

Parviainen, H. 2015, MNRAS, 450, 3233

Pätzold, M. & Rauer, H. 2002, ApJ, 568, L117

Pepe, F., Mayor, M., Rupprecht, G., et al. 2002, The Messenger, 110, 9

Pepper, J., Kuhn, R. B., Siverd, R., James, D., & Stassun, K. 2012, PASP, 124, 230

Pepper, J., Pogge, R. W., DePoy,

D. L., et al. 2007, PASP, 119, 923

Petigura, E. A., Marcy, G. W., Winn, J. N., et al. 2018, AJ, 155, 89

Petigura, E. A., Sinukoff, E., Lopez, E. D., et al. 2017, AJ, 153, 142

Plavchan, P. & Bilinski, C. 2013, ApJ, 769, 86

Pollacco, D. L., Skillen, I., Collier Cameron, A., et al. 2006, PASP, 118, 1407

Pollack, J. B., Hubickyj, O., Bodenheimer, P., et al. 1996, Icarus, 124, 62

Queloz, D., Henry, G. W., Sivan, J. P., et al. 2001, A&A, 379, 279

Quirrenbach, A., Amado, P. J., Caballero, J. A., et al. 2014, Society of Photo-Optical Instrumentation Engineers (SPIE) Conference Series, Vol. 9147, CARMENES instrument overview, 91471F

Rasio, F. A. & Ford, E. B. 1996, Science, 274, 954

Reffert, S., Bergmann, C., Quirrenbach, A., Trifonov, T., & Künstler, A. 2015, A&A, 574, A116

Reichert, K., Reffert, S., Stock, S., Trifonov, T., & Quirrenbach, A. 2019, A&A, 625, A22

Reiners, A., Ribas, I., Zechmeister, M., et al. 2018a, A&A, 609, L5

Reiners, A., Zechmeister, M., Caballero, J. A., et al. 2018b, A&A, 612, A49

Ribas, I., Tuomi, M., Reiners, A., et al. 2018, Nature, 563, 365

Rodríguez Martínez, R., Gaudi, B. S., Rodriguez, J. E., et al. 2019, arXiv e-prints, arXiv:1912.01017

Sabotta, S., Kabath, P., Korth, J., et al. 2019, MNRAS, 489, 2069

Sabotta, S., Schlecker, M., Chaturvedi, P., Guenther, E. W., & et. al. 2020, in prep., A&A

Saio, H., Kurtz, D. W., Murphy, S. J., Antoci, V. L., & Lee, U. 2018, MNRAS, 474, 2774

Schlecker, M., Mordasini, C., Emsenhuber, A., et al. 2020, arXiv e-prints, arXiv:2007.05563

Schneider, J., Dedieu, C., Le Sidaner, P., Savalle, R., & Zolotukhin, I. 2011, A&A, 532, A79

Schweitzer, A., Passegger, V. M., Cifuentes, C., et al. 2019, A&A, 625, A68

Shporer, A., Jenkins, J. M., Rowe, J. F., et al. 2011, AJ, 142, 195

Sikora, J., Wade, G., & Rowe, J. 2020, arXiv e-prints, arXiv:2009.04039

Sikora, J., Wade, G. A., & Rowe, J. 2018, in 3rd BRITE Science Conference, Vol. 8, 141–145

Simpson, E. K., Baliunas, S. L., Henry, G. W., & Watson, C. A. 2010, MNRAS, 408, 1666

Sing, D. K. 2010, Astronomy & Astrophysics, 510, A21

Siverd, R. J., Collins, K. A., Zhou,

G., et al. 2018, AJ, 155, 35

Smette, A., Sana, H., Noll, S., et al. 2015, A&A, 576, A77

Spiegel, D. S., Burrows, A., & Milsom, J. A. 2011, ApJ, 727, 57

Stephan, A. P., Naoz, S., & Gaudi, B. S. 2018, The Astronomical Journal, 156, 128

Stock, S., Kemmer, J., Reffert, S., et al. 2020, A&A, 636, A119

Stock, S., Nagel, E., Kemmer, J., et al. 2020, submitted, A&A

Szabó, G. M., Szabó, R., Benkő, J. M., et al. 2011, ApJ, 736, L4

Tal-Or, L., Zechmeister, M., Reiners, A., et al. 2018, A&A, 614, A122

Talens, G., Albrecht, S., Spronck, J., et al. 2017, A&A, 606, A73

Talens, G. J. J., Justesen, A. B., Albrecht, S., et al. 2018, A&A, 612, A57

Talens, G. J. J., Spronck, J. F. P., Lesage, A. L., et al. 2017, A&A, 601, A11

Tremaine, S. & Dong, S. 2012, AJ, 143, 94

Trifonov, T., Caballero, J., Morales, J., Ribas, I., & Reiners, A. 2020, submitted, Science

Trifonov, T., Kürster, M., Zechmeister, M., et al. 2018, A&A, 609, A117

Valenti, J. A., Butler, R. P., & Marcy, G. W. 1995, PASP, 107, 966

Van Dokkum, P. G. 2001, Publications of the Astronomical Society of the Pacific, 113, 1420

Villaver, E. & Livio, M. 2009, ApJ, 705, L81

Villaver, E., Livio, M., Mustill, A. J., & Siess, L. 2014, ApJ, 794, 3

Šubjak, J., Sharma, R., Carmichael, T. W., et al. 2020, AJ, 159, 151

Wang, W., Wang, L., Li, X., Chen, Y., & Zhao, G. 2018, ApJ, 860, 136

Wildi, F., Blind, N., Reshetov, V., et al. 2017, in Society of Photo-Optical Instrumentation Engineers (SPIE) Conference Series, Vol. 10400, Society of Photo-Optical Instrumentation Engineers (SPIE) Conference Series, 1040018

Williams, J. P. & Cieza, L. A. 2011, ARA&A, 49, 67

Wittenmyer, R. A., Butler, R. P., Horner, J., et al. 2020, MNRAS, 491, 5248

Wittenmyer, R. A., Butler, R. P., Tinney, C. G., et al. 2016, ApJ, 819, 28

Wolfgang, A., Rogers, L. A., & Ford, E. B. 2016, ApJ, 825, 19

Wong, I., Shporer, A., Daylan, T., et al. 2020, arXiv e-prints, arXiv:2003.06407

Wright, D. J., Wittenmyer, R. A., Tinney, C. G., Bentley, J. S., & Zhao, J. 2016, ApJ, 817, L20

Wright, J. T., Marcy, G. W., Howard, A. W., et al. 2012, ApJ, 753, 160

Zechmeister, M., Dreizler, S., Ribas, I., et al. 2019, A&A, 627, A49

Zechmeister, M. & Kürster, M. 2009, A&A, 496, 577

Zechmeister, M., Kürster, M., & Endl, M. 2009, A&A, 505, 859

Zechmeister, M., Reiners, A., Amado, P. J., et al. 2018, A&A, 609, A12

Zhou, G., Bakos, G. Á., Bayliss, D., et al. 2019a, AJ, 157, 31

Zhou, G., Huang, C. X., Bakos, G. Á., et al. 2019b, AJ, 158, 141

Zhou, G., Rodriguez, J. E., Collins, K. A., et al. 2016, AJ, 152, 136

Appendix A

RV data

MASCARA-1-b Tautenburg data					
time (bjd) +2450000	RV ($\frac{m}{s}$)	RV err ($\frac{m}{s}$)	time (bjd) +2450000	RV ($\frac{m}{s}$)	RV err ($\frac{m}{s}$)
7966.36	2103	874	7971.58	1328	536
7966.39	2101	1027	7971.55	1253	1104
7966.43	1931	608	7973.36	1242	539
7966.46	1349	382	7973.38	1594	864
7966.47	1395	493	7973.4	2265	780
7966.49	1735	820	7973.42	1389	1125
7971.39	1494	1223	7973.44	1725	580
7971.4	1833	591	7973.47	2027	510
7971.42	1363	484	7973.49	2488	303
7971.43	1404	404	7973.51	1728	425
7971.45	2559	538	7973.53	1421	849
7971.46	2393	1360	7973.55	1350	546
7971.48	1185	863	7973.57	1306	506
7971.49	1802	565	7973.59	877	613
7971.53	539	704	7979.34	2343	1029
7971.54	2554	758	7979.37	2170	1046
7971.55	820	1189	7979.39	2065	844
7971.57	1370	1163	7979.41	2152	682
7971.58	2285	1002	7979.43	1557	1037
7971.56	1885	465	7979.45	2510	512
7972.45	873	334	7979.47	1102	270
7972.47	667	869	7979.49	1376	1076
7972.48	978	799	7979.51	1806	337
7972.49	1345	267	7979.53	1706	353
7971.51	1046	683	7979.56	1521	736
7971.52	2120	836	7979.58	1812	892
7971.54	1119	584	7979.56	1268	1140
7971.55	1709	945	7980.33	2020	421
7971.56	1412	443			

Table A.1: Barycentric Julian dates at mean exposure and the radial velocities determined from cross-correlation.

MASCARA-1-b Tautenburg data					
time (bjd) +2450000	RV ($\frac{m}{s}$)	RV err ($\frac{m}{s}$)	time (bjd) +2450000	RV ($\frac{m}{s}$)	RV err ($\frac{m}{s}$)
7980.35	2402	303	7998.34	670	489
7980.38	2393	1133	7998.36	821	754
7980.4	1766	898	7998.38	768	1266
7980.42	1071	468	7998.45	1397	692
7980.46	1539	1061	7998.47	825	1287
7979.53	1244	859	7998.49	1159	1032
7980.55	983	694	7998.51	1612	989
7980.57	401	1265	7998.54	621	1372
7980.59	761	808	7999.36	1129	1874
7995.33	2291	455	7999.51	1262	1040
7995.35	1460	882	7999.53	1603	1099
7995.37	1389	338	7999.55	1572	507
7995.4	867	470	8000.41	315	1087
7995.42	1637	770	8000.43	626	834
7995.43	1225	566	8000.45	840	762
7995.44	102	1260	8000.47	937	828
7995.46	834	1219	8000.49	508	437
7995.47	953	851	8000.51	197	592
7995.49	628	633	8000.53	891	432
7995.5	-309	662	8000.55	1091	426
7995.52	611	1003	8000.57	1388	1534
7995.53	309	916	8001.39	945	514
7995.54	624	505	8004.37	1454	643
7995.57	1281	1758	8007.41	251	1559
7995.59	734	1520	8008.49	513	1610
7996.37	-418	2582	8012.46	979	580
7996.39	-3	2173	8013.4	549	952
7996.41	-54	2306	8014.3	1479	592

Table A.2: Barycentric Julian dates at mean exposure and the radial velocities determined from cross-correlation.

MASCARA-1-b Ondřejov data		
time (bjd) +2450000	RV $(\frac{m}{s})$	RV err $(\frac{m}{s})$
8313.41	791	1156
8313.48	5211	1054
8313.51	2453	2798
8313.54	2959	3167
8313.59	6032	3331
8314.56	2375	364
8314.41	1465	1712
8314.43	1412	1729
8334.4	2874	473

Table A.3: Barycentric Julian dates at mean exposure and the radial velocities determined from cross-correlation.

KIC 3766112 Tautenburg data			KIC 4944828 Tautenburg data		
time (bjd) +2450000	RV $(\frac{m}{s})$	RV err $(\frac{m}{s})$	time (bjd) +2450000	RV $(\frac{m}{s})$	RV err $(\frac{m}{s})$
7557.49	-469	1402	7557.51	942	982
7558.46	74	1080	7558.51	-499	1016
7562.48	-1348	569	7562.51	970	1384
7563.49	-909	1604	7563.51	653	1396
7564.48	-976	1159	7564.51	232	1254
7566.51	-815	316	7585.49	246	897
7592.39	-1121	895	7585.53	-344	1039
7585.47	-1098	711	7588.52	-217	1315
7588.5	-1292	1818	7625.41	-122	887
7625.39	-848	801	7625.41	-122	887
7625.39	-848	801	7880.47	1000	976
7883.51	-366	1144	7883.53	515	962
7884.48	-889	1219	7884.5	454	704
7889.51	576	2206	7889.45	810	744
7911.45	798	989	7911.42	572	1146
7918.5	-209	1294	7918.53	-1075	620
7924.47	-910	1675	7923.47	360	892
7940.42	-477	656	7923.53	864	1073
7944.45	-2435	666	7924.49	320	1326
8001.46	-3458	207	7940.45	636	972
8008.38	-1139	348	7944.36	-790	569
8009.43	-1241	1297	7944.37	-332	1109
8012.36	-1535	1532	8001.53	-351	1132
8013.51	-2304	263	8007.46	-1321	675
8014.5	-2067	829	8008.41	-1314	1270
			8012.39	510	805
			8012.51	-149	705
			8014.39	-315	590
			8014.52	33	871

Table A.4: Barycentric Julian dates at mean exposure and the radial velocities determined from cross-correlation.

KIC 4944828 Ondřejov data		
time (bjd) +2450000	RV ($\frac{m}{s}$)	RV err ($\frac{m}{s}$)
7884.52	-279	1023
7892.47	-1641	1105
7905.39	1051	994
7926.51	113	1120
7929.41	-896	1135
7935.52	260	849
7946.36	402	787
8314.48	-89	111
8334.5	220	959

Table A.5: Barycentric Julian dates at mean exposure and the radial velocities determined from cross-correlation.

KIC 7352016 Tautenburg data			KIC 7777435 Tautenburg data		
time (bjd) +2450000	RV $(\frac{m}{s})$	RV err $(\frac{m}{s})$	time (bjd) +2450000	RV $(\frac{m}{s})$	RV err $(\frac{m}{s})$
7557.42	-325	1115	7557.53	206	977
7558.42	-653	303	7558.52	479	1154
7562.41	-172	951	7562.53	238	1235
7563.41	-711	1164	7563.53	380	531
7564.38	-740	829	7564.53	410	943
7566.41	-585	775	7585.51	128	864
7589.43	-1664	666	7588.42	846	968
7585.40	-454	1278	7588.54	-574	1348
7588.45	-1176	1129	7625.43	69	951
7625.33	-778	657	7883.55	435	815
7625.52	-2699	1042	7884.52	108	1112
7880.49	-300	891	7889.48	1400	1186
7883.46	-298	538	7911.47	528	785
7884.43	-808	847	7919.44	-1099	1427
7884.56	-1454	618	7923.49	-423	1062
7914.43	-452	1040	7924.50	-225	877
7919.42	475	643	7940.49	538	747
7923.41	298	392	7944.39	309	759
7924.42	-926	1048	8001.55	170	842
7940.47	-239	1095	8007.44	-674	765
7944.47	-1608	617	8008.42	-1073	975
8001.49	-2128	1345	8012.40	12	1339
8008.33	-706	1178	8012.53	-182	910
8009.38	-1196	1111	8014.41	486	1082
8012.32	-1363	1003	8014.54	-185	463
8013.49	-2296	1035			
8014.45	-2559	1071			

Table A.6: Barycentric Julian dates at mean exposure and the radial velocities determined from cross-correlation.

KIC 9222948 Tautenburg data			KIC 9453452 Tautenburg data		
time (bjd) +2450000	RV $(\frac{m}{s})$	RV err $(\frac{m}{s})$	time (bjd) +2450000	RV $(\frac{m}{s})$	RV err $(\frac{m}{s})$
7557.44	-668	893	7557.40	-13	1176
7558.44	-316	737	7558.39	-461	1197
7562.46	-450	771	7562.38	256	1553
7563.46	-272	836	7563.38	148	1144
7564.46	-968	1265	7564.41	-1069	1557
7566.49	-1014	1236	7566.38	-350	1111
7590.43	-1583	1348	7568.39	174	609
7585.42	-1530	1150	7585.35	-2035	911
7588.47	-1763	956	7585.37	-1182	1117
7625.36	-1614	825	7625.31	-1147	442
7625.36	-1614	825	7625.31	-1147	442
7880.52	-927	1419	7880.44	28	800
7883.48	-734	1257	7883.43	-124	832
7884.45	-1416	1451	7884.41	-251	527
7889.43	-827	1288	7884.54	-1155	736
7911.49	823	787	7889.54	-992	1270
7912.46	485	627	7912.48	105	571
7919.46	82	1328	7919.49	484	1641
7923.43	0	1196	7923.38	263	565
7924.44	-966	1310	7924.39	-9	1235
7941.44	-511	781	7939.53	262	1212
7944.49	-366	714	7941.47	-519	1215
8001.57	-1764	1428	7942.38	-1558	496
8008.36	-2940	7302	7942.49	-456	1362
8009.41	-1095	1583	8001.51	-2615	1720
8012.34	-809	1645	8008.31	-1489	1240
8014.37	2635	5670	8009.36	-1207	1720
8014.47	-1946	1670	8012.29	-1302	1153
			8013.47	-2342	1423
			8014.43	-2357	1313

Table A.7: Barycentric Julian dates at mean exposure and the radial velocities determined from cross-correlation.

KIC 9222948 Ondřejov data			KIC 9453452 Ondřejov data		
time (bjd) +2450000	RV ($\frac{m}{s}$)	RV err ($\frac{m}{s}$)	time (bjd) +2450000	RV ($\frac{m}{s}$)	RV err ($\frac{m}{s}$)
7892.42	-366	415	7891.41	251	254
7929.45	476	993	7928.46	-3	199
7948.37	405	69	7948.42	-268	115
7995.52	-1512	606	8322.40	-25	126
8334.58	-332	167			

Table A.8: Barycentric Julian dates at mean exposure and the radial velocities determined from cross-correlation.

Appendix B

CARMENES stars and planets

CARM. ID	mass ($M_\odot$)	CARM. ID	mass ($M_\odot$)	CARM. ID	mass ($M_\odot$)
J00051+457	0.565	J04472+206	0.149	J10289+008	0.485
J00067-075	0.114	J04588+498	0.649	J10482-113	0.096
J00183+440	0.449	J05019-069	0.168	J10564+070	0.11
J01013+613	0.442	J05062+046	0.252	J10584-107	0.149
J01019+541	0.127	J05084-210	0.151	J11000+228	0.423
J01025+716	0.512	J05314-036	0.599	J11026+219	0.603
J01026+623	0.597	J05365+113	0.655	J11033+359	0.452
J01033+623	0.203	J06000+027	0.237	J11054+435	0.43
J01125-169	0.132	J06011+595	0.265	J11110+304W	0.5382
J01352-072	0.257	J06103+821	0.458	J11417+427	0.381
J02088+494	0.32	J06105-218	0.598	J11421+267	0.485
J02222+478	0.622	J06371+175	0.51	J11511+352	0.506
J02362+068	0.261	J06548+332	0.392	J12123+544S	0.635
J02442+255	0.384	J06574+740	0.248	J12156+526	0.251
J02519+224	0.251	J07446+035	0.339	J12189+111	0.135
J02530+168	0.094	J07558+833	0.239	J12312+086	0.611
J02565+554W	0.689	J08413+594	0.12	J12479+097	0.354
J03133+047	0.16	J09143+526	0.622	J13005+056	0.169
J03463+262	0.658	J09144+526	0.605	J13196+333	0.606
J03473-019	0.514	J09163-186	0.563	J13229+244	0.264
J04153-076	0.234	J09449-123	0.31	J14010-026	0.552
J04290+219	0.744	J09561+627	0.64	J14173+454	0.263
J04376+528	0.653	J10023+480	0.601	J14257+236W	0.678
J04429+189	0.537	J10122-037	0.575	J14294+155	0.555

Table B.1: CARMENES stopped GTO stars included in the analysis, part 1

CARM. ID	mass ($M_\odot$)	CARM. ID	mass ($M_\odot$)	CARM. ID	mass ($M_\odot$)
J14307-086	0.739	J18051-030	0.521	J22021+014	0.6
J14321+081	0.105	J18174+483	0.51	J22057+656	0.314
J15194-077	0.33	J18189+661	0.128	J22096-046	0.531
J15305+094	0.111	J18198-019	0.656	J22114+409	0.123
J15499+796	0.143	J18353+457	0.631	J22115+184	0.58
J16167+672S	0.699	J18356+329	0.074	J22137-176	0.171
J16254+543	0.35	J18580+059	0.622	J22252+594	0.385
J16303-126	0.323	J19169+051N	0.526	J22468+443	0.352
J16313+408	0.164	J19255+096	0.108	J22518+317	0.482
J16555-083	0.09	J19346+045	0.632	J22532-142	0.37
J16570-043	0.274	J19511+464	0.246	J22559+178	0.599
J16581+257	0.572	J20093-012	0.141	J23113+085	0.33
J17303+055	0.59	J20305+654	0.415	J23216+172	0.437
J17338+169	0.211	J20533+621	0.597	J23351-023	0.119
J17355+616	0.606	J21164+025	0.402	J23381-162	0.508
J17378+185	0.489	J21348+515	0.494	J23419+441	0.141
J17578+046	0.155	J21466+668	0.258	J23548+385	0.295
J18022+642	0.173	J22012+283	0.303		

Table B.2: CARMENES stopped GTO stars included in the analysis, part 2

CARMENES ID	period	fap	remark
J00067-075	21.17	0.5206%	planet?
J00183+440	40.65	0.5847%	Rotation peak
J01025+716	43.39	10^{-6}	Activity peak (CaIRT)
J01026+623	9.33	0.0100%	Rotation peak
J01026+623	18.9	0.3146%	Activity peak (CaIRT,Hα)
J01125-169	3.06	0.0047%	Known planet
J01125-169	80.62	0.0173%	Activity peak (dlw)
J01125-169	4.7	0.0349%	Known planet
J02088+494	60.62	0.4171%	RV loud
J02222+478	28.23	0.0072%	Activity peak (CaIRT,dlw)
J02530+168	4.91	10^{-6}	Known planet
J02530+168	11.41	10^{-6}	Known planet
J02530+168	172.34	0.0011%	Activity peak (dlw)
J03133+047	2.29	10^{-6}	Known planet
J03133+047	67.91	0.3438%	planet?
J04153-076	1.8	10^{-6}	Activity peak (crx)
J04290+219	12.53	0.0048%	Rotation peak
J04290+219	25.07	0.0036%	Activity peak (CaIRT,dlw)
J04290+219	175.22	0.0314%	Activity peak (crx)
J04376+528	16.3	0.1925%	Activity peak (CaIRT,dlw)
J04376+528	7.9	0.1966%	planet?
J04376+528	422.79	0.2191%	planet?
J04588+498	8.97	0.0081%	planet?
J05084-210	693.32	10^{-6}	period longer than time baseline
J05314-036	37.08	0.0033%	Activity peak (CaIRT,Hα,dlw)
J05314-036	10000	10^{-6}	period longer than time baseline
J05365+113	11.77	10^{-6}	Activity peak (CaIRT,Hα,dlw)
J05365+113	12.47	0.0409%	Activity peak (CaIRT,Hα,dlw)
J06011+595	83.39	0.0704%	Activity peak (dlw)
J06011+595	44.1	0.3726%	planet?
J06011+595	21.52	0.6634%	planet?
J06103+821	10000	0.0230%	period longer than time baseline

Table B.3: Output of the periodicity search of the CARMENES stopped subsample; part 1

CARMENES ID	period	fap	remark
J06105-218	2621.41	0.0002%	period longer than time baseline
J06548+332	14.21	10^{-6}	Known planet
J06548+332	67.59	10^{-6}	planet?
J06548+332	119.48	0.0003%	planet?
J06574+740	1.7	0.9875%	RV loud
J07446+035	2.78	10^{-6}	Activity peak (crx,dlw)
J08413+594	206.39	10^{-6}	Known planet
J08413+594	2236.05	10^{-6}	period longer than time baseline
J08413+594	39.3	0.0383%	planet?
J09143+526	16.32	10^{-6}	Activity peak (CaIRT,Hα,dlw)
J09143+526	1468.72	0.0201%	period longer than time baseline
J09144+526	1432.22	10^{-6}	period longer than time baseline
J09144+526	24.4	0.0012%	Known planet
J09144+526	16.66	10^{-6}	Activity peak (CaIRT,Hα,dlw)
J09561+627	18.66	10^{-6}	Activity peak (CaIRT,dlw)
J09561+627	8.93	0.0282%	planet?
J10122-037	10.65	0.0004%	Rotation peak
J10122-037	21.4	0.0056%	Activity peak (CaIRT)
J10289+008	305.89	0.0166%	planet?
J10482-113	1.52	0.0702%	Rotation peak
J10482-113	2.93	0.0321%	Activity peak (dlw)
J10564+070	2.7	10^{-6}	Activity peak (crx,dlw)
J10584-107	4.62	10^{-6}	Activity peak (crx)
J11026+219	13.74	0.4204%	Activity peak (crx)
J11026+219	13.95	0.1249%	Activity peak (crx)
J11026+219	4.54	0.0409%	planet?
J11033+359	12.94	10^{-6}	planet?
J11033+359	1960.31	10^{-6}	period longer than time baseline
J11054+435	1043.71	0.0005%	period longer than time baseline
J11417+427	41.28	10^{-6}	Known planet
J11417+427	514.72	10^{-6}	Known planet
J11421+267	2.64	10^{-6}	Known planet
J11421+267	56.29	0.9319%	planet?

Table B.4: Output of the periodicity search of the CARMENES stopped subsample; part 2

CARMENES ID	period	fap	remark
J11511+352	11.12	0.0028%	Rotation peak
J11511+352	25.5	0.5200%	planet?
J12123+544S	13.68	10^{-6}	Known planet
J12123+544S	107.28	0.4552%	planet?
J12156+526	2.54	0.0045%	RV loud
J12189+111	1.55	0.2962%	RV loud
J12479+097	1.47	0.0012%	Known planet
J13229+244	3.02	10^{-6}	Known planet
J13229+244	87.38	0.1654%	Activity peak (crx,dlw)
J14307-086	249.07	0.3527%	planet?
J14321+081	1.46	0.1494%	RV loud
J15194-077	5.37	0.0003%	Known planet
J15194-077	2.65	0.4592%	planet?
J15194-077	9.62	0.7188%	planet?
J15305+094	505.74	0.3923%	period longer than time baseline
J15499+796	10000	0.2739%	period longer than time baseline
J16167+672S	86.9	10^{-6}	Known planet
J16167+672S	361.2	10^{-6}	Activity peak (crx)
J16167+672S	22.06	0.0018%	Activity peak (CaIRT,Hα,dlw)
J16303-126	4.83	0.7732%	Known planet
J16303-126	17.88	0.0011%	Known planet
J16313+408	1.99	0.3866%	Activity peak (dlw)
J16555-083	11.18	10^{-6}	Activity peak (Hα,dlw)
J16581+257	539.22	0.0051%	period longer than time baseline
J16581+257	11.29	0.2735%	Rotation peak
J17303+055	33.77	0.6047%	Activity peak (CaIRT,Hα,crx,dlw)
J17378+185	15.52	0.0007%	Known planet
J17378+185	480.52	0.0073%	planet?
J17378+185	40.3	0.0038%	Activity peak (CaIRT,Hα)
J17578+046	311.25	0.0010%	Rotation peak
J18174+483	16.04	0.3243%	Rotation peak
J18353+457	2.62	0.1111%	Activity peak (Hα)
J18356+329	201.65	0.0685%	period longer than time baseline
J18356+329	108.57	0.8765%	period longer than time baseline
J19169+051N	104.24	10^{-6}	Known planet
J19169+051N	174.48	0.0008%	planet?
J19169+051N	23.67	0.4980%	Activity peak (crx)

Table B.5: Output of the periodicity search of the CARMENES stopped subsample; part 3

CARMENES ID	period	fap	remark
J19255+096	382.16	10^{-6}	Activity peak (dlw)
J19346+045	2.52	0.6427%	planet?
J20533+621	118.33	0.3981%	Activity peak (crx)
J20533+621	183.37	0.1655%	planet?
J21164+025	14.45	10^{-6}	Known planet
J21164+025	42.98	0.0002%	Activity peak (CaIRT)
J21348+515	26.34	0.3320%	Rotation peak
J21466+668	8.05	10^{-6}	Known planet
J21466+668	2.31	10^{-6}	Known planet
J21466+668	92.47	10^{-6}	Activity peak (Hα)
J22021+014	10.96	0.0405%	planet?
J22057+656	123.74	0.0001%	Activity peak (crx)
J22096-046	2380.57	10^{-6}	period longer than time baseline
J22096-046	10000	0.0146%	period longer than time baseline
J22115+184	381.86	0.0001%	planet?
J22115+184	39.04	0.0809%	Activity peak (CaIRT,dlw)
J22137-176	3.65	10^{-6}	Known planet
J22137-176	611.67	10^{-6}	period longer than time baseline
J22252+594	13.35	10^{-6}	Known planet
J22468+443	2.19	10^{-6}	Activity peak (crx,dlw)
J22468+443	4.36	10^{-6}	Activity peak (crx,dlw)
J22468+443	3.22	0.8860%	RV loud
J22532-142	61.17	10^{-6}	Known planet
J22532-142	30.09	10^{-6}	Known planet
J23113+085	2225.31	10^{-6}	period longer than time baseline
J23113+085	141.09	10^{-6}	planet?
J23419+441	178.74	0.0001%	planet?
J23419+441	93.21	0.5426%	Activity peak (dlw)

Table B.6: Output of the periodicity search of the CARMENES stopped subsample; part 4

Acknowledgements

I would like to give my sincere thanks to my thesis supervisors Eike Guenther and Artie Hatzes. They especially contributed to the success of this PhD project with their time, patience, fruitful discussions and helpful remarks.

I thank Petr Kabath, Marek Skarka, Tereza Klocova und Daniel Dupalka for observations and data reduction with the OES. I thank them for the fruitful collaboration in the Czech part of my project. A big thank you as well to Judith Korth and Sascha Grziwa for their collaboration in the transit search in the *Kepler* A stars. I thank the CARMENES team for an inspiring team effort: for the building of the instrument, the observations and data reduction, the RV-extraction and visualization, science discussions and a whole of six meetings during my PhD time. Special thanks to Martin Schlecker for a fruitful collaboration. I also thank Iván Muñoz and Juan Carlos Muñoz who also calculated occurrence rates from CARMENES which were very useful as a sanity check. I thank Priyanka Chaturvedi and Arite Hatzes for discussion of and comments on the planet candidates.

I thank Michael Hartmann, Christian Högner, Frank Ludwig and Uwe Laux for observations with the TCES in service mode.

I also wish to thank Jonas Greif, André Prater, Priyanka Chaturvedi for proofreading of this thesis.

I thank my "house M" colleagues Alexander Drabent, Jakob Gelszinnis, Frank Pertermann, Priyanka Chaturvedi, Mukul Mhaksey, Kamlesh Rajpurohit, Michael Hartmann, David Wöckel, Verena Wolf, Sebastian Schmidl and Thomas Sperling, who created a fun working environment. They also listened to numerous test talks and gave very helpful hints for improvement.

I am grateful to the Tautenburg exoplanet working group for interesting insights and nice discussions. I thank Artie Hatzes for putting together such a nice team and for an always open door.

I thank Massimillano Esposito for the explanation of his detection limit method and for the great opportunity of observing with HARPS at LaSilla observatory.

I thank Evangelos Nagel, Matthias Hoeft and David Wöckel for organizing regular online meetings during Corona time. It helped a lot to feel part of a team while we all worked from home.

I thank Patrick Rauer for his useful comments to improve the code of the Tautenburg Spectroscopy Pipeline which helped to make the pipeline code more readable. I thank Michael Hartmann, Priyanka Chaturvedi and Jiři Zak for important pipeline tests. They helped me to find crucial bugs and to make the pipeline compatible with the RV-program RADIAL.

Lastly, and most importantly: I am very grateful to my husband Philipp for his support and patience and to my daughter for simply beeing herself.

This work was generously supported by the Thüringer Ministerium für Wirtschaft, Wissenschaft und Digitale Gesellschaft and the Deutsche Forschungsgemeinschaft (DFG) under the project GU 464/20-1.

This thesis includes data collected by the *Kepler* mission. Funding for the *Kepler* mission is provided by the NASA Science Mission directorate. This research has made use of NASA's Astrophysics Data System Bibliographic Services.

This research has made use of the SIMBAD database, operated at CDS, Strasbourg, France, and of data from the European Space Agency (ESA) mission Gaia (`https://www.cosmos.esa.int/gaia`), processed by the Gaia Data Processing and Analysis Consortium (DPAC, `https://www.cosmos.esa.int/web/gaia/dpac/consortium`).

CARMENES is an instrument for the Centro Astronómico Hispano-Alemán de Calar Alto (CAHA, Almería, Spain). CARMENES is funded by the German Max-Planck-Gesellschaft (MPG), the Spanish Consejo Superior de Investigaciones Científicas (CSIC), the European Union through FEDER/ERF FICTS-2011-02 funds, and the members of the CARMENES Consortium (Max-Planck-Institut für Astronomie, Instituto de Astrofísica de Andalucía, Landessternwarte Königstuhl, Institut de Ciències de l'Espai, Insitut für Astrophysik Göttingen, Universidad Complutense de Madrid, Thüringer Landessternwarte Tautenburg, Instituto de Astrofísica de Canarias, Hamburger Sternwarte, Centro de Astrobiología and Centro Astronómico Hispano-Alemán), with additional contributions by the Spanish Ministry of Economy, the German Science Foundation through the Major Research Instrumentation Programme and DFG Research Unit FOR2544 "Blue Planets around Red Stars", the Klaus Tschira Stiftung, the states of Baden-Württemberg and Niedersachsen, and by the Junta de Andalucía.

Acronyms

τ-spline Tautenburg Spectroscopy Pipeline

AAPS Anglo Australian Planet Search

Carmencita CARMEN(ES) Cool dwarf Information and daTa Archive

CARMENES **C**alar **A**lto high-**R**esolution search for **M** dwarfs with **E**xo-earths with **N**ear-infrared and optical **E**chelle **S**pectrographs

CCD Charge-coupled device

CoRoT COnvection, ROtation et Transits planétaires

CRIRES CRyogenic high-resolution InfraRed Echelle Spectrograph

FAP false alarm probability

FWHM Full width at half maximum

GLS-periodogram Generalized Lomb-Scargle Periodogram

GTO Guaranteed Time Observations

HARPS High Accuracy Radial velocity Planet Searcher

HATN Hungarian-made Auto-mated Telescope Network

HIRES High Resolution Echelle Spectrometer

HPF The Habitable-zone Planet Finder

IAU International Astronomical Union

IRD Infrared Doppler

KELT Kilodegree Extremely Little Telescope

MASCARA Multi-site All-Sky CAmeRA

MAST Mikulski Archive for Space Telescopes at `https://archive.stsci.edu/`

MCMC Markov-Chain Monte Carlo

NGTS Next-Generation Transit Survey

NIRPS Near Infra-Red Planet Searcher

NZP nightly zero point

OES Ondřejov Echelle Specrograph

RMS Root Mean Square

RV radial velocity

S/N signal-to-noise ratio

SERVAL Spectrum radial velocity analyser

SOPHIE Spectrographe pour l'Observation des Phénomènes des Intérieurs stellaires et des Exoplanètes

SpT spectral type

TCES Tautenburg Coudé Echelle Specrograph

TESS Transiting Exoplanet Survey Satellite

UVES Ultraviolet and Visual Echelle Spectrograph

VLT Very Large Telescope

WASP Super Wide Angle Search for Planets

Table B.7: List of Symbols

Quantity	Symbol	Value in SI
Newtonian gravitational constant	G	$6.6742 \times 10^{-11}\,\mathrm{m^3\,kg^{-1}\,s^{-2}}$
Astronomical unit	AU	$1.495\,978\,706\,6 \times 10^{11}\,\mathrm{m}$
Parsec	pc	$3.085\,677\,580\,7 \times 10^{16}\,\mathrm{m}$
Day	d	$86\,400\,\mathrm{s}$
Year	yr	$3.154 \times 10^{7}\,\mathrm{s}$
Mass of the Sun	$\mathrm{M}_\odot$	$1.988\,92 \times 10^{30}\,\mathrm{kg}$
Radius of the Sun	$\mathrm{R}_\odot$	$6.961 \times 10^{6}\,\mathrm{m}$
Luminosity of the Sun	$\mathrm{L}_\odot$	$3.846 \times 10^{26}\,\mathrm{W}$
Mass of Jupiter	$\mathrm{M}_{\mathrm{Jup}}$	$1.898 \times 10^{27}\,\mathrm{kg}$
Radius of Jupiter	$\mathrm{R}_{\mathrm{Jup}}$	$6.9911 \times 10^{4}\,\mathrm{m}$
Mass of the Earth	$\mathrm{M}_\oplus$	$5.9724 \times 10^{24}\,\mathrm{kg}$
Radius of the Earth	$\mathrm{R}_\oplus$	$6.371 \times 10^{3}\,\mathrm{m}$
Stellar Mass	$\mathrm{M}_\star$	
Stellar Radius	$\mathrm{R}_\star$	
Planetary Mass	M_{pl}	
Period of a Planet	P_{pl}	
Right Ascension	α	
Declination	δ	
Inclination	i	
Degree	$^\circ$	
Minute (plane angle)	$'$	
Second (plane angle)	$''$	
Eccentricity	e	

Ehrenwörtliche Erklärung

Ich erkläre hiermit ehrenwörtlich, dass ich die vorliegende Arbeit selbstständig verfasst und ohne unzulässige Hilfe Dritter oder Benutzung anderer als der angegebenen Hilfsmittel angefertigt habe. Jedwede wörtlich oder sinngemäß übernommenen Ausführungen, Daten und Konzepte sind ausnahmslos unter Angabe der Quellen als solche kenntlich gemacht.

Bei der Auswahl und Auswertung folgenden Materials haben mir die nachstehend aufgeführten Personen in der jeweils beschriebenen Weise unentgeltlich geholfen:

1. Dr. Eike Guenther und Prof. Dr. Artie Hatzes – Betreuung der vorliegenden Arbeit
2. Marek Skarka, Tereza Klocova, Petr Kabath und Daniel Dupalka – Beobachtungen und Datenreduktion aus Ondřejov mit dem OES
3. Judith Korth und Sascha Grziwa – Transit Suche mit dem Computerprogramm EXOTRANS
4. CARMENES consortium – Datenreduktion, Radialgeschwindigkeiten und Aktivitätsindikatoren für 300 vorher ausgewählte M-Sterne

Weitere Personen waren an der inhaltlich-materiellen Erstellung der vorliegenden Arbeit nicht beteiligt. Insbesondere habe ich hierfür nicht die entgeltliche Hilfe von Vermittlungs- beziehungsweise Beratungsdiensten (Promotionsberater oder andere Personen) in Anspruch genommen. Niemand hat von mir unmittelbar oder mittelbar geldwerte Leistungen für Arbeiten erhalten, die im Zusammenhang mit dem Inhalt der vorgelegten Dissertation stehen.

Diese Arbeit ist weder im In- noch im Ausland in gleicher noch in ähnlicher Fassung Bestandteil einer anderen Studien- oder Prüfungsleistung.

Die geltende Promotionsordnung der Physikalisch-Astronomischen Fakultät der Friedrich-Schiller-Universität Jena ist mir bekannt.

Ich versichere ehrenwörtlich, dass ich nach bestem Wissen die reine Wahrheit gesagt und nichts verschwiegen habe.

Tautenburg, den 15. September 2020

Silvia Sabotta

Curriculum Vitae: Silvia Sabotta

silvia.sabotta.eu
✉ *silvia@sabotta.eu*

Work Experience

09/2020 – now **Research Assistant**, *Landessternwarte Heidelberg-Königsstuhl*, Heidelberg.

03/2017 – 09/2020 **Research Assistant**, *Thüringer Landessternwarte*, Tautenburg, (parental leave 07/2019 – 02/2020).

10/2016 – 02/2017 **Student Assistant**, *Faculty of Mathematics and Computer Science*, Jena.

07/2015 – 02/2017 **Student Assistant**, *Thüringer Landessternwarte*, Tautenburg.

Education

03/2017 – 02/2021 **PhD Student**,
doctor rerum naturalium, Friedrich-Schiller-University Jena and Thüringer Landessternwarte Tautenburg.
PhD thesis: 'The Frequency of Planets around A- and M-type stars'

04/2014 – 10/2016 **Master of Science**,
Physics, Friedrich-Schiller-University Jena.
Master thesis: 'Influence of plage regions on planet diameter measurements'

10/2010 – 04/2014 **Bachelor of Science**,
International Physics Studies Program, University of Leipzig.
Bachelor Thesis: 'Electrical and Optical Characterisation of Aluminum-Doped Amorphous Zinc-Tin-Oxide Thin Films'

2000 – 2009 **Abitur (A levels)**, Johann-Sebastian-Bach-Gymnasium, Mannheim.

Additional Education

Nov 2016 **Training Workshop**, *Wroclaw*, Observations and Modeling of Solar Flares.

Jun 2016 **Training Workshop**, *Bad Honnef*, Formation and Evolution of Exoplanets.

Apr 2016 **Training Workshop**, *Tautenburg*, Observations and Data Reduction with a 2 m telescope.

Scholarship

10/2010 – 10/2016 Heinrich Böll Foundation

Teaching

05/2020 – 07/2020 **Assistent in the Beginners Lab**, *Faculty of Physics and Astronomy*, Jena.

09/2018 – 10/2018 **Tutor: 3rd Tautenburg Observing School**, *Thüringer Landessternwarte*, Tautenburg.

08/2017 – 09/2017 **Tutor: Short Summer School – detect your planet**, *Astronomical Institute of the Czech Academy of Sciences*, Ondřejov.

10/2016 – 02/2017 **Seminar: Analysis 1 for students of material sciences**, *Faculty of Mathematics and Computer Science*, Jena.

10/2016 – 02/2017 **Tutor: Analysis 3 for future teachers**, *Faculty of Mathematics and Computer Science*, Jena.

Other Experience

International

09/2009 – 08/2010 **Voluntary Year**, *Action Reconciliation Service for Peace*, Brno, Czech Republic.

Publications

[1] **Sabotta, S**, M. Schlecker, P. Chaturvedi, E. W. Guenther, and et. al. The carmenes search for exoplanets around m dwarfs. occurrence rates, detection limits and survey completeness. *A&A*, 2020. in prep.

[2] L. D. Nielsen, D. Gandolfi, D. J. Armstrong, J. S. Jenkins, M. Fridlund, N. C. Santos, F. Dai, V. Adibekyan, R. Luque, J. H. Steffen, M. Esposito, F. Meru, **Sabotta, S.**, E. Bolmont, D. Kossakowski, J. F. Otegi, F. Murgas, M. Stalport, F. Rodler, M. R. Díaz, and a. o. . m. Kurtovic. Mass determinations of the three mini-Neptunes transiting TOI-125. *MNRAS*, 492(4):5399–5412, Mar. 2020, 2001.08834.

[3] P. Kabáth, M. Skarka, **Sabotta, S.**, E. Guenther, D. Jones, T. Klocová, J. Šubjak, J. Žák, M. Špoková, M. Blažek, J. Dvořáková, D. Dupkala, J. Fuchs, A. Hatzes, E. Kortusová, R. Novotný, E. Plávalová, L. Řezba, J. Sloup, P. Škoda, and M. Šlechta. Ondřejov Echelle Spectrograph, Ground Based Support Facility for Exoplanet Missions. *PASP*, 132(1009):035002, Mar. 2020, 2001.01001.

[4] **Sabotta, S.**, P. Kabath, J. Korth, E. W. Guenther, D. Dupkala, S. Grziwa, T. Klocova, and M. Skarka. Lack of close-in, massive planets of main-sequence A-type stars from Kepler. *MNRAS*, 489(2):2069–2078, Oct. 2019, 1908.04570.

[5] M. Skarka, P. Kabáth, E. Paunzen, M. Fedurco, J. Budaj, D. Dupkala, J. Krtička, A. Hatzes, T. Pribulla, Š. Parimucha, Z. Mikulášek, E. Guenther, **Sabotta, S.**, M. Blažek, J. Dvořáková, L. Hambálek, T. Klocová, V. Kollár, E. Kundra, M. Šlechta, and M. Vaňko. HD 99458: First time ever Ap-type star as a δ Scuti pulsator in a short period eclipsing binary? *MNRAS*, 487(3):4230–4237, Aug. 2019, 1906.01877.

[6] J. C. Morales, A. J. Mustill, I. Ribas, M. B. Davies, A. Reiners, F. F. Bauer, D. Kossakowski, E. Herrero, E. Rodríguez, M. J. López-González, C. Rodríguez-López, V. J. S. Béjar, L. González-Cuesta, R. Luque, E. Pallé, M. Perger, D. Baroch, A. Johansen, H. Klahr, C. Mordasini, G. Anglada-Escudé, J. A. Caballero, M. Cortés-Contreras, S. Dreizler, M. Lafarga, E. Nagel, V. M. Passegger, S. Reffert, A. Rosich, A. Schweitzer, L. Tal-Or, T. Trifonov, M. Zechmeister, (...), and **Sabotta, S.** (...). A giant exoplanet orbiting a very-low-mass star challenges planet formation models. *Science*, 365(6460):1441–1445, Sept. 2019, 1909.12174.

[7] P. Kabáth, M. Skarka, **Sabotta, S**, and E. Guenther. The role of small telescopes as a ground-based support for exoplanetary space missions. *Contrib. Astron. Obs. Skalnaté Pleso*, 49:462–468, 2019.

[8] S. Benatti, D. Nardiello, L. Malavolta, S. Desidera, L. Borsato, V. Nascimbeni, M. Damasso, V. D'Orazi, D. Mesa, S. Messina, M. Esposito, A. Bignamini, R. Claudi, E. Covino, C. Lovis, and **Sabotta, S.** A possibly inflated planet around the bright young star DS Tucanae A. *A&A*, 630:A81, Oct. 2019, 1904.01591.

[9] A. Quirrenbach, P. J. Amado, I. Ribas, A. Reiners, J. A. Caballero, W. Seifert, J. Aceituno, M. Azzaro, D. Baroch, D. Barrado, F. Bauer, S. Becerril, V. J. S. Bèjar, D. Benítez, M. Brinkmöller, C. Cardona Guillén, C. Cifuentes, J. Colomé, M. Cortés-Contreras, S. Czesla, S. Dreizler, K. Frölich, B. Fuhrmeister, D. Galadí-Enríquez, J. I. González Hernández, R. González Peinado, E. W. Guenther, E. de Guindos, H. J. Hagen, A. P. Hatzes, P. H.

Hauschildt, J. Helmling, T. Henning, O. Herbort, L. Hernández Castaño, E. Herrero, D. Hintz, S. V. Jeffers, (...), and **Sabotta, S.** (...). CARMENES: high-resolution spectra and precise radial velocities in the red and infrared. In *Proceedings of the SPIE*, volume 10702 of *Society of Photo-Optical Instrumentation Engineers (SPIE) Conference Series*, page 107020W, July 2018.

[10] E. W. Guenther, O. Barragán, F. Dai, D. Gand olfi, T. Hirano, M. Fridlund, L. Fossati, A. Chau, R. Helled, J. Korth, J. Prieto-Arranz, D. Nespral, G. Antoniciello, H. Deeg, M. Hjorth, S. Grziwa, S. Albrecht, A. P. Hatzes, H. Rauer, S. Csizmadia, A. M. S. Smith, J. Cabrera, N. Narita, P. Arriagada, J. Burt, R. P. Butler, W. D. Cochran, J. D. Crane, P. Eigmüller, A. Erikson, J. A. Johnson, A. Kiilerich, D. Kubyshkina, E. Palle, C. M. Persson, M. Pätzold, **Sabotta, S.**, B. Sato, S. A. Shectman, J. K. Teske, I. B. Thompson, V. Van Eylen, G. Nowak, A. Vanderburg, J. N. Winn, and R. A. Wittenmyer. K2-106, a system containing a metal-rich planet and a planet of lower density. *A&A*, 608:A93, Dec. 2017, 1705.04163.

[11] G. Chen, E. W. Guenther, E. Pallé, L. Nortmann, G. Nowak, **Kunz, S.**, H. Parviainen, and F. Murgas. The GTC exoplanet transit spectroscopy survey. V. A spectrally-resolved Rayleigh scattering slope in GJ 3470b. *A&A*, 600:A138, Apr. 2017, 1703.01817.

[12] I. Juvan, M. Bluemcke, D. Baak, **Kunz, S.**, S. Schmidl, S. Klose, D. A. Kann, A. Nicuesa Guelbenzu, and F. Ludwig. GRB 160410A: TLS Tautenburg observations. *GRB Coordinates Network*, 19309:1, Jan. 2016.

Talks

11/2020 **Exoplanet Demographics Conference**, *'Detection Limits and Occurrence Rates of the CARMENES M Dwarf Survey'*, IPAC/Caltech (virtual).

06/2020 **TLS institute colloquium**, *'Occurrence rates, detection limits and survey completeness from CARMENES'*, Tautenburg.

05/2019 **10th CARMENES science meeting**, *'Detection limits and sample completeness'*, Sevilla.

03/2019 **PSF theory group meeting of the MPIA**, *'Finding the frequency of close-in planets around hot and cool stars'*, Heidelberg.

01/2019 **Tautenburg Presentation Series**, *'Finding detection limits for planets around A and M type stars'*, Tautenburg.

11/2018 **9th CARMENES science meeting**, *'Detection Limits for the CARMENES sample'*, Barcelona.

10/2018 **PLATOSpec workshop 2**, *'Limits of ground based RV surveys'*, Ondřejov.

01/2018 **Tautenburg Presentation Series**, *'166 (im)possible planets around A stars'*, Tautenburg.

10/2017 **Exo-Coffee at IAC**, *'Blue atmosphere or stellar activity – is the blue atmosphere of the exoplanet GJ 3470 b real?'*, Teneriffe.

06/2017 **European Week of Astronomy and Space Science**, *'Blue atmosphere or stellar activity – is the blue atmosphere of GJ 3470 b real?'*, Prague.

05/2017 **Astronomical Institute Institute colloquium**, *'Blue atmosphere or stellar activity – is the blue atmosphere of GJ 3470 b real?'*, Ondřejov.

11/2016 **Physikerinnentagung**, *'Blue atmosphere or stellar activity – Are bright stellar regions (plage) occulted during transit?'*, Hamburg.

09/2016 **AG meeting**, *'Blue atmosphere or stellar activity – Are bright stellar regions (plage) occulted during transit?'*, Bochum.

Public Outreach

05/2018 **Talk: 8th Science Slam of the Graduate Academy**, *'Can you eat ice cream on an exoplanet?'*, Jena.

03/2018 **Video: Show your research**, *'How frequent are planets around very hot and cold stars?'*, Jena.

11/2017 **Talk: Searching for Life - Lange Nacht der Wissenschaften**, *'How do sunsets look like on exoplanets?'*, Jena.

10/2016 **Talk: Lange Nacht der Sterne**, *'Blaue Planeten und wie sie beobachtet werden'*, Tautenburg.